THE UNIVERSITY OF ALBERTA

Studies on the Neck Coiled-coil and Highly Charged regions of Kinesin-Like Motor Proteins Kif3A and Kif3B

By

Mundeep Singh Chana ©

A THESIS
SUBMITTED TO THE FACULTY OF GRADUATE STUDIES AND RESEARCH IN PARTIAL FULFILLMENT OF THE REQUIREMENTS FOR THE DEGREE OF MASTER OF SCIENCE

DEPARTMENT OF BIOCHEMISTRY

EDMONTON, ALBERTA

FALL 2002

National Library
of Canada

Acquisitions and
Bibliographic Services

395 Wellington Street
Ottawa ON K1A 0N4
Canada

Bibliothèque nationale
du Canada

Acquisitions et
services bibliographiques

395, rue Wellington
Ottawa ON K1A 0N4
Canada

Your file Votre référence

Our file Notre référence

The author has granted a non-exclusive licence allowing the National Library of Canada to reproduce, loan, distribute or sell copies of this thesis in microform, paper or electronic formats.

The author retains ownership of the copyright in this thesis. Neither the thesis nor substantial extracts from it may be printed or otherwise reproduced without the author's permission.

L'auteur a accordé une licence non exclusive permettant à la Bibliothèque nationale du Canada de reproduire, prêter, distribuer ou vendre des copies de cette thèse sous la forme de microfiche/film, de reproduction sur papier ou sur format électronique.

L'auteur conserve la propriété du droit d'auteur qui protège cette thèse. Ni la thèse ni des extraits substantiels de celle-ci ne doivent être imprimés ou autrement reproduits sans son autorisation.

0-612-81378-9

Canada

THE UNIVERSITY OF ALBERTA

LIBRARY RELEASE FORM

NAME OF AUTHOR: Mundeep S. Chana

TITLE OF THESIS: Studies on the Neck Coiled-coil and Highly Charged regions of Kinesin-Like Motor Proteins Kif3A and Kif3B

DEGREE: Master of Science

YEAR THIS DEGREE GRANTED: 2002

Permission is hereby granted to the University of Alberta Library to reproduce single copies of this thesis and to lend or sell such copies for private, scholarly, or scientific research purposes only.

The author reserves all other publication and other rights in association with the copyright in the thesis, and except as herein before provided neither the thesis or any substantial portion thereof may be printed or otherwise reproduced in any material form whatever without the author's written permission.

Mundeep Chana

Permanent Address:
4328-46 Street
Edmonton, AB
T6L 6L9

DATE: Aug, 21 2002

THE UNIVERSITY OF ALBERTA

FACULTY OF GRADUATE STUDIES IN RESEARCH

The undersigned certify that they have read, and recommend to the Faculty of Graduate Studies in Research for acceptance, a thesis entitled "STUDIES ON THE NECK COILED-COIL AND HIGHLY CHARGED REGIONS OF KINESIN-LIKE MOTOR PROTEINS KIF3A AND KIF3B" submitted by Mundeep Singh Chana in partial fulfillment of the requirements of the degree of Master of Science.

Dr. Robert S. Hodges
(Supervisor)

Dr. Charles F. ~~B. Holmes~~

Dr. Joel H. Weiner

Dr. Randall Irvin

DATE: Aug. 12, 2002

ABSTRACT

These studies were aimed at characterizing the coiled-coil forming region in the necks of the kinesin-like motor proteins, Kif3A and Kif3B, and illuminating the contributions of the electrostatic residues in the flexible hinge region of Kif3A and Kif3B to heterodimer formation by these two proteins. Synthetic peptides based on the neck regions of the motor proteins Kif3A and Kif3B were used to characterize the homodimeric and heterodimeric neck region coiled-coils of the proteins. The ability of complementary charged regions to specify heterodimer formation in coiled-coils was examined by synthesizing analogs of the neck coiled-coil regions of Kif3A and Kif3B, with and without various negatively and positively charged extensions to the C-terminus of the neck coiled-coil, and by characterizing these analogs by circular dichroism spectroscopy. The regions of the necks we studied were able to form coiled-coils and overall the unstructured charged regions control specificity of heterodimerization without affecting stability of the heterodimeric coiled-coil.

ACKNOWLEDGEMENTS

I would especially like to thank my supervisor Dr. Robert S. Hodges for his guidance and support throughout my years in his laboratory. In addition I would like to thank Dr. Brian Tripet for his guidance and support during my introductory years of graduate training. I would like to extend a thank you to Dr. Colin Mant for his interest in the project and for all the polishing of the published material. Who would have guessed that a four months summer project would grow into four publications, two international symposia, and a Master of Science Degree?

I would like to pay special thanks to Bob Luty for teaching me how to use a circular dichroism spectrometer and for analyzing my peptides. I thank Les Hicks for carrying out and analyzing the analytical ultracentrifugation sedimentation equilibrium runs for this project. Thanks to Michael Carpenter for help with amino acid analysis. Thanks to Lorne Burke for his special touch with HPLCs.

I would like to thank my friend Jessica Agrell-Smith for her support during my degree.

I would like to thank the members of Dr. Hodges laboratory for making the lab such an enjoyable place to come to every morning. Thank you to Stan Kwok, Darin Lee, Jennifer Litowski, Paul Cachia, Elsi Vacano, and Morris Aarbo.

A number of organizations contributed financially to this project. The 75th Anniversary Award from the Faculty of Medicine and Dentistry for MSc. Research, research allowances from the Medical Research Council of Canada, the National Institute of Health, the University of Colorado Health Sciences Center, and the University of Alberta Biochemistry Department.

For all that lies within,

And for all that lies hereafter.

I would like to dedicate this thesis

To my father, Gurmeet Singh Chana,

To my supervisor Dr. Robert Stanley Hodges,

And my friend, Jessica Agrell-Smith.

TABLE OF CONTENTS

Page

Chapter I. Introduction

I. Kinesin and Kinesin-like Proteins

1. General introduction to the Kinesin field: A brief history 1
2. Isolation of Kinesin 9
3. Characterization of Kinesin 11
    - i. Quaternary Structure 11
    - ii. Enzymatic Activity 12
    - iii. Mechanochemical Motor Domain 16
    - iv. Microtubule-based Movement 18
4. The Kinesin Superfamily 19
5. Kif3 Heterotrimeric motor protein: A kinesin-like protein. 20

II. Coiled-coils 24

1. Hydrophobic Repeat 24
2. Hydrogen Bonding associations 29
3. Electrostatic interactions in coiled-coils 29

III. Electrostatics 30

Chapter II. Materials and Methods

A. Materials 37

1. Chemicals and reagents 37

B. Methods

1. Peptide synthesis 38
2. Peptide purification 45
3. Amino acid analysis 48
4. Mass spectrometry 48
5. Circular dichroism spectroscopy 51
    - A. % α-helix calculation 52
    - B. Protein unfolding measurements 52
    - C. Calculation of denaturation midpoints 53

6. Preparation of oxidized peptides 57
7. Sedimentation equilibrium studies 58
8. Redox experiments 58
9. Heterostranded peptide formation 59

Chapter III The role of unstructured highly charged regions on the stability and specificity of dimerization of two-stranded α-helical coiled-coils: Analysis of the neck-hinge region of the kinesin-like motor protein Kif3A.

A. Introduction 63
B. Results 66
  i. Autonomous folding of predicted neck coiled-coil region 66
  ii. Secondary structure of the charge-rich hinge region 72
  iii. Role of charge-rich regions in dimer formation 77
  iv. Effect of charge-rich regions on coiled-coil stability 86
C. Discussion 89

Chapter IV An investigation into the effects of highly charged regions on the stability of the neck region coiled-coil of kinesin-like motor protein Kif3B.

A. Introduction 94
B. Results 97
  i. Folding of the predicted neck coiled-coil of Kif3B 97
  ii. Secondary structure of the charge-rich hinge region 98
  iii. Role of oppositely charged regions in dimer formation 99
  iv. Stability of the neck coiled-coil Kif3B with Kif3A 111
  v. Selective heterodimer formation 118
C. Discussion 121

Chapter V Stability and specificity of heterodimer formation for the neck regions of the motor proteins Kif3A and Kif3B.

A. Introduction 125
B. Results 128

i. Secondary structure of the complementary charged regions of Kif3A and Kif3B 128
ii. Folding of the neck region coiled-coil 130
iii. Role of complementary charged region in dimer formation 133
iv. Effect of complementary charged region on coiled-coil stability . 137
C. Discussion 143

Chapter VI Future Investigations 150

Bibliography 169

LIST OF TABLES

Table Page

II-1 List of reagents used and suppliers 37

III-1 Circular dichroism data of disulfide-bridged Kif3A synthetic pepetides 71

III-2 Circular dichroism data of reduced Kif3A synthetic pepetides 74

III-3 Denaturation data for disulfide-bridged Kif3A synthetic peptides 80

IV-1 Circular dichroism data of Kif3B synthetic peptides .106

IV-2 Denaturation data for Kif3B synthetic peptides 113

IV-3 Circular dichroism data of reduced Kif3B synthetic peptides 117

V-1 Circular dichroism data of synthetic peptides 136

V-2A Denaturation data for synthetic coiled-coil peptides 142

V-2B Denaturation data for synthetic peptides with one charge segment 142

V-2C Denaturation data for synthetic peptides with both charge segments 142

VI-1 Circular dichroism data of reduced synthetic peptides from N-type kinesin superfamily proteins 158

VI-2 Neck region coiled-coil stability data 162

LIST OF FIGURES

Figure		Page
I-1	Vesicle transport in Nerve Cell	5
I-2	Electron micrographs of vesicles tethered to microtubules	6
I-3	Schematic of conventional dimeric kinesin	13
I-4	Schematic of KIF3 heterotrimeric motor protein	23
I-5	Figure showing pattern of amino acids promoting α-helix	27
I-6	Schematic illustration of a parallel two-stranded α-helical coiled-coil	28
II-1	Figure showing amino acid activation and coupling	40
II-2	Figure showing mechanism for deprotection of amino acid	42
II-3	Reversed-phase HPLC chromatographs of crude and pure peptide 1	46
II-4	Reversed-phase HPLC chromatographs of crude and pure peptide 2	47
II-5	Electrospray mass spectrometry spectra of pure peptides 1 and 2	50
II-6	Circular dichroism spectra of an alpha-helix and random coil	54
II-7	Urea/Temperature melting curves of peptides with extrapolation plot	55
II-8	Mass spectrometry spectra depicting DTNP derivitization of peptide	61
II-9	Mass spectrometry spectra depicting heterodimer formation of peptide	62
III-1	Amino acid sequences of the Kif3A peptides	68
III-2	Circular dichroism spectra of synthetic peptides, P2, P5, and P1	69
III-3	Circular dichroism spectra of reduced peptides P2, P3, and P1	73
III-4	Thermal Denaturation of peptides P1, P2 and P3	76
III-5	Circular Dichroism spectra of synthetic peptides derived from Kif3A	78
III-6	RP-HPLC elution profiles of start and end points from redox experiments	81

III-7 The formation of oxidized, heterostranded peptides as a function of time 84

III-8 Formation of heterostranded peptides in the presence of NaCL 85

III-9 Denaturation profiles of disulfide bridged Kif3A synthetic peptides 87

III-10 Extrapolation of Tm data to the absence of urea for Kif3A peptides 88

IV-1 Schematic of Kif3A/Kif3B and sequence of neck-hinge regions 101

IV-2 Amino acid sequences of synthetic Kif3B peptides 103

IV-3 Circular dichroism spectra of peptides P7, P10, and P6 105

IV-4 Circular dichroism spectra of oxidized and reduced synthetic Kif3B peptides 109

IV-5 Guanidine-HCl and urea denaturation profiles of Kif3B synthetic peptides ..112

IV-6 Temperature and urea denaturation profiles of Kif3B synthetic peptides 114

IV-7 Comparison of Kif3A and Kif3B coiled-coil stability using urea 116

IV-8 The formation of oxidized, heterostranded peptides through redox equilibrium experiments for peptides P3+P4, and P8+P9 120

V-1 Schematic of Kif3A/Kif3B and sequence of complementary charge-rich regions 129

V-2 Circular dichroism spectra of complementary charge-rich region 131

V-3 Amino acid sequences of Kif3A and Kif3B peptides 132

V-4 Circular dichroism and denaturation profiles of homo and heterodimeric neck coiled-coils 135

V-5 The formation of oxidized, heterostranded peptides as a function of time 139

V-6 Formation of heterostranded peptides in the presence of NaCL 140

V-7 Guanidine-HCl and urea denaturation of peptides P3, P8, and P3/P8 144

V-8 Guanidine-HCl and urea denaturation of peptides P1, P6, and P1/P6 145

VI-1 Kinesin superfamily tree 151

VI-2A Sequence alignment of kinesin-like protein neck regions, N1-N5 154

VI-2B Sequence alignment of kinesin-like protein neck regions, N6-N11 155

VI-3 Sequences of kinesin-like protein neck regions peptides characterized 156

VI-4 Circular dichroism spectra of analysed peptides 157

VI-5 Denaturation profiles of the synthetic peptides 161

VI-6 A cross-sectional view of two neck region coiled-coils 163

VI-7 Helical propensity plot of two neck region coiled-coils 165

VI-8 Potential intrachain electrostatic interactions of two neck regions 166

LIST OF ABBREVIATIONS

Amino acids:

Ala, A	alanine
Arg, R	arginine
Asn, N	asparagine
Asp, D	apartic acid
Cys, C	cysteine
Gln, Q	glutamine
Glu, E	glutamic acid
Gly, G	glycine
His, H	histidine
Ile, I	isoleucine
Leu, L	leucine
Lys, K	lysine
Met, M	methionine
Phe, F	phenylalanine
Pro, P	proline
Ser, S	serine
Thr, T	threonine
Trp,W	tryptophan
Tyr, Y	tyrosine
Val, V	valine

Boc or t-Boc	tert-butyloxycarbonyl
CD	circular dichroism
DCM	dichloromethane
DIEA	N,N-diisopropylethylamine
DMF	N,N-dimethylformamide
DTT	dithothreitol
EDT	1,2-ethandithiol
GdnHCl	guanidine hydrochloride
$[\mathrm{GdnHCl}]_{1/2}$	guanidine hydrochloride denaturation midpoint
HBTU	2-(1H-benaotriazol-1-yl)-1,1,3,3-tetramethyluronium hexafluorophosphate
HF	hydrofluoric acid
HOBt	1-hydroybenzotriazole
RP-HPLC	reversed-phase-high performance liquid chromatography
I.D.	internal diameter
KAP3	kinesin-like accessory protein 3 isoforms
Kif3A	kinesin family motor protein 3A
Kif3B	kinesin family motor protein 3B
m	slope of free energy versus denaturant concentration plots
MW	molecular weight
NMP	N-methylpyrrolidinone

SEC	size-exclusion chromatography
SpKRP85	*Strongylocentrotus purpuratus* **K**inesin **R**elated **P**rotein-85kDa
SPPS	solid-phase peptide synthesis
TFA	trifluoroacetic acid
TFE	2,2,2-trifluoroethanol
T_m	temperature denaturation midpoint
$[\text{urea}]_{1/2}$	urea denaturation midpoint
XlKlp3A	*Xenopus laevis* **K**inesin-**l**ike **p**rotein subunit 3A
ΔG_u	free energy of unfolding
$\Delta\Delta G_u$	change or difference in free energy of unfolding

CHAPTER I

INTRODUCTION

This thesis deals with studies of the neck region of kinesin-like motor proteins. The first part of this introductory chapter comprises a general overview of the kinesin field beginning with a description of initial studies conducted to identify and characterize the kinesin molecule. Our work was carried out using peptides from the MmKif3A/B motor protein and so a description of this protein will conclude this section of the introduction. Many of the studies conducted were an attempt to understand how the stability of two-stranded α–helical coiled-coils might be affected by regions rich in charged residues, and so there is a section addressing the coiled-coil motif and one addressing the functional role of charged residues in proteins.

I. Kinesin and Kinesin-like Proteins

1) *General introduction to the kinesin field:* A brief history.

The discovery of the kinesin motor protein was a result of investigations initiated in an attempt to explain the movement of membranous particles in nerve cell axons. Neurons have an intriguing topology. Emanating from a central cell body, there are multiple extensions, termed dendrites, and usually a single long appendage, termed the axon (see Fig. I-1A). As early as the 19th century it was discovered that the dendrites and axons were replenished by the cell body; their removal from the cell body led to their subsequent decay. It was postulated that a type of circulation within the cell might lead to the continual rejuvenation of the neuron's extensions.

The axon, being larger and longer than dendrites, has been the favored extension for investigation. In the 20th century, with light microscopy alone, small particles were observed moving through axons on straight pathways. Experiments using a variety of neurons were conducted using radiolabeled precursor molecules. The rate of movement of the radioactivity down the axon was examined for compounds such as the enzymes involved in the metabolism of neurotransmitters such as norepinephrine, acetylcholine, and serotonin. The rate of movement of radioactivity was determined by measuring, over time, the amount of radioactivity reaching a lesion in the axon.

Radiolabeled molecules were found in membrane bound vesicles after sedimentation of the cell contents. Notably, neurosecretory granules, containing hormones and hormone binding proteins, glycoproteins, plasma membrane precursors, and organelles such as the mitochondrion and portions of the smooth endoplasmic reticulm (SER), were all found to be transported down the axon at velocities approaching 400mm/day. This type of transport was termed fast axonal transport. Furthermore, this type of intracellular transport appears to be a rational consequence of the compartmentalization found in eukaryotic cells. For example, secretion of a protein requires the movement of membrane bound vesicles from the endoplasmic reticulm (ER) to the Golgi, and finally to the cell surface. Thus large cells with a polarized structure such as neurons require the organized transport of membrane bound vesicles, formed in the cell body, to the periphery of the axon. [For extensive reviews see: Grafstein and Forman, 1980; Smith, 1980].

Along with swiftly moving particles, seen with light microscopy, tubular rod-shaped filaments were also seen. These were characterized as microtubules, composed of alpha and beta subunits, which polymerize to give filaments with stable and dynamic ends, termed the minus and plus ends, respectively. The minus end is located in the cell body and the ever shortening and elongating plus end is located in the axon [Inoue, 1997, Review].

With the development of electron microscopy in the latter half of the 20th century, close-up views of the internal structure of the axonal organelles could be observed. In an attempt to characterize the organelles moving from the cell body to the axon, the anterograde direction, a portion along the length of an axon was frozen using liquid nitrogen, a technique that became known as a cold block. An alternate method was to create a lesion along a small portion of the axon's length. Organelles partaking in fast transport in the anterograde and retrograde directions conglomerated at the proximal (closest to the cell body) and distal regions of the cold block, respectively. On the proximal side, tubulovesicular particles (membrane limited structures) and mitochondria were observed to predominate [Smith, 1980, review; Tsukita and Ishikawa 1980]. The blocked organelles were closely associated with microtubules and their longitudinal arrangement gave them the look of pearls on a string (see Fig. I-1B, C). Further, electron microscopy led to the observation of cross-bridges between transported vesicles and microtubules (see Fig. I-2A, B, C). A model was proposed giving a role to the cross-bridge structures in the movement of membrane-enclosed vesicles along the microtubules. The cross-bridge structures were thought to behave similarly to the behavior of myosin heads with F-actin [Schmitt, 1968]. The cross-bridges were thought to oscillate while continually binding, unbinding, and rebinding to microtubules. Hence the cross-bridge structures were thought to be protein (see Fig. I-2D).

Fig. I-1. Panel A depicts a schematic representation of a typical nerve cell. Panel B shows membrane bound vesicles, round structures, associated with long fibers identified as microtubules (adapted from Miller and Lasek, 1985). Panel C shows an axon, crushed in the center to create a lesion. The arrowhead pointing upward shows the point of lesion, the arrowhead facing downward points at the axonal membrane. The dark regions right of the lesion are organelles such as mitochondria, on the left and near the top, are small particles, which are small membrane bound vesicles. Notice the linear structures they form. Prox, represents proximal, or side of the lesion closest to the cell body, while Dist, represents distal, or the side of the lesion furthest from the cell body (adapted from Smith, 1980).

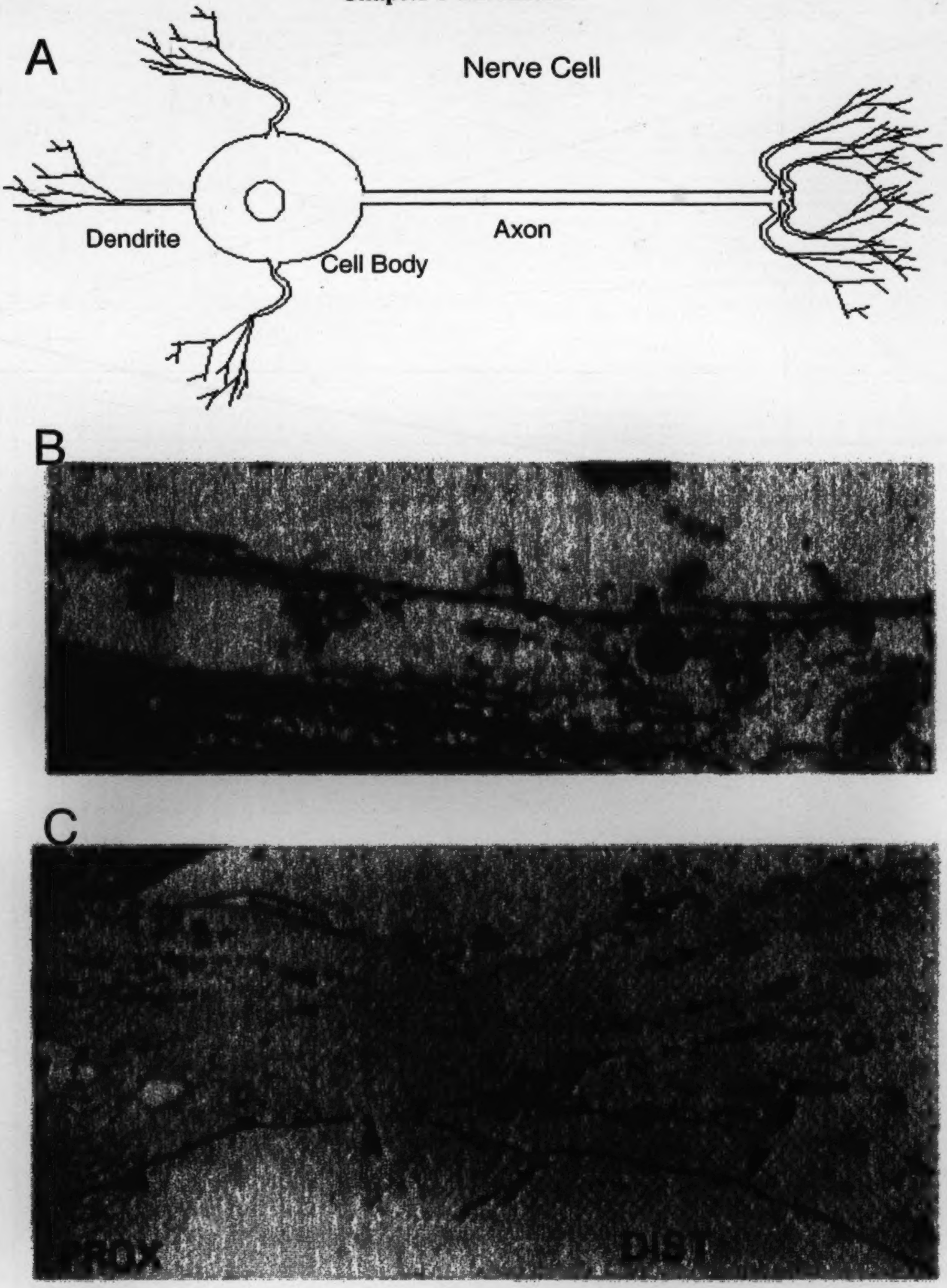
A
Nerve Cell
Dendrite
Cell Body
Axon
B
C
PROX
DIST

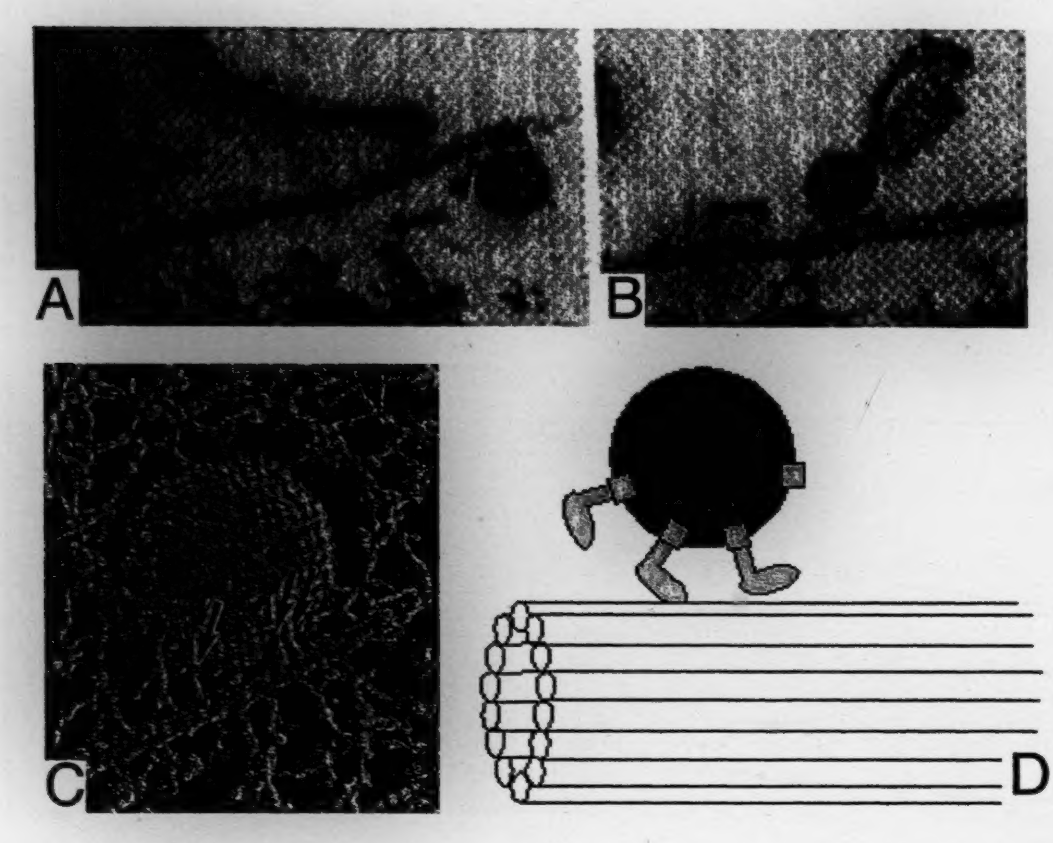

Fig. I-2. Panels A and B show lower resolution electron micrographs of vesicles associated with microtubules. The arrow heads are pointing to cross-bridge structures that tether the vesicles to the microtubule (adapted from Miller and Lasek, 1985). Panel C shows a higher resolution electronmicrgraph of a membrane bound vesicle tethered to a microtubule. The arrows are pointing to cross-bridge structures (adapted from Hirokawa and Yorifuji, 1986). Panel D depicts schemtatic model of a cross-bridging protein responsible for microtubule-based fast axonal transport of membrane bound vesicles.

In the early 1980s, along with the development of video-enhanced contrast-differential interference contrast (AVEC-DIC) microscopy, enabling better resolution of moving organelles, a number of key experiments focused on identifying the protein translocator responsible for fast axonal transport. In 1981, it was shown that there were three different waves in axonal transport, a fast component where membrane bound organelles were found to move at 400 mm/day, and two slow components with transfer rates of 0.3-1.0 mm/day and 2-4.0 mm/day, respectively [Tytell et al., 1981]. Using 2-D gel electrophoresis it was discovered that each transport component was composed of a distinct set of proteins. It was thought that perhaps each rate component represented a discrete macromolecular assembly that moved as a unit [Tytell et al., 1981]. With the increased resolution of AVEC-DIC microscopy it was possible to see structures as small as one-tenth the resolution limit of the light microscope. With this technological advancement, researchers were able to track particles 30nm in diameter. For the first time they could identify more particles than could ever be seen before moving in the anterograde direction [Allen et al, 1982]. This phenomenon was not unlike going to the country and observing stars that were always present but because of our city location we were unable to detect them.

1982 saw the development of an extruded axoplasm from the giant squid axon [Brady and Lasek, 1982]. Extruded axoplasm was the result of removing the plasma membrane and insulating layer of glial cells from the axon. Removal of the axonal contents is like squeezing toothpaste from a tube. The benefits of mechanically extruded axoplasm over a detergent permeablized axon are that (1) microtubules that delineate the linear pathways that most particles follow could be seen better since there is less light scattering; (2) there is less likelihood of components being lost or extracted; (3) the resulting preservation of polypeptide components and axonal organization leads to a greater extended life span for the model; (4) the fact that fast axonal transport continues in extruded axoplasm discounts the theory that fast axonal transport might be regulated by action potentials traversing the axonal membrane [Brady and Lasek, 1982].

The extruded axoplasm system led to a further refinement in the search for the reasons behind fast axonal transport. From extruded axoplasm, dissociated axoplasm was developed by mechanically disrupting the axoplasm. This technique enabled the isolation of individual microfilaments with associated organelles to be observed with AVEC-DIC and electron microscopy [Schnapp et al, 1985]. With this system of dissociated axoplasm, researchers were able to observe single microfilaments support bi-directional organelle movement. Through labeling the microfilaments with anti-alpha-tubulin antibodies, the isolated filaments were shown to be composed of tubulin. Lastly, a single dissociated transport filament could be isolated, rapidly frozen and observed by electron microscopy. The filaments were seen to have structural characteristics exactly the same as purified microtubules; hence, researchers were able to identify the microfilaments in axoplasm responsible for fast axonal transport to be microtubules composed of tubulin. Furthermore, they were able to observe that a direct relationship exists between organelle movement and microtubules. Moreover, the observation that single microtubule filaments supported bi-directional movement indicated that the transport filaments have more than one “track” for organelle movement [Schnapp et al., 1985].

The improved visualization of microtubule filaments in dissociated axoplasm also led to improved visualization of organelle movement. It was seen that mitochondria moved along filaments while attached by a portion of their entire lengths; unattached segments of mitochondria exhibited Brownian motion. Organelles could be seen to switch filaments, so that, when mitochondria switched filaments, one end was seen attached to a crossing filament while the other end remained attached to the original filament; the trailing end subsequently detached from the original and reattached to the crossing filament. These observations led to the hypothesis that organelles have multiple attachment sites for microtubules [Vale et al, 1985a]. Investigators determined that organelle movement requires ATP [Vale et al, 1985a], and by showing that organelles moved on dissociated axoplasmic microtubules, they proved that organelle movement did not require the microtubules to be associated with the interlocking network of thin neurofilaments found in the axonal cytoplasm. These findings cast doubt on two previously postulated hypotheses that explain transport by contraction of a cytoplasmic lattice [Ellisman and Porter, 1980] or cytoplasmic streaming through low viscosity channels [Weiss and Gross, 1982].

2) *Isolation of kinesin*

The year 1985 could be described as the "Big-Bang" for the kinesin field. With the isolation of a soluble factor that could promote organelle movement on stabilized microtubules, it was possible to show that the soluble factor was proteinaceous. It was shown that heat or trypsin treatment of the soluble factor, prior to adding it to the reconstituted system of stabilized microtubules and purified organelles, inhibited organelle movement [Vale et al, 1985b]. Organelles were observed making stable complexes with microtubules in the presence of AMP-PNP, adenylylimidodiphosphate; a nonhydrolyzable form of ATP [Vale et al, 1985b]. Initial purification of the soluble factor, or translocator protein, made use of this property, and so microtubules with bound organelles were isolated and the protein translocator was released from microtubules with ATP [Vale et al, 1985c]. The protein was initially identified from squid axoplasm and was found to have a mammalian homologue in bovine and chicken brain tissue [Brady, 1985]. The protein was found to have two subunits, a heavy subunit approximately 110 kD and a light subunit approximately 65 kD. The protein was termed kinesin from the Greek *kinein*, to move [Vale et al, 1985c]. Later it was determined that the kinesin molecule was likely to be composed of two heavy subunits or chains and two light subunits or chains resulting in a tetramer [Bloom et al., 1988]. Heavy chain and light chain are terms coined to describe the two subunits of kinesin. However, the spacial organization of the four chains was still unknown.

Using a cold block, whereby a small segment of an axon is frozen to arrest transport of vesicles, investigators were able to cool squid axons and concentrate moving vesicles on microtubules on both sides of the cold block. The microtubules on the periphery of the axon were isolated and the concentrated vesicles were subjected to electron microscopy. Examination of the concentrated vesicles by electron microscopy revealed cross-bridges between the vesicles and microtubules. The mean distance of organelles and vesicles from microtubules was measured and determined to be 17nm, and the length of the cross bridges was 16-18nm in length [Miller and Lasek, 1985] suggesting that the cross-bridging structures were responsible for holding the vesicles near microtubules. In permeabilised and reactivated walking-leg crayfish axons, bi-directional organelle movement was seen on microtubules. Examination with electron microscopy of the axon at the periphery and in central locations led to the observation of cross-bridges between membrane bound organelles and microtubules. In this instance the measurement of the cross-bridges was 25nm ± 4nm. It was thought that the cross-bridges were visualizations of the kinesin molecule [Miller and Lasek, 1985; Hirokawa and Yorifuji, 1986] because it had been shown to be responsible for microtubule directed movement [Vale et al, 1985b; Vale et al 1985c]. The first direct evidence to show kinesin binding to vesicular structures and microtubules was presented in 1989 [Pfister et al., 1989]. Monoclonal antibodies were developed to the two subunits of the kinesin molecule. The antibodies were used to show that kinesin bound to punctate cytoplasmic structures, indicative of membrane bound organelles, in a variety of cultured mammalian cell types. Furthermore, double-labeling experiments made use of antibodies of tubulin and kinesin to show that kinesin was found highly concentrated where microtubules were found in abundance [Pfister et al., 1989]. Three of the kinesin antibodies were specific to the heavy chain, and two were specific to the light chain.

3) *Characterization of kinesin*

i) *Quaternary Structure*

Electron microscopy and antibody decoration were used to elucidate the spacial arrangement of the four chains in the proposed kinesin tetramer [Hirokawa et al., 1989]. Kinesin had been predicted to be a highly elongated molecule, [Bloom et al., 1988] and upon its visualization through electron microscopy, the molecules were seen to be rod-shaped with an overall length of 80.4 nm ± 8.1 nm [Hirokawa et al., 1989]. Morphologically, the molecule was seen to have two globular structures that were termed heads. The opposite end was termed the tail and was found to have a fan-like structure [Hirokawa et al., 1989]. The two ends of the molecule were connected with a relatively straight shaft, which was occasionally observed to have a bend, called a hinge [Hirokawa et al., 1989]. The long and short diameters of the head were found to be 10 ± 2 and 9 ± 2 nm, respectively. The tail region was determined to have a width of 15 ± 3 nm. The position of the occasionally observed hinge was found 35 nm from the near edge of the heads [Hirokawa et al., 1989]. Next, using antibodies with epitopes for the light chain, kinesin molecules were observed decorated with either of the two antibodies, termed L1 or L2. The antibodies were clearly shown, through electron microscopy, to bind to the fan-shaped tail region. When the antibodies with epitopes to the heavy chains were bound to kinesin, the head regions appeared unusually large and globular. Thus the light chains were thought to comprise the fan-shaped tail region while the heavy chains were thought to comprise the globular head region [Hirokawa et al., 1989] (see Fig. I-3). Upon observing, by electron microscopy, the kinesin molecule bound to microtubules, it was further determined that kinesin, using its globular head regions, bound to microtubules [Hirokawa et al., 1989]. Investigators visualized the globular head regions to be close to the microtubules while the fan-shaped tail regions were further away.

ii) Enzymatic Activity

It was determined that axonal transport is dependent upon ATP to provide the necessary energy for organelle movement [Grafstein and Forman, 1980]. Upon the isolation of kinesin, it was found that kinesin is a microtubule-activated ATPase [Vale et al., 1985a]. On its own, however, kinesin's ATPase activity was determined to be low. A hydrolysis value of 0.06 – 0.08 umol ATP/ min•mg of kinesin was reported in one case; however upon the addition of purified microtubules, the ATPase activity was seen to increase to 2.1 [Kuznetsov and Gelfand, 1986]. Upon kinetic analysis of kinesin's ATPase activity,

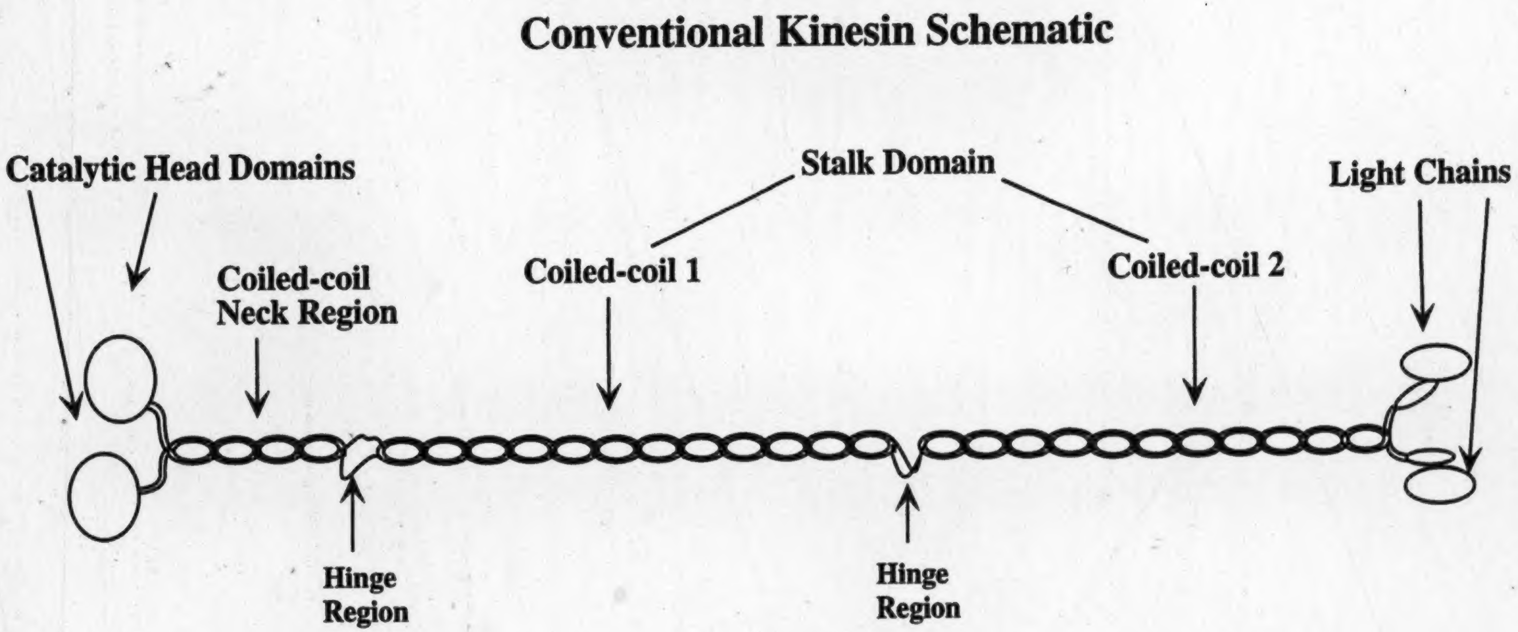

Conventional Kinesin Schematic

Catalytic Head Domains
Coiled-coil Neck Region
Stalk Domain
Coiled-coil 1
Coiled-coil 2
Light Chains
Hinge Region
Hinge Region

Fig. I-3. A schematic of conventional dimeric kinesin. The overall structure was determined by electron microscopy [Hirokawa et al., 1989]. The catalytic head domain crystal structure was solved [Kull et al., 1996; Sacks et al., 1997] to high resolution. The stalk domain's ability to form a coiled-coil in solution was shown [de Cuevas et al., 1992], prior to the neck region's ability to form a coiled-coil [Morri et al., 1997; Tripet et al., 1997]. Conventional kinesin's catalytic subunits are found at the N-terminus and exhibit microtubule-activated ATPase activity. The high resolution structure of the light chains has not been solved to date.

it was found that kinesin's Km for ATP decreased when microtubules were introduced [Kuznetsov and Gelfand, 1986]. The rate-limiting step in the cycle of ATP hydrolysis by myosin and dynein is the dissociation of the products of hydrolysis. The mechanism of kinesin stimulation, however, differs from that of myosin and dynein and so during this initial characterization of kinesin's ATPase activity, it was thought that the rate-limiting step of the mechanochemical cycle of kinesin was the hydrolysis of ATP itself [Kuznetsov and Gelfand, 1986]. Thus, the lower concentration of ATP required for kinesin to reach Vmax/2 implies that binding of the protein to microtubules increases its affinity for ATP. There seems to exist a type of communication between the nucleotide-binding pocket of kinesin and the microtubule-binding domain. In 1988, evidence was put forward for ADP dissociation as the rate-limiting step for kinesin ATPase activity. It was also observed that ADP dissociation was increased through the binding of microtubules [Hackney, 1988; Sadu and Taylor, 1992]. Similar to myosin, kinesin must cycle through bound and unbound states between itself and its polymer, i.e. microtubules. Perhaps conformational changes in the microtubules binding site can be relayed to the nucleotide-binding site to enhance kinesin's catalytic efficiency, ATP binding, or dissociation of hydrolysis products. Kinesin's microtubule activated ATPase activity was confirmed by other researchers [Cohn et al., 1987; Penningroth et al., 1987; William et al., 1988]. Furthermore, through demonstrating how both ATP hydrolysis and kinesin's microtubule translocating ability were sensitive to the same inhibitors, it was shown that both activities were coupled [Cohn et al., 1987]. Lastly, the requirement of Mg^{+2} ions equimolar to ATP for enzymatic activity was also shown [Cohn et al., 1987]. Mg-free ATP behaved as a competitive inhibitor and quenched ATPase activity.

Through the use of [α–^{32}P] labeled ATP, investigators were able to determine that the heavy chain was responsible for binding ATP [Penningroth et al., 1987]. Also, through the development of monoclonal antibodies to kinesin's heavy chain, Ingold et al. (1988) were able to inhibit kinesin's microtubule mobility, presumably through antibody binding and blocking of the microtubule binding site on the protein's heavy chain subunits. Interestingly, inhibition of microtubule binding through antibody binding to the catalytic domains led to the stimulation of kinesin's ATPase activity [Ingold et al., 1988]. This finding further supports the idea that a binding interaction at the microtubule binding site may transmit a change to the nucleotide binding environment through side-chain interactions in kinesin's catalytic core. Evidence to further the idea that the heavy chain subunit was responsible for ATPase activity and microtubule binding was found when examiners isolated a 45Kda fragment from the kinesin heavy chain with ATPase and microtubule binding abilities [Kuznetsov et al., 1989]. This fragment was unable to support translocation on microtubules and was seen to have an enhanced ATPase activity. It was postulated that somehow the uncoupling of the ATPase and translocating activities might activate the ATPase [Kuznetsov et al., 1989].

Concomitant to kinesin's isolation, peculiarities in its behavior were noticed. Indeed, its unique behavior enabled its isolation. Immediately upon characterization of its activity, kinesin was compared to myosin and dynein, two mechanochemical motors. Kinesin formed a strong complex with microtubules when presented with a non-hydrolyzable ATP analogue [Lasek and Brady, 1985]. Kinesin's mechanochemical cycle seemed to differ from that of myosin and dynein, and was investigated using ATP analogues and inhibitors of ATPase activity. Intermediate states in kinesin's hydrolysis cycle were prolonged and kinesin's affinity for microtubules was assessed [Romberg and Vale, 1993]. The results show that when in the ATP or ADP•P bound state, kinesin will adhere to a microtubule, while myosin's affinity for F-actin is weak in these nucleotide bound states. Further, kinesin-ADP was discovered to dissociate from microtubules while myosin-ADP will form rigour complexes with F-actin (rigour complexes is a term coined to describe the strong binding associations between the myosin and F-actin proteins in the completely ATP depleted state) [Romberg and Vale, 1993].

It has been noted that the binding of ATP to kinesin is associated with a conformational change in its structure [Sadu and Taylor, 1992]. -A conformational change has also measured for the binding of ATP to myosin or dynein [Taylor, 1992; Holzbaur and Johnson 1986]. Myosin and dynein dissociate their respective polymers upon ATP binding, while kinesin does not. The question that remained to be answered was how kinesin utilized its conformational change upon ATP binding. Could it be stored for use later or is ATP binding directly coupled to mechanical work?

iii) Mechanochemical Motor Domain

Early on, investigators began comparing kinesin to myosin and dynein, but were these comparisons warranted? All three seem to transduce chemical energy to mechanical motion and each interacts with a filamentous protein structure. Upon solving the crystal structure for kinesin's catalytic core in 1996, comparisons between kinesin and myosin were seen to be justified since seven of the eight β-strands, and all six major helices of the kinesin motor domain, were seen to overlap with corresponding structural elements in myosin with a root mean squared deviation of 3.5Å [Kull et al., 1996]. Upon analysis of the molecule, a core of eight-stranded mostly-parallel β-sheet, flanked on either side by three α-helices, was seen. This first crystal structure was solved with Mg•ADP in the nucleotide binding pocket [Kull et al., 1996].

The structural similarity between kinesin's core and myosin's was not foreseen. No sequence similarity between the proteins is notable, and the regions of sequence responsible for forming the secondary structural units of the catalytic cores in the two proteins are not found with the same topology within the two proteins. With different lengths, (kinesin's catalytic core~340aa's while myosin's~850aa's), different sequences, and different linear organization of the structural forming regions, the two proteins are still able to fold into tertiary structures that overlap [Kull et al., 1996].

Upon the availability of the crystal structure of rat brain kinesin [Sack et al., 1997], the comparisons to myosin became questionable. This rat brain crystal structure was more ordered at its N and C termini. The C-terminus was seen to form 2 β-strands, β9 and β10, with the latter being seen to interact with β7 in the core of the molecule. Following β10 there is an extended loop, L13, following loop13; begins α7, the coiled-coil of the neck-region. In this structure it was noted that the neck helix is not where one would expect it when compared to myosin's lever arm helix. Moreover, kinesin's neck helix ran in a different direction relative to the core domain, approximately at a right angle [Sack et al., 1997]. Investigators felt that the difference in the structural placement and orientation of the neck helix suggested that kinesin's mechanism of force generation was different from myosin's mechanism as well. Furthermore, they cite the difference between the kinetics of the two mechanochemical cycles of the two proteins. For example, while myosin spends most of its cycle dissociated from actin, and is non-processive, kinesin spends most of its cycle attached to microtubules and is capable of continued uni-directional motion. Also, kinesin is seen to function as a dimer while conventional myosin forms filamentous structures.

iv) Microtubule-based Movement

Although it has been postulated that kinesin moves to its successive microtubule binding sites in a hand-over-hand manner, how it achieves this has been a question researchers thought might be explained by the unraveling of the neck coiled-coil. Structurally, the dimer is too small to "walk" in 8nm steps along microtubules, yet it has been observed to make over 100 steps at 8nm per step without dissociating. Originally, the helix of the neck coiled-coil was thought to serve as a mechanical amplifier of ATP hydrolysis. However, evidence to date does not favor this idea. Rather, the ability of kinesin to reach its successive binding site is thought to be through the disorder-to-order transition of the neck linker region of kinesin, namely β9, β10 and L13, which precedes the neck coiled-coil [Rice et al., 1999]. Using paramagnetic resonance, fluorescence, and cryro-electron microscopy Rice et al. (1999) were able to show that there is a large structural change in the β9, β10 and L13 regions during the ATPase cycle of kinesin.

Though the hypothesis whereby the unwinding of the neck coil as the method used to reach each successive tubulin-binding site has fallen out of favour, the neck coiled-coil was specifically shown to help tether the molecule to tubulin through an electrostatic attraction with tubulin [Thorn et al., 2000]. Perturbation of the neck coiled-coil has also been shown to decrease the rate of the kinesin's movement [Romberg et al., 1998]. Lastly, it is essential for kinesin to be a dimer in order to move processively in a hand-over-hand manner along a microtubule and to enable it to approach rates of movement similar to fast axonal transport. The neck coiled-coil for kinesin has been shown to form in solution, while the coiled-coil of kinesin-like proteins is predicted to form by sequence similarity, but none have been explicitly shown [Tripet et al., 1997]. While the neck linker region sequence homology is conserved among kinesin-like proteins [Fletterick and Vale, 1997], the coiled-coil region, though seemingly present in the majority of identified sequences, does not appear to be as highly conserved.

4) *The kinesin superfamily*

Kinesins are known as molecular motors because they transduce the chemical energy of adenosine triphosphate (ATP) into mechanical motion and move in a processive manner. After the initial discovery of a kinesin from squid axonal extracts (Vale *et al.*, 1985a), many other kinesin-like proteins were discovered (Review: Miki *et al.*, 2001). This finding led to the organization of a new superfamily of kinesin-related proteins (Goodson *et al.*, 1994; Kim and Endow, 2000), and recently many of the related kinesin proteins found in different organisms have been grouped, categorized and placed into sub-families (Miki *et al.*, 2001). PCR techniques using primers for the catalytic domain were used to isolate novel motor regions. Interestingly, when the known sequences are aligned based on their catalytic motor regions, they are not only grouped by sequence similarity, they also tend to be grouped based on the spacial organization of the protein. This yielded three general classes of kinesin-like motor proteins, termed N-type, C-type and M-type, referring to the location of the catalytic head domains in the protein [Fletterick and Vale, 1997]. Furthermore, the sequence alignments of the motor domains grouped proteins with similar cellular functioning, and this led investigators to propose that a motor was fine-tuned to suit its biological functions. Though their biological specificity is thought to be dictated by the tail regions, it is felt that classification of all kinesin superfamily proteins based on tail regions could lead to the same groupings based on motor-head domain sequences. Thus, the protein molecules, though they contain three distinct domains, are not completely independent of each other. Each is suited specifically for its role in the transport process; thus each domain plays its role in generating an unique and highly specific transport protein [Fletterick and Vale, 1997]. For example, there are bipolar kinesin-like proteins that form tetramers through their α-helical stalk domains. Also, conventional kinesin is known to form a homodimer with its motor-stalk-containing domains, giving it two heads; not all kinesins reportedly function with two heads, since some apparently work as monomers. Further, not all kinesin-like proteins that form dimers with their motor-stalk domains form homodimers; some form heterodimers and have motor-stalk domains that are neither the same sequence nor the same length [Kim and Endow, 2000]. Also, each different type of kinesin-like protein is thought to carry a distinct set of membrane bound organelles or vesicles. This hypothesis is supported by the growing evidence that the types of cargo carried by a specific kinesin-like protein are unique to that protein [Review: Kamal and Goldstein, 2000; Review: Goldstein and Philp, 1999].

5) *Kif3 heterotrimeric motor protein: A kinesin-like protein*

Conventional kinesin has been shown to be composed of two heavy and two light chains [Bloom et al., 1988; Kuznetsov et al., 1988; Hirokawa et al., 1989]. The second protein in the kinesin superfamily of proteins to be completely characterized was found to be a heterotrimeric complex composed of two motor subunits with microtubule activated ATPase activity and an accessory protein [Wedaman et al., 1996]. This heterotrimeric protein was termed kinesin-II but is also called the Kif3 complex where Kif represents kinesin family [Yamazaki et al., 1996].

Cole et al. (1993) set out to sequence and characterize the subunits of the Kif3 complex, isolated from sea urchin. The 85kDa subunit was fully sequenced, and termed spKRP85 for *Strongylocentrotus purpuratus* **K**inesin **R**elated **P**rotein-85kDa. The heterotrimeric complex was shown to move in the anterograde direction on microtubules [Cole et al., 1993]. Kondo et al. (1994) reported a mouse analogue, Kif3A, for **Ki**nesin **F**amily. In 1995, Rashid et al. published the sequence of the 95kDa subunit found in sea urchin, followed by the sequence publication of Kif3B by Yamazaki et al., (1995). The accessory proteins in sea urchin and mouse were sequenced and reported in 1996 [Wedaman et al., 1996; Yamazaki et al., 1996]. These proteins have since been named KAPs for **K**inesin-like **A**ssociated **P**roteins.

Upon analysis of the spKRP85/95 and Kif3A/B motor subunits, it was noted that the N-terminal regions (approximately residues 1-350) were likely to comprise a motor domain similar to conventional kinesin, based on sequence homology. The N-terminal domains were predicted to be separated from the small globular C-terminal domains by a central α-helical segment thought to form a coiled-coil similar to the one shown for conventional kinesin [de Cuevas et al., 1992]. A similar stalk-like structure as seen for conventional kinesin was noted for the Kif3A/B complex in electron micrographs [Yamazaki et al., 1995].

From sequence analysis, it appeared that spKRP85 and Kif3A were orthologues, having a 73% homology along their full lengths; it was predicted that spKRP95 would be the orthologue to Kif3B [Rashid et al., 1995]. It is interesting to note that while spKRP85 has 699 amino acids, Kif3A is comprised of 701, while both spKRP95 and Kif3B were originally reported to have 742 amino acids, with the extra residues found at the C-termini [Rashid et al., 1995; Yamazaki et al., 1995].

Within the same organism, spKRP85 was found to have 52% identity with the full-length spKRP95, and 73% within the motor region. Kif3A and Kif3B were found to have 47% identity along their full length and 61% in their motor regions. Interestingly, in the similarity profiles between spKRP85/Kif3A and spKRP95/Kif3B, a short region of sequence between the proteins was found to have strikingly low homology. This region was found located in the predicted coiled-coil stalk domain, but indicated low probability for α-helix formation [Cole et al., 1993; Rashid et al., 1995; Yamazaki et al., 1995]. When these regions were further scrutinized, it was noted that spKRP85/Kif3A had a stretch of amino acids that were comprised of a number of negatively charged amino acids closely spaced side-by-side (11 and 13 for spKRP85 and Kif3A, respectively). This negatively charged segment was followed by a segment of positively charged amino acids (9 for both proteins). This region of sequence disparity in spKRP95/Kif3B, was found to begin with a stretch of positively charged amino acids (8 in each protein) and is followed by a segment of negatively charged amino acids (11 and 14 for spKRP95 and Kif3B, respectively) (see Fig. I-4).

It was postulated that these complementary charged regions could help the motor subunits form spKRP85/95 and Kif3A/B heterodimers through the destabilization of homodimers, and stabilization of heterodimers through electrostatic attractions [Rashid et al., 1995]. It was also noted that non-ideal and charged residues were located in the stalk region's **a** and **d** positions [Rashid et al., 1995]. The **a** and **d** positions are classically

Schematic of the heterotrimeric Kif3 Motor Protein

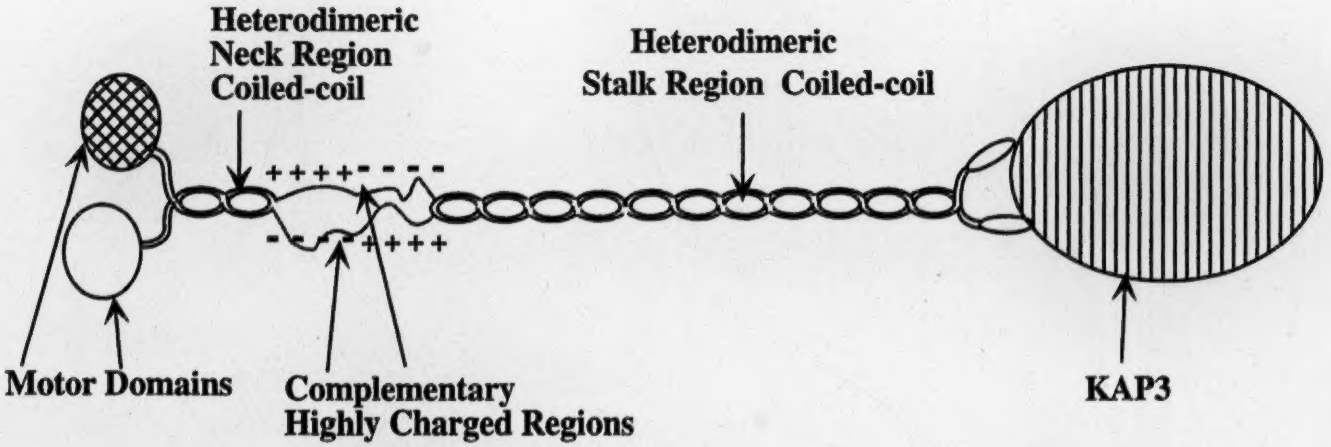
Heterodimeric
Neck Region
Coiled-coil
Heterodimeric
Stalk Region Coiled-coil
+ + + + - - - -
- - - - + + + +
Motor Domains
Complementary
Highly Charged Regions
KAP3

Fig. I-4. A schematic of the kinesin-like heterotrimeric motor protein (Kif3A/Kif3B/KAP3). This protein consists of two different polypeptide chains, Kif3A and Kif3B, which resemble conventional kinesin heavy chains. Each polypeptide chain contains an N-terminal globular motor domain, followed by a potential neck coiled-coil region a highly charged hinge region, a coiled-coil stalk region and the C-terminal tail region (which binds to an accessory unit, the kinesin-like associated protein KAP3).

reserved for hydrophobic residues in a coiled-coil, [Hodges et al., 1972] and it was predicted that the formation of heterodimers would prevent electrostatic repulsions at the hydrophobic core of the coiled-coil stalk [Rashid et al., 1995]. This hypothesis has been bolstered by the recent findings of De Marco et al. (2001).

Investigations of the Kif3 complex found in sea urchins led to observations of the Kif3 complex bringing condensed chromosomes to the metaphasic plate during mitosis, as well as new membrane to the cleavage furrow during cytokinesis [Morris and Scholey, 1997]. In *Caenorhabditis elegans* and *Chlamydomonas*, the Kif3 complex was found to be important in maintaining sensory neurocilia and the flagella, respectively [Cole et al., 1998], and it has been located in the photoreceptor rod cells in fish retina [Beech et al., 1996; Muresan et al., 1999]. Lastly, the Kif3A complex has been shown to be involved in the left-right asymmetry determination during embryonic development and mutations in the gene are thought to lead to *situs inversus* or the misplacing of internal organs in mammals [Marszalek et al., 1999; Takeda et al., 1999].

II. Coiled-coils

1) *Hydrophobic repeat*

The rod shaped region observed by electron microscopy in kinesin [Hirokawa et al., 1989] and the Kif3 heterodimeric complex [Hiroto et al., 1995] were thought to be long α-helical regions that were predicted to form coiled-coils. These predictions were verified by CD analysis of conventional kinesin [de Cuevas et al., 1992; Tripet et al., 1997]. The coiled-coil motif is typically comprised of two parallel α-helix forming polypeptide chains. Coiled-coils were predicted to form in the stalk regions because the sequences were noted to have the characteristic hydrophobic repeat. The regular 3-4 spacing of the hydrophobic residues will lead to the formation of an amphipathic helix, and can be characterized by a seven-residue (heptad) repeat designated **abcdefg,** where positions **a** and **d** contain hydrophobic residues. The 3-4 hydrophobic repeat (HXXHXXXHXXH.... where H is a hydrophobic residue) ensures that there is a strip of hydrophobes along one side of the helix (see Fig. I-5). A characteristic of α-helices that contributes to their ability to form a coiled-coil is the fact that there are 3.6 residues per each full turn. This non-integral number of residues per turn, prevents the stacking of hydrophobic residues throughout the length of the sequence. Instead, the hydrophobes shift around the circumference of the helix such that the hydrophobic residues snake around the helix. Thus, the hydrophobic strip winds its way down the helix from the N-terminus to the C-terminus.

A coiled-coil is a dimer formed through the association of two amphipathic helices, and they associate through the burial of their hydrophobic residues away from their surrounding aqueous environment (see Fig. I-6A). As a consequence of the hydrophobes coiling around the helical structure, the individual helices accomplish the burial of their hydrophobes through coiling about each other. Thus, the separate α-helices, which can be seen as coils, twist about each other to form a coiled-coil. Hence, the main need for formation of coiled-coils is the correct periodicity of hydrophobic and hydrophilic residues, which will control the type of secondary structure present in order to maximize the burial of hydrophobic side chains in the core of the protein [DeGrado et al., 1989; Kaiser & Kezdy, 1983; Kamtekar et al., 1993; Xiong et al., 1995]. The 3-4 hydrophobic repeat (HXXHXXXHXXH.... where H is a hydrophobic residue) was experimentally demonstrated in the 284-residue coiled-coil tropomyosin, in which 71 of 82 **a** and **d** positions contained hydrophobic residues [Hodges et al., 1972]. Extensive studies on the role of the **a** and **d** positions in coiled-coil folding and stability have been reviewed [Adamson et al., 1993; Betz et al., 1995; Cohen & Parry, 1994; Hodges, 1992, 1996; Kohn & Hodges, 1998]; also see Tripet et al., (2000) and Wagschal et al., 1999).

Not only is the presence of a hydrophobic residue important in either of the hydrophobic positions, the amino acid's side-chain structure is also deemed important. For example, though the aromatic ring of phenylalanine and the indole ring of tryptophan are hydrophobic, they are not the best side-chains because of their large size. In fact β-branched amino acids have been shown to prefer the first, or **a** position [Zhou et al., 1992; Wagschal et al., 1999], while leucine is preferred in the **d** position [Harbury et al., 1993; Tripet et al., 2000]. Thus, not only is hydrophobicity important for stable coiled-coil formation, the side-chain packing is also of importance, (Fig. I-6B). The fact that the **a** and **d** positions do not contribute equally to stability and that they are indeed not equivalent was shown in the elegant experiments of Zhou et al., (1992a,b, 1993) and through analysis of the GCN4 coiled-coil X-ray crystal structure [O'Shea et al., 1991]. Comparison of the crystal structures of coiled-coils has revealed two distinct types of packing arrangements at the **a** and **d** positions of two-stranded coiled-coils. In the case of the **a** position, the C^{α}-C^{β} vector projects out of the interior of the core roughly parallel to the C^{α}-C^{β} vector, and thus is termed "parallel packing". In contrast, at a **d** position, the C^{α}-C^{β} vector projects, roughly, perpendicular to the C^{α}-C^{β} vector, and thus is termed "perpendicular packing". As a result of these steric differences, differences in the

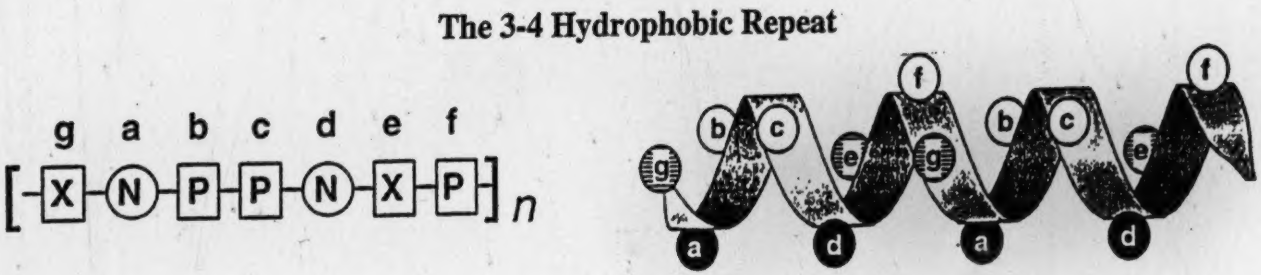

Fig. I-5. The pattern of polar (P) and nonpolar (N) amino acid residues that promotes α-helical secondary structure. Open balls represent polar side-chains, closed balls represent nonpolar side chains and hatched balls represent side-chains that could be polar or nonpolar. In an amphipathic α-helix, the **[g-a-b-c-d-e-f]**$_n$ nomenclature is used to label the various positions of the seven-residue sequence repeat. Placement of hydrophobic residues only at positions **a** and **d** leads to the so-called 3-4 (or 4-3) hydrophobic repeat, in which the spacing between hydrophobes is three (**d** is three positions down from **a**) followed by four (**a** is four positions down from **d**). The **e** and **g** positions (hatched balls) are able to contribute to either the polar or nonpolar face of the helix and may contain polar or nonpolar residues.

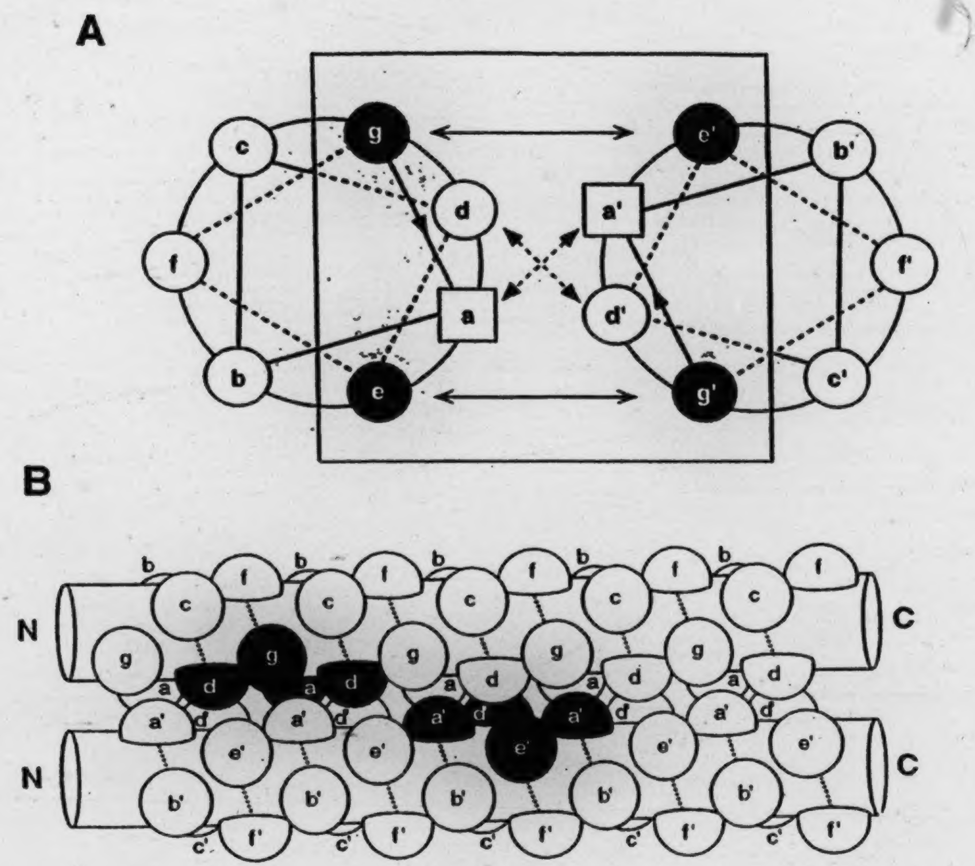

Fig. I-6. Schematic illustrations of a parallel two-stranded α-helical coiled-coil. In **(A)** the coiled-coil is viewed in a cross-sectional helical-wheel representation where the direction of polypeptide chain propagation is into the page from N to C terminus. Interchain **a-a′** and **d-d′** (prime indicating a position on the other helix) van der Waals packing interactions between side-chains in the hydrophobic core are depicted with arrows. Potential interhelical interactions between residues at position **g** of one helix and position **e′** of the other helix are also depicted with arrows. Residues that make up the entire dimerization interface are included in the box. In **(B)**, the coiled-coil is viewed from the side. N and C refer to the N and C termini, respectively. The "knobs into holes" packing at the dimer interface is depicted. For example, the side-chain at position **a′** packs into the hole between four residues on the upper helix. Similarly, a side-chain at position **d** packs into the hole between four residues on the lower helix.

frequency of occurrence, and contribution to coiled-coil stability of certain residues, has been ascribed to their ability to pack better in each of these positions.

2) *Hydrogen bonding associations*

The more tightly the side-chains can pack together in the hydrophobic core, the better able they will be to exclude water. The exclusion of water is important for the α-helical backbone so that H-bonding associations with the peptide backbone will be maintained. The better able a peptide backbone is at forming H-bonding associations, which favor an α-helical structure, the greater the likelihood of helix formation. It has been noted that, statistically, certain amino acids are found more often in helical structures than other secondary structures [Chou & Fasman, 1978; Munoz & Serrano, 1994]. These α-helix-favoring residues are thought to have a helical propensity, and the more of them found in a sequence, the greater the likelihood that sequence will form an α-helix. The thermodynamic contributions of each amino acid, to an α-helical structure have also been assessed [Tripet et al., 2000; Wagschal et al., 1999; Zhou et al., 1994]. The side-chains of amino acids with high helical propensity must be able to adopt more easily the phi and psi angles required for helix formation; this may promote H-bonding associations within the backbone.

3) *Electrostatic interactions in coiled-coils*

Another force that can contribute to the stability of a coiled-coil is ionic attractions. Typically, electrostatic forces can be found to involve amino acid side chains on both polypeptides; this is known as an interchain interaction [Lavigne et al., 1996]. These interactions usually occur from a **g** position on one chain to the **e** position in the subsequent heptad of the partner chain. Often, a residue on the partner chain is denoted by its letter with a prime, so that in this case we would expect a g-e′ interaction or an i-i′+5 interaction. Another type of stabilizing electrostatic interaction occurs between charged residues on the same chain, known as intrachain electrostatic interaction. They have also been noted to affect coiled-coil stability, though not as greatly as interchain attractions [Zhou et al., 1992].

Nature has used the coiled-coil as a motif to bring proteins together such as the DNA binding transcription factors fos-jun or myc-max. Not only is the coiled-coil able to form a dimer, its dimer forming ability can be regulated. This can be seen for the jun transcription factor, found to form a jun-fos heterodimer preferentially as a result of the interchain electrostatic interactions between the **g** and **e′** positions of each transcription factor [O'Shea et al., 1989]. For the transcription factors myc and max, the formation of the max homodimers has been noted but, again, there is a preference for heterodimer formation, and this is again controlled through preferential electrostatic interactions, although in this instance the interaction occurs between residues found in the **a** and **d** positions [Lavigne et al., 1995].

III. Electrostatics

Electrostatic interactions are seen in protein-protein interactions throughout cell biological processes. Their contribution to protein folding remains a topic of study, and though they appear to contribute, to some extent, to stabilizing a protein's three-dimensional fold, their roles in orienting and directing proteins to increase successful interactions have been increasingly studied.

The amino acid make-up of proteins involved in macromolecular assemblies characterizes their associations by providing complementary surfaces for interacting macromolecules. Further, they are responsible for providing the binding strength to hold the macromolecule together. The twenty different amino acids, in addition to the structure of their side-chains, differ in their polarity and charge such that the twenty commonly occurring amino acids are composed of hydrophobic or non-polar, polar uncharged and charged side-chains.

In 1976, the preeminent force for the association of two macromolecules was considered to be the burial of hydrophobic surface area. Hydrogen bonding associations and salt-bridges (H-bonded ion pairs) were considered to provide very little in terms of binding energy, but were thought to provide specificity because the presence of unpaired charges and hydrogen bonding groups was thought unfavorable [Fersht, 1984, (Review); Hunenberger et al., 1999]. Elements involved in bringing two subunits or an enzyme-ligand together such as burial of hydrophobic residues, formations of H-bonding associations, and electrostatic interactions are the same forces that contribute to determining the specificity and stability of a protein's final 3-dimensional structure. Burial of hydrophobic residues and surface area is still considered to contribute greatly to protein folding [Creighton, 1990; Dill, 1990; Pace et al., 1996]. Not only is there a favorable interaction between hydrophobic side-chains through van der Waals associations but, unlike for charged side-chains, desolvation of hydrophobic side-chains also contributes to the free energy of the folded state.

Charged residues such as Glu, Asp, Arg, Lys, and His can participate in protein folding and recognition in two additional ways: either through forming H-bonding associations to form a salt-bridge or by the long range force of attraction, or repulsion termed electrostatic interaction.

Realisation of the contribution of H-bonding associations to stability seems to have emerged in the two decades following the late '70s [Creighton, 1990]. It has been suggested that, taking into account the unfavorable desolvation of the polar functional group involved, an individual H-bonding association could donate 0.6 kcal/mol to the stability of a folded protein. The major problem with H-bonding associations is that in order for them to be present in a protein structure, their polar components, the carboxyl oxygen and amide nitrogen atoms, must be desolvated. One way for polar functional groups participating in H-bonding associations to overcome their loss of solvation energy was shown to be through being partially solvent exposed or to participate in more than a single association. This way, the polar functional groups can either minimize their loss of solvation energy or maximize the number of H-bonding associations each functional group participates in to overcome the loss of solvation energy [Ben-Naim, 1991].

Proteins have been shown to be only marginally stable in solution, showing stabilities approximately just 5-10 kcal/mol when the buried hydrophobic surface would lead to predictions of values much greater [Privalov et al., 1988]. It has been noted that not all H-bonding associations for polar atoms in folded proteins are fulfilled and it has been suggested that the burial of polar residues in proteins counters the hydrophobic effect, thus explaining the discrepancy between theory and empirical evidence [Vogt et al., 1997].

These views seem to be supported by analyses of thermophilic proteins, which show a greater number of polar atoms on their surfaces and greater burial of nonpolar atoms compared to their mesophilic counterparts [Vogt et al., 1997]. Furthermore, the number of unsatisfied internal H-bonding associations in thermophiles was seen to be lower than for the mesophilic counterparts. Thus H-bonding associations can stabilize a protein given the functional groups involved can overcome the penalty of desolvation.

Whether charged amino acids forming a salt bridge in the core of a protein contributes to a protein's overall stability would be best determined by comparing the stability of the folded molecule to the stability of the unaltered protein when it is completely unfolded. However, this is not always the case when analyses are done experimentally. Experimental analyses have been conducted where pKa shifts of specific salt bridges have been measured. A particular example is the His30-Asp71 salt bridge in T4 lysozyme in which the experimental reference molecule, for pKa-shift experiments, would not be the unfolded protein, but rather it would be either a negatively or positively charged ion-pair-containing protein, depending on whether the pH of the solution was basic or acidic. Also, mutations have been used to discern the contribution of the His30-Asp71 ion-pair to T4 lysozyme's stability. The reference molecule for the mutations of His30 or Asp71 would be the mutant protein, which is less than ideal since structural relaxations may occur upon the introduction of a mutant side-chain [Anderson et al., 1990; Hendsch et al., 1994]. One type of analysis makes use of solved crystal structures of proteins and solves the electrostatic potential of buried salt bridges between themselves and between the salt bridges and the partial charges on the atoms of the protein using the Poisson-Boltzman equation. Such an analysis takes into account the free energy of desolvation, the free energy of coulombic interaction, and the free energy of interaction of the salt bridge with other protein atoms. The computational analysis bases its results on a reference state termed a hydrophobic isostere of the molecule. Essentially, it is the same molecule, with the same side-chain packing but the charge component of the salt-bridge is "turned off" [Hendsch & Tidor, 1994; Lounnas & Wade, 1997]. The findings indicate that, relative to their hydrophobic isosteres, salt bridges destabilize a protein. These calculation-based conclusions are mirrored in the experimental work on a DNA binding protein known as ARC repressor protein. Random mutagenesis of a salt-bridged triad led to the discovery of more stable mutants with hydrophobic residues replacing the charged amino acids. Functional mutants were crystallized to show that the hydrophobes replacing the charged triad had a similar packing interaction to the wild-type charged residues [Waldburger et al., 1995].

The formation of a salt-bridge is seen as the necessary consequence of desolvating charged polar groups [Ben-Naim, 1991]. The amount that H-bonding associations contribute to the free energy of folding is thought to vary due to the distance between charged or polar functional groups (hence the length of the H-bond) and the number of H-bonding associations that the charged or polar functional groups form [Creighton, 1990; Hendsch, 1994; Pappenberger et al., 1997]. Salt bridges tend to destablize proteins relative to their hydrophobic isosteres because the coulombic interaction between the charged atoms does not appear to counterbalance energetically their desolvation free energy [Hendsch & Tidor, 1994]. One way to have them contribute, favorably, to stabilizing a fold, is to ensure that they are more solvent exposed. This has been shown to be an effective way to increase the stability of the ubiquitin protein [Loladze et al., 1999]. Lastly, the charged atoms of a salt bridge can interact with the partial charges of the atoms in a protein, and this can increase the contribution of the salt bridge to a protein's free energy of folding. It has been estimated that partial charges up to 8 Å in distance, from a salt bridge interaction, can help stabilize that buried charged pair [Lounnas & Wade, 1997]. The desolvation penalty can be further reduced through protein-salt bridge contacts by the formation of a network of H-bonding associations between the salt bridge and other polar and charged groups in the protein. An example of a protein-charge electrostatic interaction leading to the stabilization of a two-stranded alpha-helical coiled can be seen between the charged side-chain of glutamic acid and the helix dipole [Kohn et al., 1997a].

The role for long-range electrostatic forces in protein folding and macromolecular association appears, generally, to lie in the realm of steering and orientating molecules prior to their specific binding through the meeting of hydrophobic surfaces. The current theory for the role of electrostatics also involves their interaction in the formation of an encounter complex, an unspecified number of loosely associated macromolecules. Again, this is formed prior to their formation of a tight, hydrophobically held complex [Camacho et al., 1999]. Empirical examples of charge controlled, enzyme-ligand, protein-protein, and protein-nucleic acid binding abound in the literature [(enzyme-ligand): Bagger & Wagner, 1998; Fischer et al., 1998; Radic et al., 1997; Soriano et al., 1998; Wade et al., 1998; Vijayakumar et al., 1998, (protein-protein): Kohn et al., 1995, O'Shea et al., 1989; Vaughan et al., 1999, (protein-nucleic Acid): Nadassy et al., 1999].

The Poisson-Boltzman equation, used to describe the interactions of charge species in solution, has been increasingly used to calculate electrostatic contributions to protein-protein recognition. Classical electrostatic theory of charged solutes in solution has made resurgence in the scientific literature [Review; Honig & Nicholls, 1995]. Early attempts at calculations treated proteins as solid spheres with a uniform charge distribution on their surfaces. However, with greater computational power available to investigators, solving the Poisson-Boltzman equation for charged solutes has led to the ability for analysis of charges on proteins at atomic resolution. Investigators can now more accurately assess the contribution of charged amino acids to protein recognition by assigning separate dielectric constants to the protein and solvent, through no longer treating the charged residues as if they were evenly distributed on a uniform spherical surface. This type of refined analysis takes into account the non-uniformity of protein surfaces such that a distinct placement of charged residues leads to the formation of microenvironments in terms of a protein's surface electrostatic potential.

Thus, long-range electrostatic interactions are thought to contribute to protein recognition through the non-uniform distribution of charged residues on a protein's surface [Honig & Nicholls, 1995]. For proteins with a net negative charge that interact with net negative ligands, there are thought, based on calculations of electrostatic potential, force fields steering the ligand, electrostatically, toward the microenvironment of the positively charged region in the active site.

CHAPTER II

MATERIALS AND METHODS

A. Materials

1. Chemicals and reagents

Unless otherwise stated, all chemicals and solvents used were analytical grade. Most of the chemicals used in this project are available from common sources, so suppliers are listed below generally only for uncommon chemicals as well as a few other selected reagents that were used (Table II.1). All solutions were prepared in water that was run through a Milligen Milli-Q deionization purification system. DIEA, DCM were distilled prior to use in peptide synthesis

Table II.1 List of reagents

Reagent	Supplers(s)
Amino Acids (protected for peptide synthesis	Advanced Chemtech, Louisville, KY Bachem, Torrance, CA Novabiochem, San Diego,CA
DCM	BDH Inc., Toronto, ON
DIEA	Caledon Laboratories, Georgetown, ON
DMF	General Intermediates of Canada, ON
GdnHCl (ultra pure)	ICN Biomedicals Inc., Aurora, OH
HF	Matheson Gas Products, Edmonton, AB
HBTU	Advanced Chemtech, Louisville, KY Novabiochem, San Diego, CA
HOBt	Advanced Chemtech, Louisville, KY
MBHA resin	Bachem, Torrance, CA
NMP	General Intermediates of Canada, Edmonton, AB
TFA	General Intermediates of Canada, Edmonton, AB
TFE	Aldrich Chemical Co., Milwaukee WI
Urea (ultra pure)	Life Technologies Inc., Gaithersburg, MD

B. Methods

1.Peptide synthesis

Peptide synthesis can be performed by two general types of procedures: the classical solution-phase method and solid-phase peptide synthesis (SPPS), based upon the method developed by Merrifield (1963). In SPPS, the growing peptide chain is attached to an insoluble matrix (polymeric resin bead), which allows easy washing away of excess reagents and reaction by-products at each synthesis step. SPPS is convenient for most peptide synthesis because of its efficiency, speed, and successful automation. Solution-phase synthesis is still used, however, in large-scale synthesis and specialized applications. Some good general references for solid-phase synthesis include Bodansky, (1988), Fields, (1997), Novabiochem, (2000), and Stewart & Young, (1984).

A general outline of the SPPS procedure is given in Figures II-1 and 2. Peptide synthesis is always carried out in the C- to N-terminal direction through the activation of the incoming amino acid's carbonyl group; made electron deficient through various techniques.

Normally, the four major steps in SPPS consist of: anchoring, deprotection, coupling, and cleavage (release). The added steps of acetylation and neutralization can be used to terminate any α-amino groups that remain unreacted after the coupling (amide bond formation) step, and neutralize any remaining acid from the deprotection step with the added bonus of abstracting a proton from the free amino groups, thereby making them more electronegative or electron rich. Typically, the amino acids used in SPPS must be derivatized at the N^{α} group as well as at any reactive side-chain functionalities to prevent side reactions during formation of the peptide bond. The methodology used for deprotection, neutralization, coupling, and acetylation was a modified procedure taken from Ball et al. (1996). The typical cycle of reactions used to elongate the peptide, bound to a solid support, was deprotection, neutralization, coupling, and acetylation.

A. Anchoring

Anchoring consists of placing the first amino acid onto the resin linker, typically a functional group such as an amine capable of forming an amide bond. The resin comes with a specific maximum level of substitution, i.e., the number of free amine groups per dry gram weight of resin. For longer peptides it is desirable to use a lower substitution and this can be done either manually, by reacting the resin with activated amino acid for a short period of time and then acetylating the unreacted free amino groups on the resin, or by purchasing a lower substitution resin. The peptides in the current study were all synthesized with a C-terminal amide, which required the use of a linker that presents an amino moiety that can be directly reacted (coupled) with the carboxylate group of the first amino acid to form an amide bond. Figure II-1, bottom panel, depicts anchoring of the first amino acid.

The synthetic peptides used in these studies were prepared by manual solid-phase synthesis methodology (Merrifield, 1997; Serada et al., 1993) using a 4-methylbenzylhydrylamine (MBHA) hydrochloride resin with conventional N-t-butyloxycarbonyl chemistry. The peptides were prepared at a 0.25 millimole scale and 0.5g of MBHA resin with a substitution of 0.5mmol/g was used for each peptide.

B. Deprotection

Deprotection of our newly added amino acid is required at its α-amino group. As stated above, the amino acids used were N^{α}-derivatized with a t-butyloxycarbonyl group

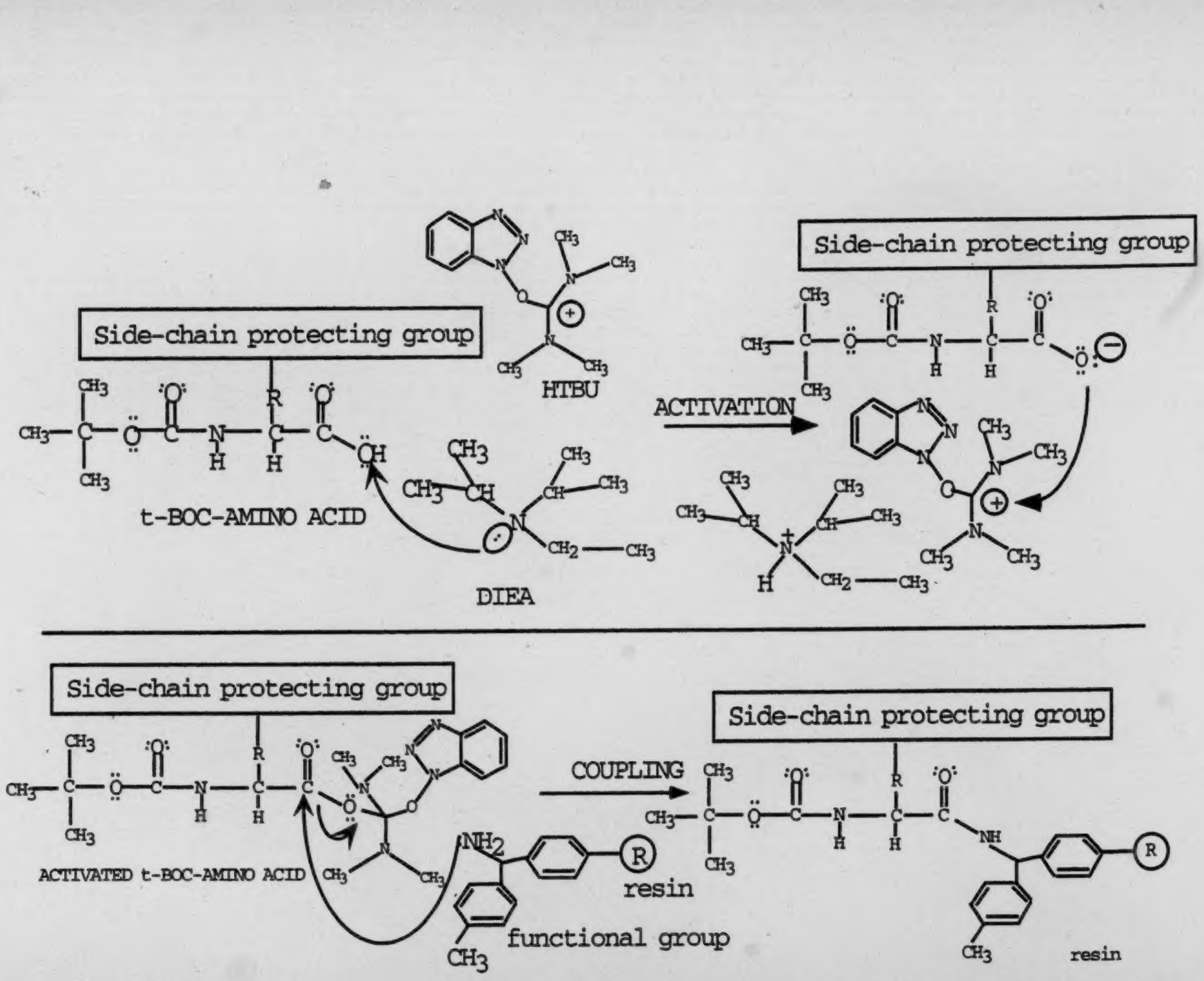
Side-chain protecting group
t-BOC-AMINO ACID
HTBU
DIEA
ACTIVATION
Side-chain protecting group
Side-chain protecting group
ACTIVATED t-BOC-AMINO ACID
COUPLING
resin
functional group
Side-chain protecting group
resin

Figure II-1. The top panel shows the activation of an Nα-protected amino acid with 2-(1H-benzotriazole-1-yl)-1,1,3,3-tetramethyluronium (HBTU). The activation is initiated through the addition of the tertiary amine, N,N isoproplyethylamine (DIEA). The bottom panel shows an activated amino acid being added to the functional linker moiety of 4-methylbenzhydrylamine(MBHA) resin. The linker group in this case is an amine that is a nucleophile, which displaces the activating group HBTU in an SN2 style reaction. The product is a protected amino acid linked to the resin through an amide bond.

and, thus, in preparation for addition of another amino acid to our growing peptide chain, we removed the t-Boc group through rinsing with a 7mL, 90% trifluoroacetic acid (TFA) in dichloromethane (DCM). The peptide was allowed to stand for one min. in the rise mixture before the mixture was flushed. This was followed by 5 min. of shaking the peptide-resin in another 7mL of 90% TFA in DCM. The t-Boc group is acid labile and it was found to be readily removed in mixtures of TFA/DCM ranging from 50-90% although the reaction time was increased to 25 min. at 50% TFA. Fig. II-2 depicts deprotection.

C. Neutralization

Neutralization was carried out prior to the addition of an amino acid. This step will lead to the removal of a proton from the now free amino groups, giving the neutral NH_2-peptide species instead of the NH_3^+-peptide species. This step aids the next coupling step by creating a more electron rich, nucleophilic amino group, thus enhancing the amide bond forming reaction. We chose to neutralize the peptide-resin with 3 washes with 5% diisopropylethanolamine (DIEA) in DCM (7mL). To prepare the peptide resin for the addition of the next amino acid (coupling), we followed our neutralization step with 3 separate washes, using 7mL each time, of DCM, 3 washes of dimethylformamide (DMF), and 3 washes with N-methylmorpholine (NMP) for a total of 21mL for each solvent. The peptide-resin was now ready to have activated amino acid added. We chose NMP as the coupling solvent for its resin swelling properties, thereby making the amino groups of the attached peptide more accessible to the added reagents. We also chose this reagent because its polar character facilitates the formation of the activated ester moiety

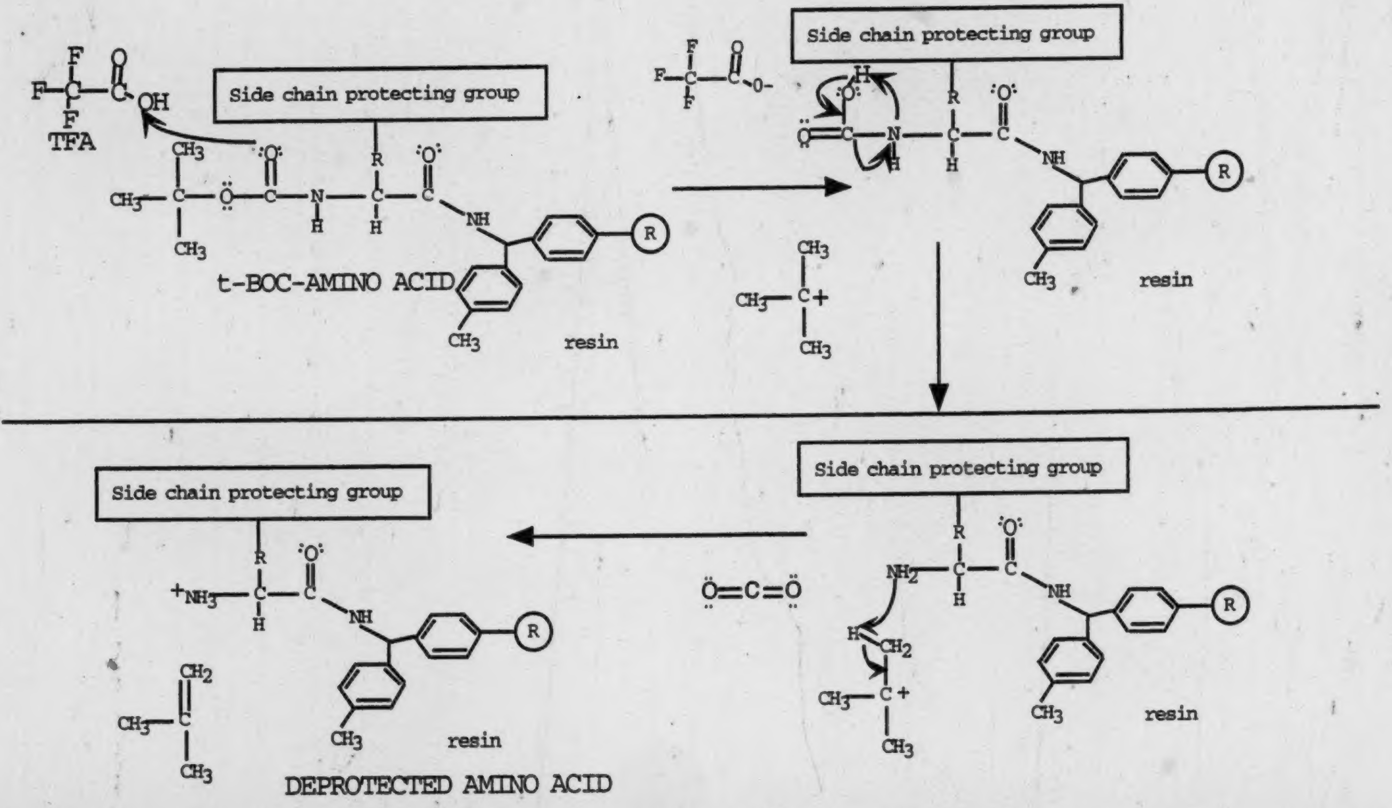
TFA
Side chain protecting group
t-BOC-AMINO ACID
resin
Side chain protecting group
resin
Side chain protecting group
resin
Side chain protecting group
resin
DEPROTECTED AMINO ACID

Figure II-2. From top left to right, the Na-protected amino acid with a side-chain protecting group, undergoes the acidolysis of its Na-protecting group, tert-butyloxycarbonyl. The organic acid trifluoracetic acid donates its proton to the carbonyl oxygen of the protecting group leading to the stable tert-butyl carbocation and N-terminally carbamylated amino acid. This decomposes through the production of carbon dioxide to give a freely exposed amino group (bottom right). Further b-elimination in the tert-butyl carbocation leads to the stable 2-methly-propene side-product.

utilized for the addition of the next amino acid to the growing peptide chain; see coupling below.

D. Coupling

Coupling of the amino acid to the growing peptide chain was done through the addition of coupling reagents that make the carbonyl carbon of the amino acid more electropositive. The coupling reagents of choice were 2-(1H-benzotriazole-1-yl)-1,1,3,3-tetramethyluronium hexafluorophosphate (HBTU) and 1-hydroxy-benzotriazole (HOBT). The peptides were synthesized from the C-terminus to the N-terminus; hence the free amino group would be located on the growing peptide, bound to the resin. The next amino acid was added to the growing peptide chain by activating the incoming amino acid's carbonyl group. The coupling reaction contained 1.0mmol of amino acid, giving a 4X excess of amino acid to free amino group on the resin. Amino acids were activated in a 2.0mL solution of 0.45M HBTU/HOBT in DMF plus 0.5mL of a 4:1 mixture of DIEA/NMP giving a final volume of 2.5mL. The amino acids were allowed to activate and form an activated ester moiety at room temperature for 5 minutes before introducing them to the resin for coupling. Fig. II-1, top panel, depicts amino acid activation; the bottom panel depicts the activated ester moiety. After activation the amino acid was added to the resin, where coupling time was generally kept at1h, during which the reaction vessels were placed on a shaker. Afterwards, the coupling mixture was drained from the reaction vessels and the resin was washed 3X with DCM. After each coupling step, the extent of each coupling was qualitatively determined by conducting a Kaiser test (Fontenot et al., 1991), where the reagents turn blue in the presence of free amines. The extent of the coupling reaction was determined by comparing the degree of yellow (negative, meaning no free amines) between our resin and a blank with no added resin. Any unreacted amino groups were capped by acetylation.

E. Acetylation

Acetylation was used to terminate any unreacted amino groups from our coupling step. The peptide-resin was mixed with 2.0mL of 50:50 DCM:DMF to which 50μL of each of acetic anhydride and DIEA were added. The reaction vessel was allowed to shake for 5 min. to "cap" any unreacted amino groups. Acetylation was also carried out to aid in the purification of the final peptide since it is easier to purify truncated peptides away rather than longer deletion peptides that would be very similar to our desired peptide. After shaking, the acetic anhydride was drained from the reaction vessels and the peptide resin was washed 3X with DCM, 1 alternating wash of DMF, DCM, then DMF, and finally 3X with DCM. After this wash, the peptide-resin was ready to undergo another cycle of deprotection, neutralization, coupling and acetylation until the final amino acid was added. After the final amino acid was added, the peptide was subjected to another deprotection step followed by an acetylation to give a peptide with an N^{α}-acetyl group.

F. Cleavage

After the addition of the last amino acid and the final acetylation, the peptide was released (cleaved) from its solid support using a Low TFMSA – High HF procedure. 100mg of peptide-resin was placed in a 50mL round bottom flask containing a micro-stirbar. The reaction flask was cooled to –5°C. The following chemicals were added in order: 100μL of m-cresol, 300μL of DMS, 500μL of TFA, and 100μL of TFMSA. The mixture was allowed to stir at –5°C for 3 h. Next, the contents of the flask, were transferred to a fritted glass funnel of medium porosity. The peptide-resin was washed 3X with cold diethyl-ether and dried under vacuum suction to remove any residual ether. The dried solid was transfer to a clean HF flask containing a micro-stirbar. To the HF flask containing the dried peptide-resin, 100µL of anisole, 100µL of DMS, and 20µL of p-thiocresol was added, followed by 10mL of HF. The mixture was stirred and kept at –4°C using an ice-salt-water slurry for 1.5 h. The HF was removed under vacuum and cold ether was used to transfer the contents to a fritted glass funnel of medium porosity and a further 3 washes with cold ether were carried out. The ether was stored, and the peptide was dissolved and extracted from the glass frit using a 50:50 mixture of acetonitrile:water containing 0.05% TFA which was subsequently lyophilized. The crude peptide that results from the cleavage is depicted in Fig. II-3.

2. *Peptide purification*

Purification of each peptide was performed by reversed-phase high-performance liquid chromatography on a Varian 5000 (Varian, Walnut Creek, CA) using a Brownlee Aquapore RP-300 C_8 column (250 X 7.0 mm. inner diameter, 7.0µm particle size, 300-Å pore size) with a linear AB gradient (ranging from 0.2% to 1.0% B/min) at a flow rate of 2mL/min, where solvent A is aqueous 0.1% trifluoroacetic acid and solvent B is 0.1% trifluoroacetic acid in acetronitrile. The column was kept at 80°C throughout the duration of the purification using a column heater. A typical purification increased the acetonitrile concentration at 1%B/min. for 10 min, followed by a less steep gradient of 0.25%B/min. for the duration of the purification. Fractions were analysed for purity by electrospray

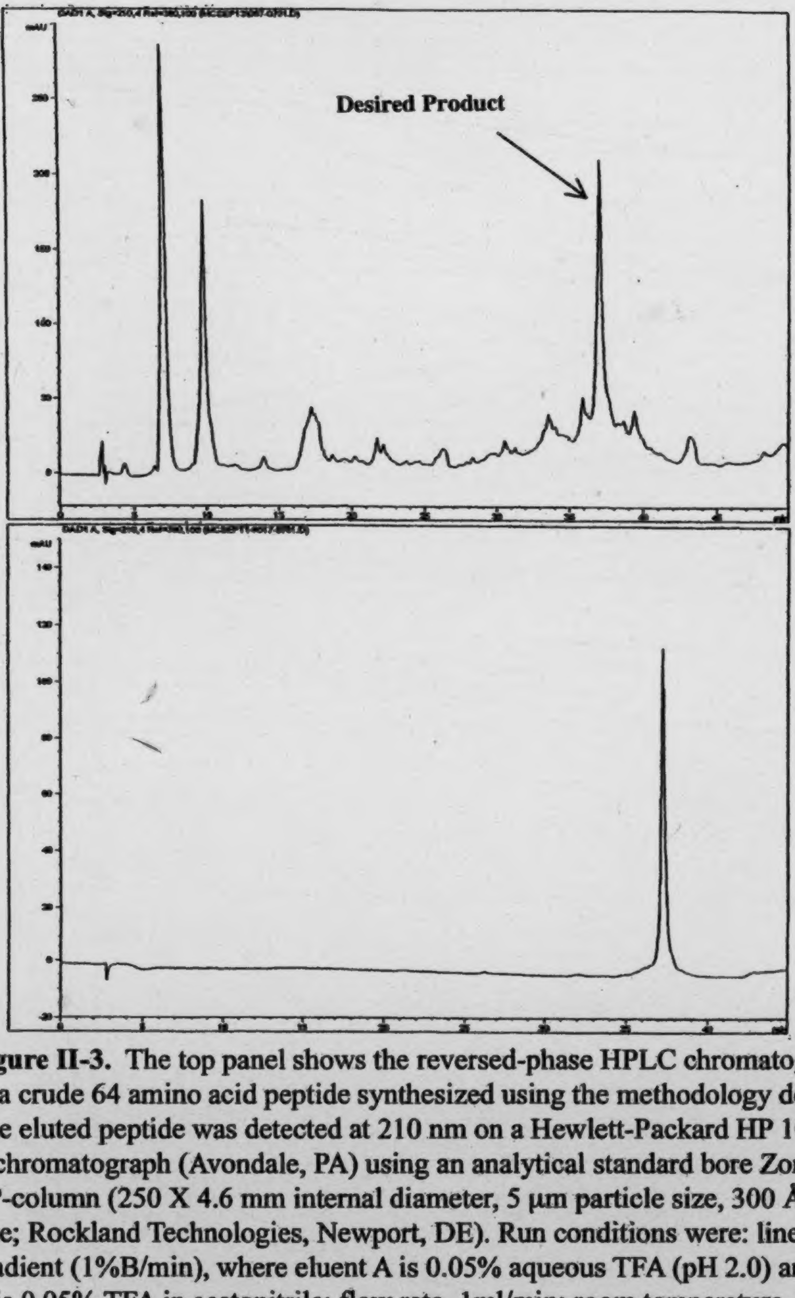

Figure II-3. The top panel shows the reversed-phase HPLC chromatograph of a crude 64 amino acid peptide synthesized using the methodology described. The eluted peptide was detected at 210 nm on a Hewlett-Packard HP 1090 Series II chromatograph (Avondale, PA) using an analytical standard bore Zorbax C8 RP-column (250 X 4.6 mm internal diameter, 5 µm particle size, 300 Å pore size; Rockland Technologies, Newport, DE). Run conditions were: linear AB gradient (1%B/min), where eluent A is 0.05% aqueous TFA (pH 2.0) and eluent B is 0.05% TFA in acetonitrile; flow rate, 1ml/min; room temperature. The bottom panel shows a purified fraction used for experimentation and secondary structure determination. The sequence of the peptide is CGGKDALLRQFQKEIEELKKKL EEGEEVSGSKISGSEEDDEEGELGEDGEKRKKRRDQAGKKV.

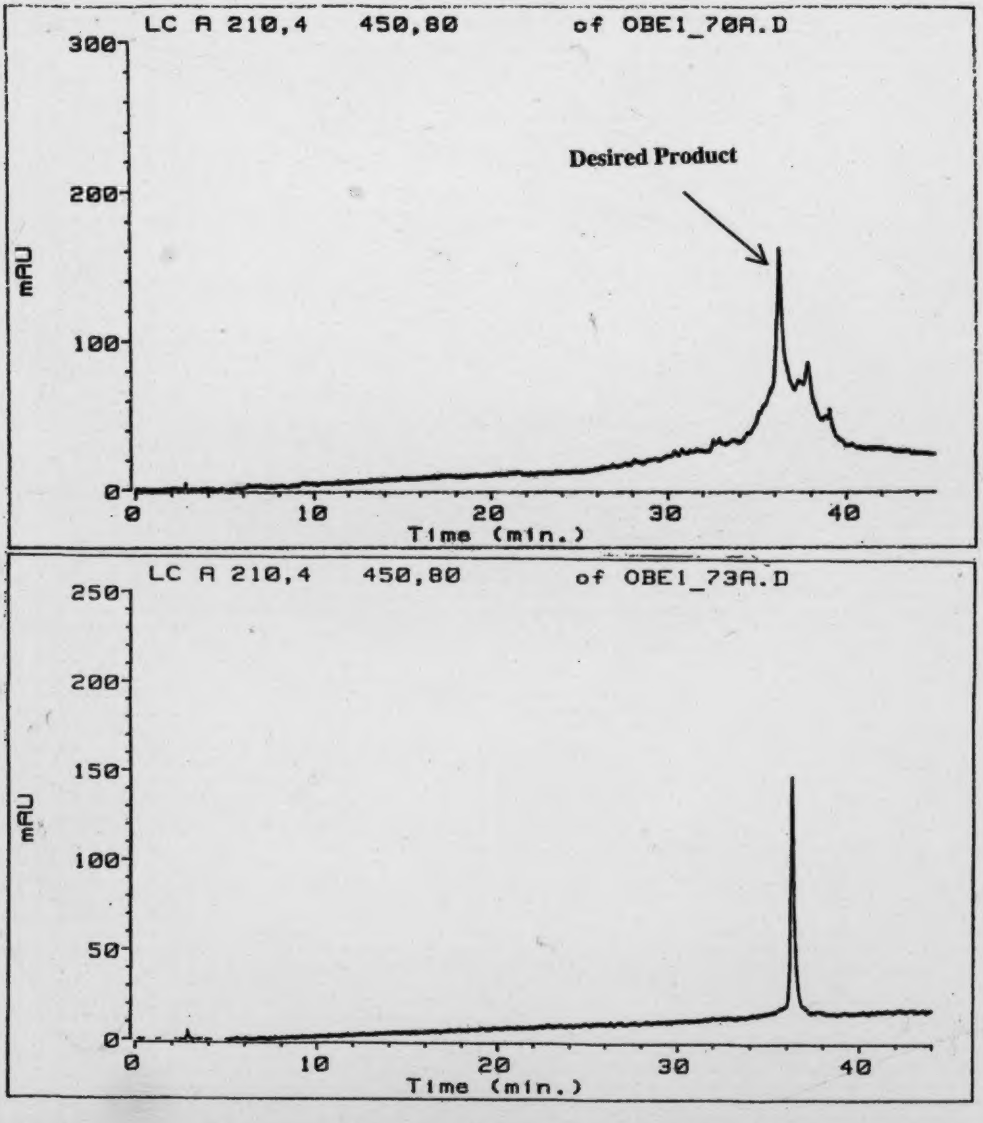

Figure II-4. The top panel shows the RP-HPLC chromatograph of a crude 39 amino acid peptide synthesized using the methodology described. The peptide is run on an analytical standard bore Zorbax C8 RP-column at a 1%B/min gradient rate and 1ml/min flow rate. The bottom panel shows a purified fraction used for experimentation and secondary structure determination. The sequence of the peptide is CGGKDALLREFQEEIARLKAQLEKRSIGRRKRREKRREG.

mass-spectrometry, amino acid composition analysis, and analytical reversed-phase HPLC. A typical pure fraction obtained from our purification procedure is shown in Fig. II-3 and Fig. II-4.

3. *Amino acid composition analysis*

For amino acid analysis, purified peptides were hydrolyzed in 6N HCl containing 0.1% phenol for 1.5 h at 160^{o}C in evacuated, sealed tubes. Following HCl removal by vacuum, samples were re-dissolved in an appropriate volume of sample dilution buffer (0.2 M NaCitrate/HCl, thiodiglycol 0.5%, benzoic acid 0.1%, pH2 buffer) and run on a Beckman model 6300 amino acid analyzer utilizing post column ninhydrin detection analysis. Typical runs consisted of isocratic gradient steps using the following buffers: 0.2 M NaCitrate, pH 3.0; 0.2 M NaCitrate/HCl, pH4.3; and 0.2 M NaCitrate, 0.9 M NaCl 5% Phenol, pH 6, with coincident temperature changes between 46-66^{o}C.

4. *Mass spectrometry*

The correct molecular masses of the purified peptides and proteins were confirmed by electrospray mass spectrometry using a Fisons VG Quattro mass spectrometer (VG Biotech, Cheshire, England) calibrated with horse heart myoglobin (Mr 16, 951.51). Briefly, the samples (~10μL at 1μg/μl conc.) were injected and delivered to the analyzer using a 50μL/min flow of 50:50 acetonitrile:water buffer in positive ion mode and scanned 7-10 times. Acquired data were then baseline subtracted, smoothed and centered. Determination of the transformed molecular weight was carried out by choosing "Manual mode processing" and picking adjacent ion peaks for the

Figure II-5. The two panels show typical mass spectral analyses of a peptide fraction. The top panel shows a 39 residue peptide and the bottom a 64 amino acid peptide. Spectra were collected in positive mode from an eluent solution of 50:50 (v/v) water and acetonitrile containing 0.1% TFA. The mass spectrum (shown on the right) contains several peaks at different mass to charge ratios (the mass spectrometer measures the mass to charge ratio rather than the absolute mass). The polypeptide in the top panel contains 14 Lys residues; each can pick up a proton. For the 39 residue peptide in the top panel, the +6 peak (at 786 as a result of the ion with 6 positive charges) is most abundant, followed by the +7 peak (at 674), the +5 peak (at 943), and a small +8 peak (at 590). The data are transformed to deconvolute the mass/charge axis to absolute mass, as shown on the left of the top panel. The calculated mass is an average based on all the peaks present in the mass spectrum. The deconvoluted mass of 4709.98 Da is very close to the theoretical value of 4710.49 Da. The bottom panel is of the 64 residue peptide which has 15 Lys residues. The ion distribution approximately follows a gaussian distribution centered about +8. The calculated mass of 7222.35 is close to the theoretical 7221.9.

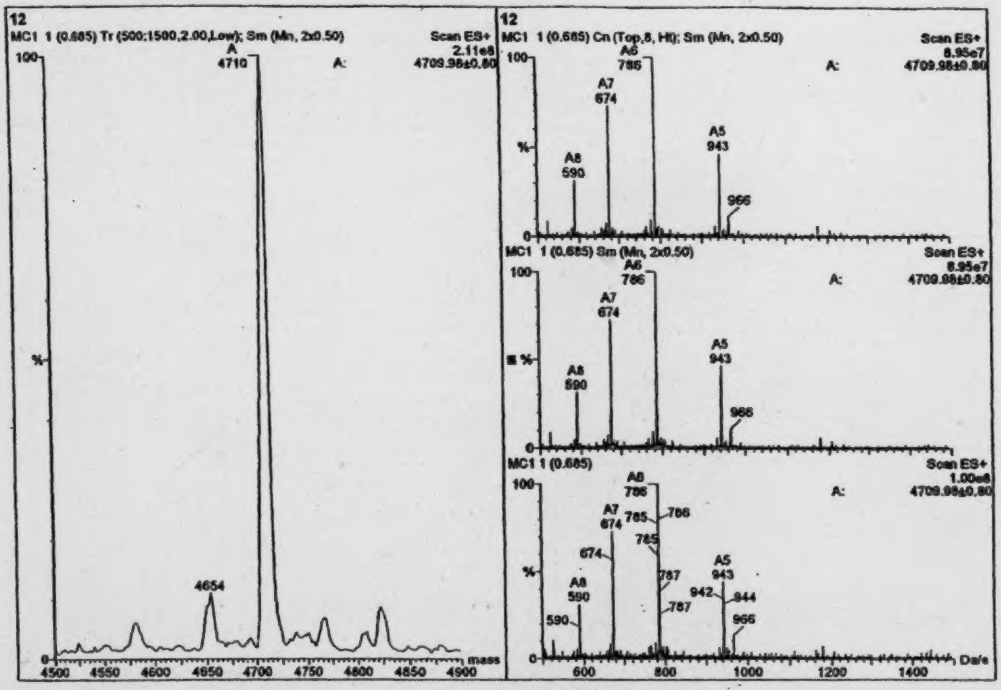
12
MC1 1 (0.685) Tr (500:1500,2.00,Low); Sm (Mn, 2x0.50)
Scan ES+
2.11e8
4709.98±0.80
A
4710
A:
4654
100
%
0
4500 4550 4600 4650 4700 4750 4800 4850 4900 mass
12
MC1 1 (0.685) Cn (Top,8, Ht); Sm (Mn, 2x0.50)
Scan ES+
8.95e7
4709.98±0.80
A6 786
A7 674
A8 590
A5 943
966
MC1 1 (0.685) Sm (Mn, 2x0.50)
Scan ES+
8.95e7
4709.98±0.80
A6 786
A7 674
A8 590
A5 943
966
MC1 1 (0.685)
Scan ES+
1.00e8
4709.98±0.80
A6 786
A7 674
785
786
674
785
787
787
A8 590
590
A5 943
942
944
966
600 800 1000 1200 1400 Da/e

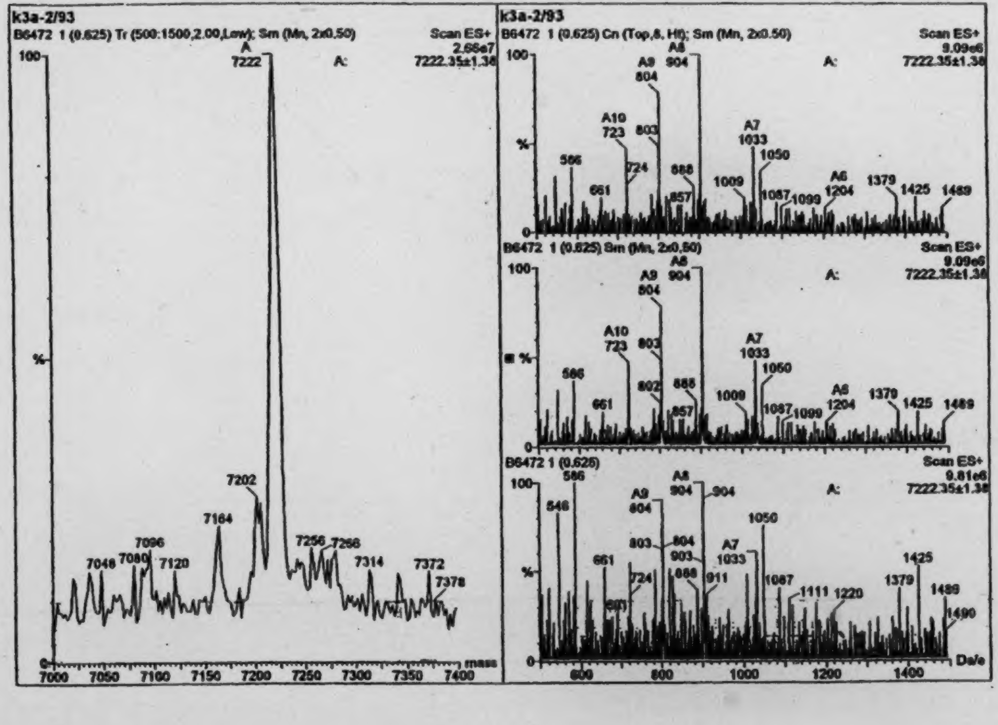
k3a-2/93
B6472 1 (0.625) Tr (500:1500,2.00,Low); Sm (Mn, 2x0.50)
Scan ES+
2.68e7
7222.35±1.38
A
7222
A:
7202
7164
7096
7048
7080
7120
7256
7266
7314
7372
7378
100
%
0
7000 7050 7100 7150 7200 7250 7300 7350 7400 mass
k3a-2/93
B6472 1 (0.625) Cn (Top,8, Ht); Sm (Mn, 2x0.50)
Scan ES+
9.09e6
7222.35±1.38
A8 904
A9 804
A10 723
803
724
586
661
888
857
A7 1033
1050
1009
1087
1099
A6 1204
1379
1425
1489
B6472 1 (0.625) Sm (Mn, 2x0.50)
Scan ES+
9.09e6
7222.35±1.38
A8 904
A9 804
A10 723
803
802
586
661
888
857
A7 1033
1050
1009
1087
1099
A6 1204
1379
1425
1489
B6472 1 (0.625)
Scan ES+
9.81e6
7222.35±1.38
586
548
A9 804
A8 904
904
1050
803
804
903
A7 1033
661
724
888
911
1087
1111
1220
1379
1425
1489
1490
600 800 1000 1200 1400 Da/e

transformation. The molecular masses were determined with an uncertainty of ± 2-3 Da. A typical mass spectral analysis is shown in Fig. II-5.

5. *Circular dichroism spectroscopy*

Circular dichroism (CD) spectra were recorded on a Jasco J-720 spectropolarimetre, interfaced to an Epson-Equity 386/25 computer running the Jasco DP-500/PS2 system software (version 1.33a). The temperature-controlled cuvette holder was maintained at the desired temperature with a Lauda model RMS circulating water bath. The instrument was calibrated with an aqueous solution of re-crystallised d-10-(+)-camphorsulfonic acid at 290.5 nm. Results were expressed as mean residue molar ellipticity [θ] ($\text{deg}\cdot\text{cm}^2\cdot\text{dmol}^{-1}$) calculated by using the equation :

$$[\theta] = (\theta_{obs} \cdot \text{MRW})/(10 \times l \times c)$$

where, θ_{obs} is the observed ellipticity expressed in millidegrees, MRW is the mean residue molecular weight (molecular weight of the peptide divided by the number of amino acids), l is the optical path length in cm, and c is the final peptide concentration in mg/mL. For wave scans, data were collected from 190 to 250 nm at 0.05-nm intervals, and the average of 10 scans reported (see figure II-6). GdnHCl and urea denaturation studies were carried out by preparing mixtures of a stock solution of peptide in buffer (0.1M KCl, 0.05M PO_4, pH 7), buffer alone and a solution of 8M GdnHCl or 10M urea in buffer where the ratios of buffer and 8M GdnHCl or 10M urea solutions were varied to give the appropriate final GdnHCl or urea concentrations. Urea/temperature studies were carried out by preparing mixtures of a stock solution of peptide in buffer (0.1M KCl, 0.05M PO_4, pH 7), buffer alone, and a solution of 10M urea in buffer where the ratios of buffer and 10M urea solutions were varied to give the appropriate final urea concentrations. The peptides in the urea/temperature studies were then subjected to thermal denaturation at fixed concentrations of urea. All peptide concentrations were determined by amino acid analysis on a Beckman model 6300, amino acid analyzer.

A. % α-helix -To solve the % α-helix the following equation was used: $-40{,}000(1-4.6/n)= [\theta_{theor}]$ (Gans et al., 1991)

where n = the length of reduced peptide, $[\theta_{theor}]$ = theoretical molar ellipticity for a peptide with helix forming sequence throughout its length, n. To calculate the % α-helix, $[\theta_{obs}]$ was subsequently divided by $[\theta_{theor}]$.

B. Protein unfolding measurements – Denaturation midpoints: $GdnHCl_{1/2}$, $urea_{1/2}$, and T_m values were determined by following the change in molar ellipticity at 222 nm using a Jasco J-720 spectropolarimeter (as described above). Ellipticity readings for GdnHCl and urea denaturations were normalized to the fraction of the peptide population that was folded (f_f) using the standard equation $f_f = ([\theta] - [\theta]_u) / ([\theta]_n - [\theta]_u)$, where $[\theta]_n$ and $[\theta]_u$ represent the ellipticity values for the fully folded and fully unfolded peptide population, respectively. $[\theta]$ is the observed ellipticity at 222nm at any denaturant condition.

Ellipticity readings for urea/temperature denaturations, where peptides were thermally denatured in fixed concentrations of urea, were normalized to the fraction of peptide population folded (f_f) using equation: $f_f = ([\theta]_{[XM]} - [\theta]_{u\,[8M]}) / ([\theta]_{n\,[YM]} - [\theta]_{u\,[8M]})$, where $[\theta]_{[XM]}$ represents the observed ellipticity at 222 nm at each temperature point for a fixed concentration of urea, i.e., the observed ellipticity for the peptide, in a fixed concentration of urea, as the temperature was changed. $[\theta]_{[YM]}$ is the ellipticity value for when the peptide population is fully folded at 4°C and the lowest used concentration of urea. $[\theta]_{u\,[8M]}$ represents the ellipticity value for a fully unfolded peptide population. It is the smallest ellipticity value for each peptide observed at an 8M concentration of urea at 88°C. Figure II-7 depicts the data generated from this type of "mixed-mode" denaturation technique.

The calculation of apparent T_m (T_m in the absence of urea) was estimated by extrapolating the observed T_m values at each urea concentration to zero concentration, assuming that the T_m values and urea concentration are linearly related by the equation $T_m^{urea} = T_m^{H2O} - m[urea]$. T_m^{urea} values were experimentally determined.

C. Calculation of denaturant midpoints, free energy of unfolding (ΔGu^{H_20}) and differences in the free energies of unfolding ($\Delta\Delta Gu^{H_20}$).

Denaturation midpoint values for the unfolding of the various peptides from folded (f) to unfolded (u) states were determined by following the change in molar ellipticity at 222 nm at 20°C. Ellipticity readings were normalized to the fraction of the peptide folded (f_f) or unfolded (f_u) using the standard equations:

$f_f = ([\theta] - [\theta]_u) / ([\theta]_n - [\theta]_u)$

$f_u = (1 - f_f)$

Each curve was then fit to a sigmoidal equation (e.g., (max-min)/(1+(denaturant conc./midpoint)^slope)+min).

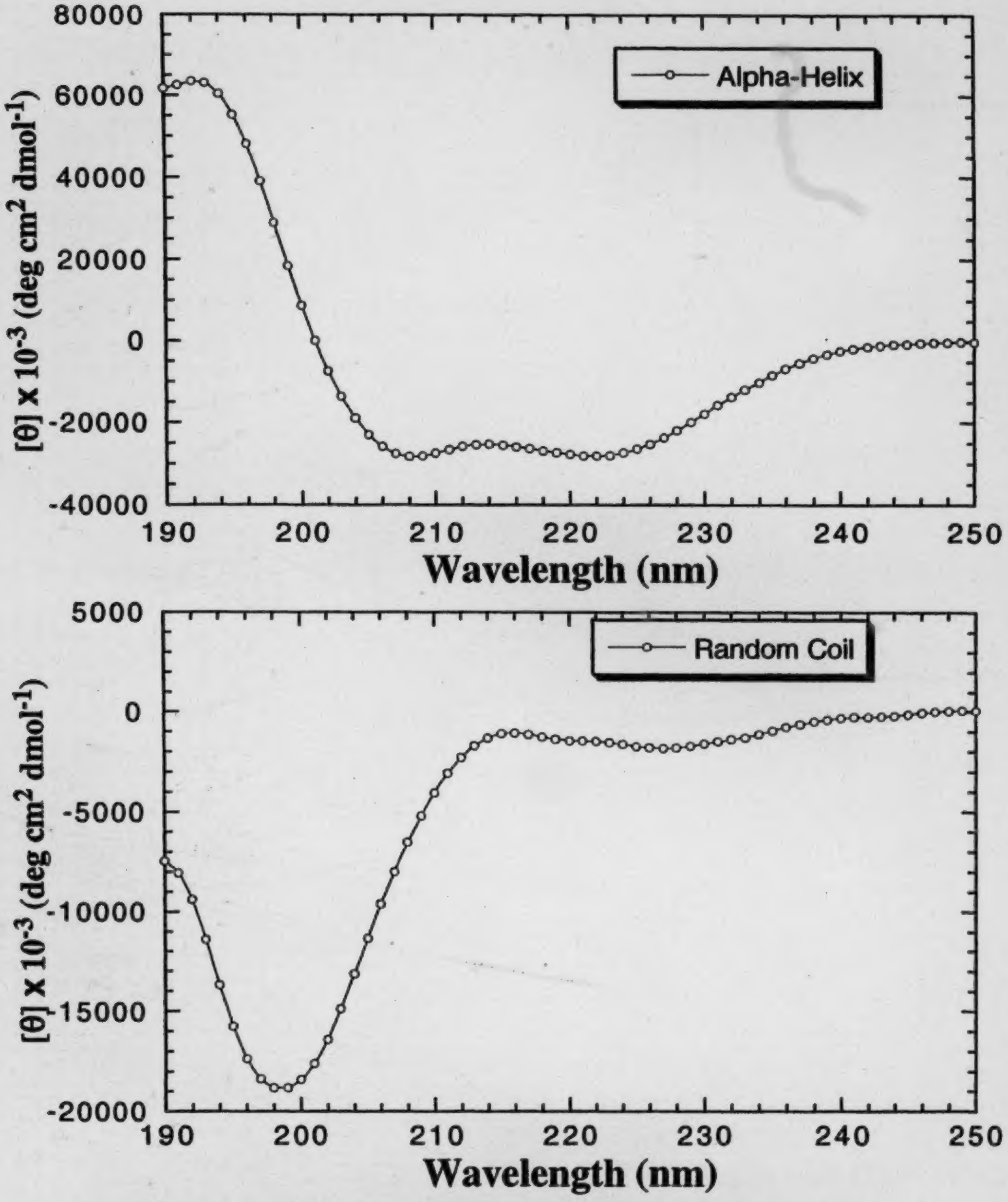

Figure II-6. The top panel shows the circular dichroism spectrum of a fully folded two-stranded alpha-helical coiled-coil. The molar ellipticity values at each wavelength is from the average of 10 scans over the range of 190 to 250 nm. The molar ellipticity values were recored every 0.05 nm but values every 1 nm are shown here for clarity. The bottom panel shows the characterisic circular dichroism spectrum of a random coil peptide.

Figure II-7. Panels A and B depict the temperature melting curves of two peptides denatured at varying concentrations of urea. The T_m value has shifted to the left with increasing concentrations of urea. The alpha-helical content was monitored at 222 nm over the course of the denaturations. The ellipticity values were normalized to 1.0 fraction folded, for each peptide, at each individual urea concentration. The fraction folded values were plotted against temperature to disclose the temperature at which the peptide populations were 50% folded. This temperature was taking to be the T_m. Each of the T_m values, recorded for a peptide, was plotted against urea concentration to yield the plot in panel C. The shift in the T_m value, for each peptide, when denatured by temperature in increasing concentrations of urea, gives a linear correlation between the T_m and urea concentration used in the temperature denaturation. This linear correlation can be used to extrapolate to a urea concentration of 0M to give the T_m in benign medium.

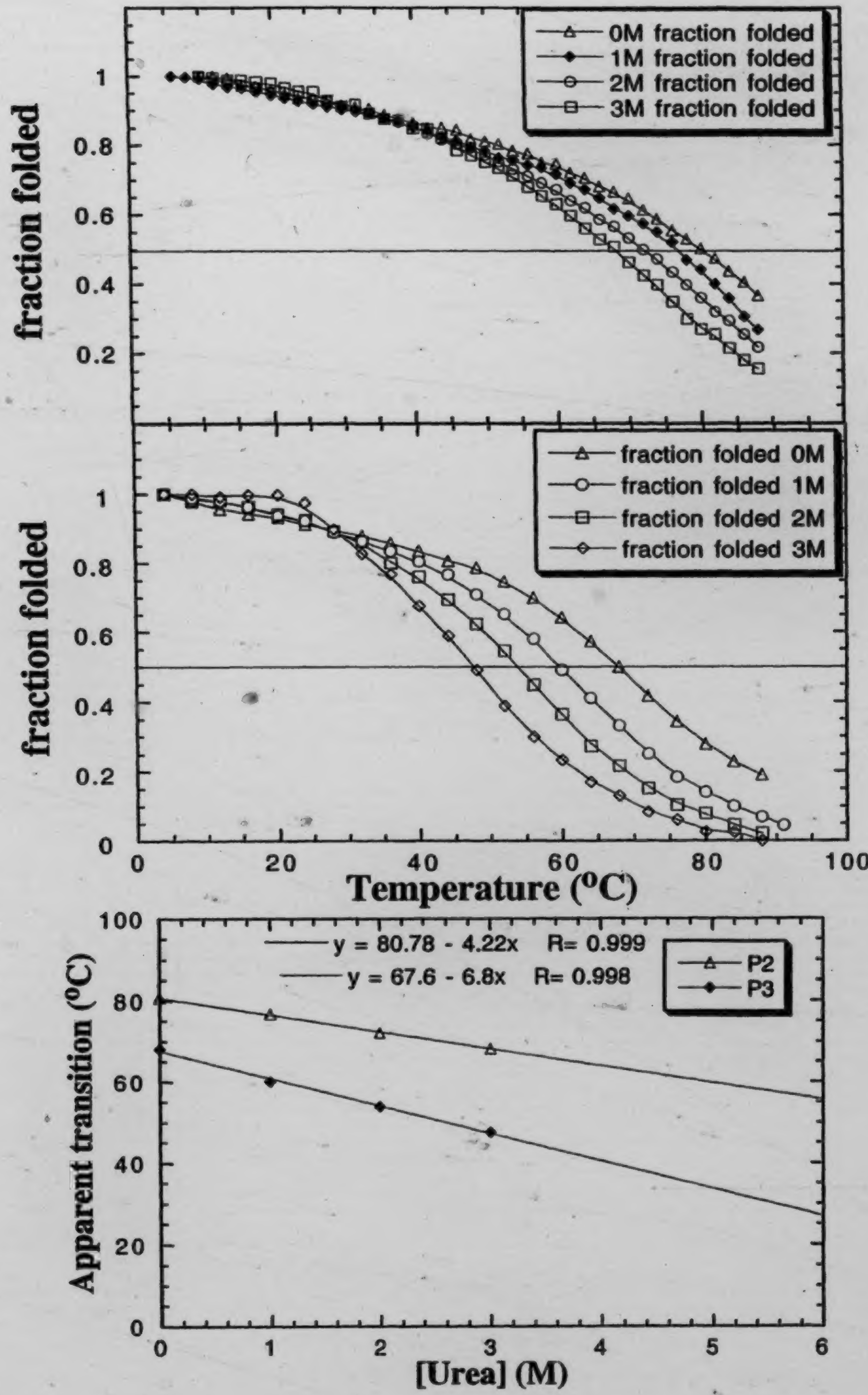
0M fraction folded
1M fraction folded
2M fraction folded
3M fraction folded
fraction folded
1
0.8
0.6
0.4
0.2
fraction folded 0M
fraction folded 1M
fraction folded 2M
fraction folded 3M
fraction folded
0
20
40
60
80
100
Temperature (°C)
100
80
60
40
20
0
y = 80.78 - 4.22x R= 0.999
y = 67.6 - 6.8x R= 0.998
P2
P3
Apparent transition (°C)
1
2
3
4
5
6
[Urea] (M)

Calculation of ΔGu^{H_20} (the free energy of unfolding in the absence of guanidine hydrochloride) was estimated by extrapolating the free energy of unfolding at each denaturant concentration to zero concentration assuming they are linearly related by the equation $\Delta Gu = -RT \ln (K_u)$, where $K_u = (f_u/f_f)$ for the oxidized peptides and $(2P_t(f_u^2/(1-f_u))$ for reduced peptides (De Francesco et al., 1991) and P_t is the total peptide concentration (M).

When the difference in free energy change ($\Delta\Delta Gu^{H_20}$) was sought between a series of analogues relative to a specific analogues, the $\Delta\Delta Gu^{H_20}$ values were calculated using the equation given by Serrano and Fersht (1989):

$\Delta\Delta Gu = ([\text{denaturant}]_{1/2,A}-[\text{denaturant}]_{1/2,B})(m_A+m_B)/2$, where $[\text{denaturant}]_{1/2,A}$ and $[\text{denaturant}]_{1/2,B}$ are the midpoints of unfolding of analogue A and B, respectively, derived from the plots of fraction folded versus GdnHCl concentration, and m_A is the slope determined from the equation $\Delta G_u = \Delta G^{H_20} - m\,[\text{denaturant}]$ (as described above). This approach calculates the value of $\Delta\Delta G_u$ at the denaturant concentration half-way between the $[\text{denaturant}]_{1/2}$ values of the peptides being compared. This method has been shown to be more accurate for determining small differences in protein stability because small errors from extended extrapolation are avoided and linearity between ΔG_u and denaturant concentration is assumed across only a small range of denaturant concentration.

6. *Preparation of oxidized peptides*

Formation of homo-two-stranded disulfide-bridged molecules was carried out by dissolving 5 mg of each peptide into 2 mL of 100mM NH_4HCO_3 pH 8 buffer and the reaction vessel stirred overnight at room temperature. Oxidized peptides were re-purified by RP-HPLC and oxidation verified by mass spectrometry (as described above).

7. *Sedimentaion equilibrium studies*

Conventional sedimentation equilibrium experiments were performed on a Beckman Model XL-I analytical ultracentrifuge (Beckman, Palo Alto) at 20°C. Standard charcoal-filled Epon double sector centerpieces (12 mm) were used, and a sample volume of 120 uL was added into each sample sector. Peptide samples were initially dialyzed against the desired buffer at 4°C overnight prior to analysis. Experiments were conducted at various rotor speeds depending on the size of the complex (~18, 000 to 32,000 rpm). Data were acquired by averaging 5 radial scans at a spacing of 0.001 cm. Equilibrium was confirmed by the superimposition of the concentration gradient measured after 20 and 24 h. The data were fit to the following equation:

$$c_r = c_0 \exp\{[M_{W,\,app}(1- v_2\rho)(r^2-r_0^2)\omega^2]/2RT\}$$

where $M_{W,\,app}$ is the apparent molecular mass, v_2 is the partial specific volume, c is the molar concentration, r is radial distance, and ρ is the solvent density. The partial specific volume of each sample was calculated from amino acid composition using the program SEDINTERP (Hayes et. al., 1998).

8. *Redox experiments*

Oxidized, homo-two-stranded peptides were mixed together from stock concentrations to final concentrations of 100μM each in 0.1M KCl, 0.05M PO_4, pH 7.0 buffer (Monera et al., 1993; O'Shea et al., 1989). To the mixture, reduced and oxidized glutathione were each added at 1.0 mM final concentration. The final reaction volume was 800μL and reactions were carried out at room temperature in Reacti vials (Chromatographic Specialties, Inc.) with fitted triangular stir bars and screw caps fitted with rubber septums. Prior to the reaction, buffers were equilibrated overnight with nitrogen gas by blowing a steady stream of N_2 through the buffers for 16 h.

15μL aliquots were taken from the Reacti vials at set time intervals and the reaction was quenched with either 10μL of 3% aqueous phosphoric acid or 10μL of 5% trifluroacetic acid. The time-points were monitored by reversed-phase HPLC (Zorbax, 300SB- C_8, 150 X 2.1 mm I.D., 5μm particle size, 300Å pore size; Agilent Technologies) to disclose the peptide ratios (homostranded and heterostranded) in the reaction mixture. Typically, $H_2PO_4^{-2}$ was used as our ion pairing agent during RP-HPLC for monitoring redox reactions.

9. *Heterostranded peptide formation*

Hetero-two stranded peptides were made using two techniques. To prepare the Kif3A/Kif3B coiled-coil, the reagent 2,2'-dithiobis(5-nitropyridine) (DTNP) was utilized (Rabanal et al., 1996). DTNP activated a peptide's cysteine sulfur atoms and, upon the introduction of another peptide with a free sulfhydryl group, the 5-nitro-2-pyridinesulfenyl group was removed through an S_N2 style nucleophilic substitution reaction to produce hetero-stranded oxidized peptide. The benefit of DTNP activation is that the heterostranded peptide is formed at pH 4.5 and so no homostranded peptides are formed.

The reaction's progress can be monitored with either RP-HPLC or mass spectrometry. Fig. II-8 and Fig. II-9 depict the progress of this reaction by mass spectral analysis. Fig. II-8 shows the change in the molecular mass of a synthetic MmKif3A neck region coiled-coil peptide through the derivatization by DTNP. Fig. II-9 shows the mass of synthetic MmKif3B neck region coiled-coil peptide before and after it has reacted with the DTNP derivatized MmKif3A peptide. The final mass is the combination of the two reduced peptides.

The second technique we used to form heterostranded peptides was to mix the two reduced peptides together at equimolar amounts at pH 5.0. The peptides were stirred at room temperature for 3-4 h and then the pH was raised to 8.0 using a small amount of KOH. The reaction was monitored using RP-HPLC. This technique was used only for peptides possessing complementary charged regions on their C-terminus. This technique led to the formation of 100% heterostranded peptide.

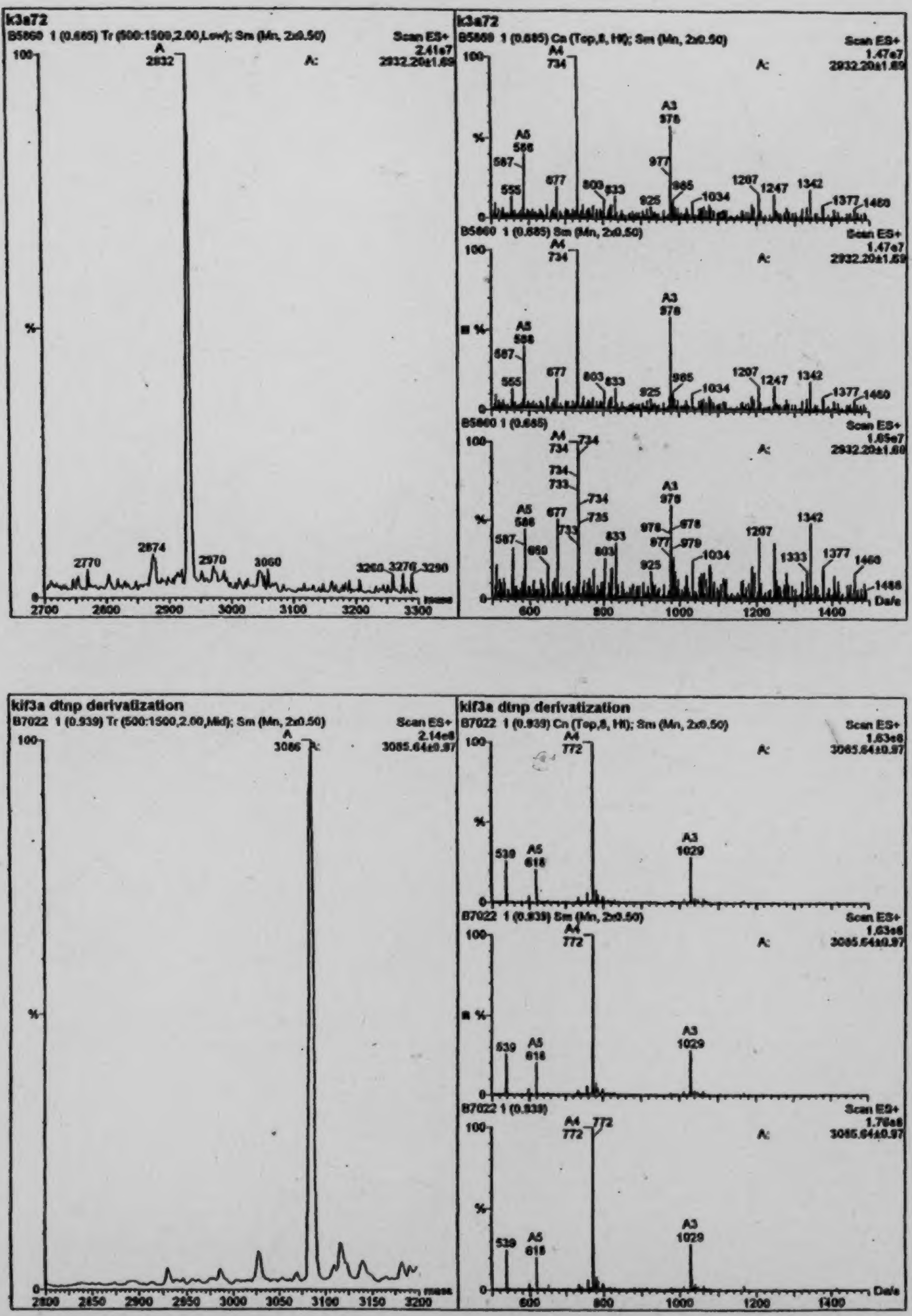

Figure II-8. The top panel shows the molecular mass of synthetic MmKif3A coiled-coil peptide, 2932.2 Da. The bottom panel shows the MmKif3A peptide derivatized with DTNP, giving a final mass of 3085.64 Da. The difference in mass arises from the addition of the 5-nitro-2-pyridinesulfenyl group, added to the peptide's cysteine side-chain sulfur atom by mixing the peptide with DTNP in 3:1 acetic acid:water

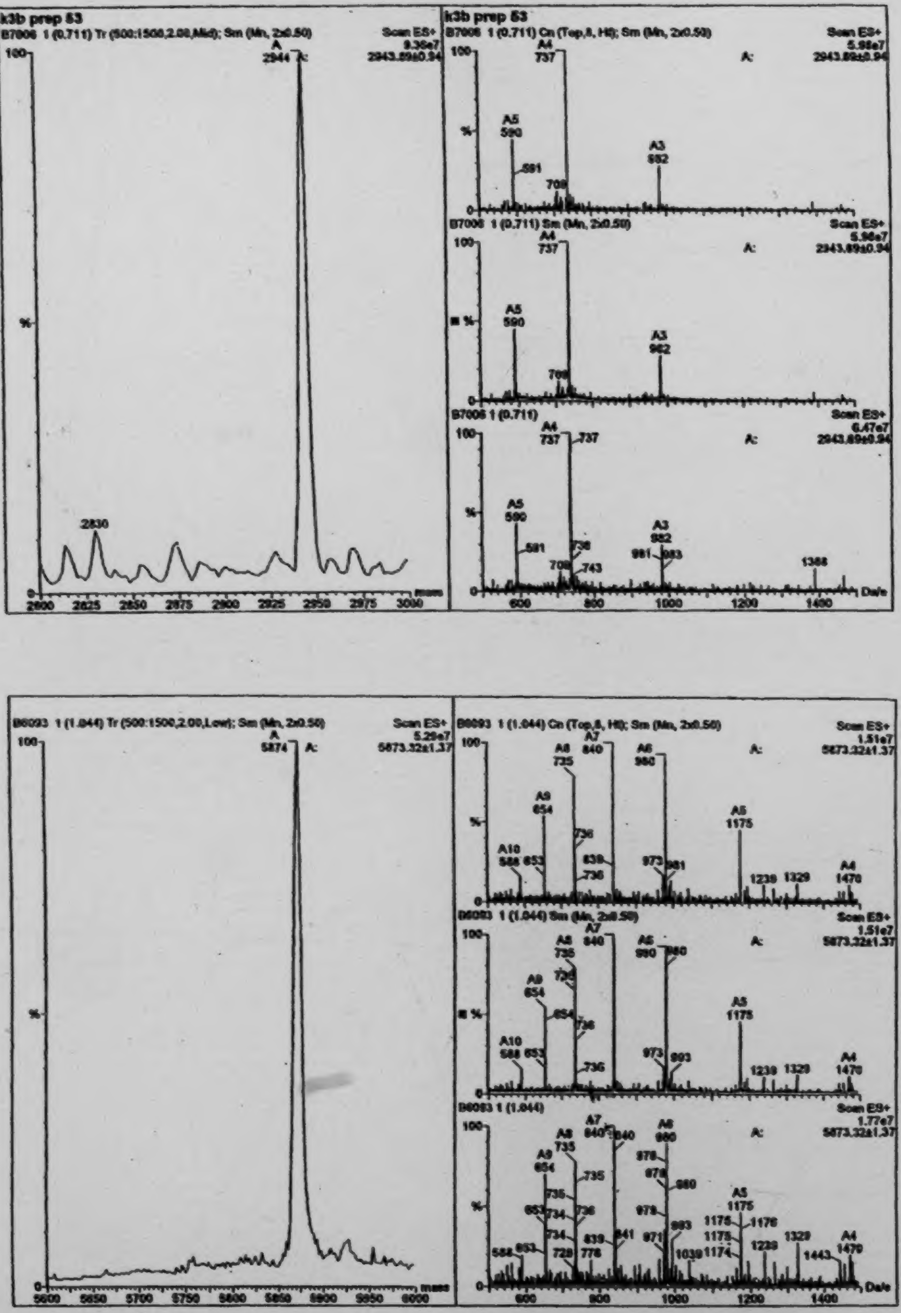

Figure II-9. The top panel shows the molecular mass of synthetic MmKif3B coiled-coil peptide (2943.89 Da) prior to adding it to the derivatived MmKif3A peptide. The bottom panel shows the final molecular mass of the heterostranded peptide that is formed after mixing the two peptides. 5873.32 Da is the sum of the two reduced peptides less 2 Da because forming a disulfide bridge leads to the loss of two protons.

CHAPTER III

The Role of Unstructured Highly Charged Regions on the Stability and Specificity of Dimerization of Two-Stranded α-Helical Coiled-Coils: Analysis of the Neck-Hinge Region of the Kinesin-like Motor Protein KIF3a[1]

A. Introduction

Intracellular transport of, membrane bound vesicular structures, and organelles, is a natural consequence of the compartmentalization found in eukaryotic cells. For example, secretion of a protein requires the movement of membrane bound vesicles from the endoplasmic reticulum to the Golgi and finally to the cell surface. Also, large cells with a polarized structure such as neurons require the movement of pre-synaptic vesicles, formed in the cell body, to the periphery of the axon. Intracellular transport of this type relies on the dynamic cytoskeleton and its associated proteins. A structural component of the cytoskeleton includes microtubules, which are polarized filaments that have stable – ends and dynamic + ends that extend outward to the periphery of non-polarized cells, and to the axon from the cell body in polarized cells such as neurons. Two proteins associated with microtubules are kinesin (Allen *et al.*, 1985; Brady, 1985, Vale *et al.*, 1985) and dynein (Gibbons *et al.*, 1965; Summers *et al.*, 1971). Kinesins are responsible for fast anterograde movement toward the + end of the microtubules and dynein for retrograde movement toward the - end of the microtubules. In addition, some kinesin-like motor proteins have also been shown to display retrograde movement (McDonald *et al.*, 1990; Case *et al.*, 1997). Kinesins are known as molecular motors since they transduce the chemical energy of adenosine triphosphate (ATP) into mechanical motion and move in a processive manner. After the initial discovery of a kinesin from squid axonal extracts (Vale *et al.*, 1985), many other kinesin-like proteins were discovered (Review: Miki *et al.*, 2001). This led to the organization of a new super family of kinesin-related proteins (Goodson *et al.*, 1994; Kim and Endow, 2000). Recently, many of the related kinesin proteins found in different organisms have been grouped, categorized and placed into sub-families (Miki *et al.*, 2001).

---

[1] A version of this chapter has been published: Chana, M.C., Tripet, B.P., Mant, C.T., and Hodges, R.S. (2002). *Journal of Structural Biology*, In press.

The catalytic core of the kinesin superfamily of proteins has structural similarity to the catalytic core of myosin and G-proteins (Review: Vale, 1996). For example, in a similar manner to myosin, many kinesins function as multi-protein complexes that include heavy and light chains. The heavy chains are responsible for ATP hydrolysis, binding the intracellular network of microtubules and providing processive movement or fast transport. In addition, for some kinesins, the heavy chains form a dimer via a two-stranded α-helical coiled-coil (de Cuevas *et al.*, 1992; Hirokawa *et al.*, 1989; Yang *et al.*, 1989).

Kinesin and myosin heavy chains share structural similarity, with many of discovered kinesins beginning with an N-terminal globular head domain, followed by a flexible neck region and a C-terminal stalk coiled-coil. The neck region of conventional kinesin consists of a neck linker and a neck coiled-coil (Morii *et al.*, 1997; Tripet *et al.*, 1997), followed by a hinge (Kozielski *et al.*, 1997; Sack *et al.*, 1997) termed hinge 1. The neck linker and coiled-coil, taken together, have been termed the neck region and are included with the globular head domain in forming the motor domain (Vale *et al.*, 1997). The transduction of chemical energy into mechanical movement has been shown to involve the neck linker region (Rice *et al.*, 1999), while the neck coiled-coil is thought to fine-tune the motor's run distance (Thorn *et al.*, 2000).

A unique feature of the kinesin-like heterodimeric motor protein Kif3A/Kif3B is the highly charged regions that interrupt the coiled-coil between the neck and stalk. These highly charged regions exhibit opposite polarity from one chain to the other (Fig. III-1, top panel). These regions have been proposed to specify heterodimer formation (Rashid *et al.*, 1995). The hinge region has been shown to have a string of negatively charged amino acid side-chains followed by a string of positively charged amino acid side-chains for kinesin-like SpKRP 85 (Rashid *et al.*, 1995) and MmKif3A proteins (Yamazaki *et al.*, 1995), both now termed Kif3A (Miki *et al.*, 2001). For kinesin-like SpKRP 95 and MmKif3B proteins, both now termed Kif3B (Miki *et al.*, 2001), which heterodimerize with SpKRP 85 and MmKif3A, respectively, hinge 1 contains a stretch of positively charged amino acids followed by a stretch of negatively charged amino acids. It was shown that Kif3A forms a heterodimer with Kif3B *in vivo* (Rashid *et al.*, 1995; Yamazaki *et al.*, 1995), and it was postulated that heterodimer formation could be the result of charged amino acid interactions leading to the destabilization of homodimers, or alternatively the stabilization of heterodimers (Rashid *et al.*, 1995).

To elucidate whether preferential heterodimer formation can be attributed to electrostatic interactions in hinge 1, a region rich in charged residues that follows the neck region of Kif3A and Kif3B, the present study was designed to show: (1) whether the predicted Kif3A neck coiled-coil region (Rashid *et al.*, 1995) would form an autonomous folding unit; (2) whether there is structure in the charged hinge 1 region of Kif3A; (3) whether electrostatics have a role in specifying heterodimer formation even when the two strands of the coiled-coil are identical; and (4) whether negatively and positively charged extensions can affect the stability of the putative Kif3A coiled-coil neck region.

B. Results

Autonomous folding of predicted neck coiled-coil region

As a first step towards characterizing the biophysical properties of the neck region of Kif3A and the putative role of its hinge region, it was first necessary to determine whether the putative neck coiled-coil-forming sequence of Kif3A was an autonomous folding unit and would form a two-stranded α-helical coiled-coil in the absence of the rest of the Kif3A molecule. In this regard, peptide P2 (residues 356-377) was synthesized (Fig. III-1, bottom panel) and analyzed by circular dichroism spectroscopy (CD). The CD spectrum of disulfide-bridged P2 (Fig. III-2A) is characteristic of a fully folded α-helical coiled-coil based upon the following characteristics: high molar ellipticity value in benign medium, double minima at 208 nm and 222 nm and a maximum at 190 nm; an α-helical content of 94% and 21 calculated α-helical residues out of 22 (Table III-1); the addition of 50% trifluoroethanol (TFE) does not increase the α-helical content (determined at 222 nm) (Table III-1); the $[\theta]_{222}/[\theta]_{208}$ ratio in benign medium (1.03) is characteristic of coiled-coils, i.e., >1.0 (Lau *et al.*, 1984) and this value decreases to 0.90 in the presence of the helix-inducing solvent TFE. Although TFE stabilizes the helical structure of individual P2 strands, it denatures tertiary and quaternary structure, i.e., the coiled-coil is dissociated to single-stranded α-helices as was clearly demonstrated by high-performance size-exclusion chromatography of coiled-coils (Lau *et al.*, 1984a,b; Monera *et al.*, 1993; Zhou *et al.*, 1992a,b; Mant *et al.*, 1997).

Figure III-1. Top Panel shows a schematic of the kinesin-like heterodimeric motor protein (Kif3A/Kif3B). This protein consists of two different polypeptide chains Kif3A and Kif3B, which resemble conventional kinesin heavy chains. Each polypeptide chain contains a N-terminal globular motor domain, followed by a potential neck coiled-coil region, a highly charged hinge region, a coiled-coil stalk region and the C-terminal tail region (which binds to an accessory unit, the so-called kinesin associated protein KAP). Bottom Panel shows the amino acid sequences of the Kif3A peptides used in this study and the sequence of Kif3B for reference. The native mouse Kif3A sequence 356-416 is shown above the synthetic peptides P1-P5 prepared for this study. The open box around the native sequence indicates the predicted neck α-helical coiled-coil region. The heptad repeat of the coiled-coil is denoted *abcdefg*, where positions **a** and **d** are the non-polar residues (shown in bold) involved in the 3-4 hydrophobic repeat. The boxed regions below the peptide sequences denote the predicted coiled-coil region and the highly negatively charged and positively charged regions. The negatively charged residues and positively charged residues are indicated by a (-) or (+) sign, respectively. CGG represents a flexible linker added N-terminally to each peptide. Ac- denotes N^{α}-acetyl and –amide denotes C^{α}-amide. All of the synthetic peptides are aligned to the native sequence except P4, which consists of the coiled-coil region 356-377 combined with the positively charged region 403-416 and deleting the negatively charged region 378-402. The flexible CGG linker was added to the N-terminus of each peptide to allow the formation of homodimeric or heterodimeric coiled-coils through the use of a covalent linkage. The disulfide bond enabled us to observe the selective formation of homo- or heterodimeric coiled-coils during Redox experiments (see Methods). The disulfide linkage also removed the monomer-dimer equilibrium when studying coiled-coil stability.

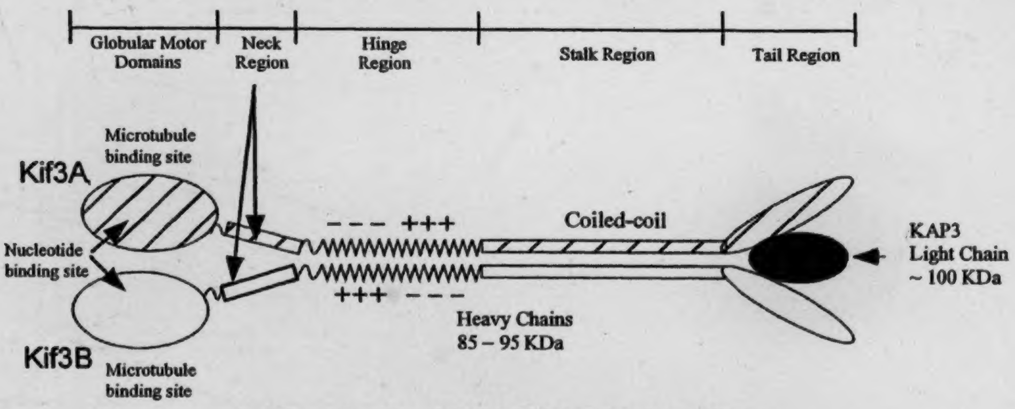
Globular Motor Domains
Neck Region
Hinge Region
Stalk Region
Tail Region
Kif3A
Microtubule binding site
Nucleotide binding site
--- +++
Coiled-coil
KAP3 Light Chain ~ 100 KDa
+++ ---
Heavy Chains 85 – 95 KDa
Kif3B
Microtubule binding site

Kinesin-like Kif3A/Kif3B Heterodimer

```
                 Neck Region                    Charge-Rich Hinge Region

          351        363         375        387        399        411
KIF3B     |          |           |          |          |          |
Native    KDALLREFQEEIARLKAQLEKRSIGRRKRREKRREGGGSGGGEEEEEEGEEGEEDGDDKD
Sequence  defgabcdefgabcdefgabcd
          356                  377             395        403        416
KIF3A     |                    |               |          |          |
Native    KDALLRQFQKEIEELKKKLEEGEEVSGSDISGSEEDDEEGELGEDGEKRKKRRDQAGKKKV
Sequence  defgabcdefgabcdefgabcd


P1 Ac-CGGKDALLRQFQKEIEELKKKLEEGEEVSGSDISGSEEDDEEGELGEDGEKRKKRRDQAGKKKV-amide
      |     Coiled coil       |--    -    ------ -  -- -|++++++-   +++|

P2 Ac-CGGKDALLRQFQKEIEELKKKLEEG-amide
      |     Coiled coil       |

P3 Ac-CGGKDALLRQFQKEIEELKKKLEEGEEVSGSDISGSEEDDEEG-amide
      |     Coiled coil       |--    -    ------|

P4 Ac-CGGKDALLRQFQKEIEELKKKLEEGKRKKRRDQAGKKKV-amide
      |     Coiled coil       |++++++-   +++|

P5                         Ac-CGGEEVSGSDISGSEEDDEEGELGEDGEKRKKRRDQAGKKKV-amide
                              |--    -    ------ -  -- -|++++++-   +++|
```

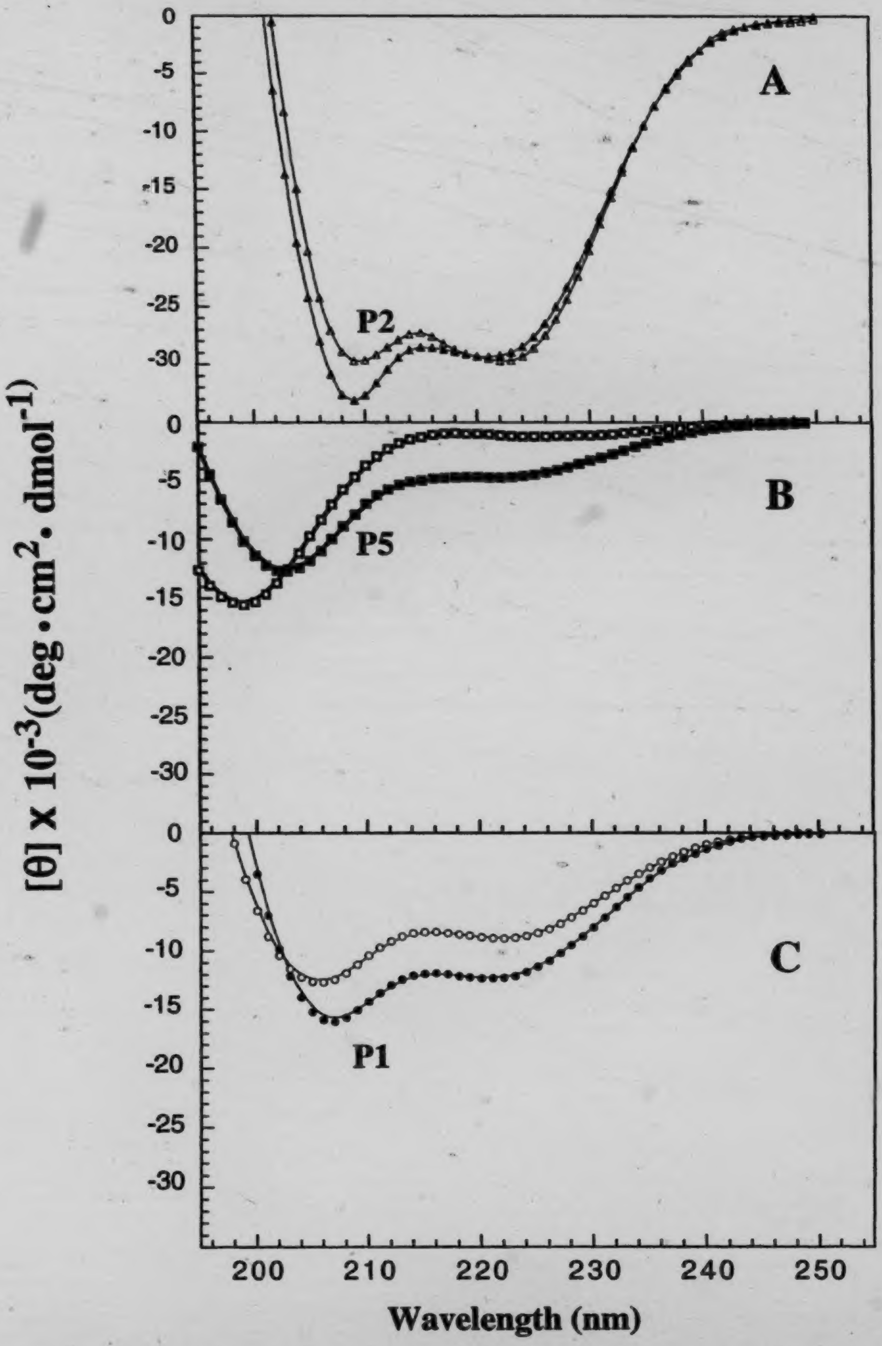

Figure III-2. Circular dichroism (CD) spectra of synthetic disulfide-bridged two-stranded peptides P2, P5, and P1 in a benign buffer (0.1 M KCl, 0.05 M PO_4, pH 7) (open symbols) and in the presence of 50% trifluoroethanol (TFE)–benign buffer (closed symbols) at 25°C are shown in Panel A (peptide P2), Panel B (peptide P5), and Panel C (peptide P1). The peptide sequences are shown in Fig. III-1.

Similarly, the CD spectrum of P2 in its reduced state (Fig. III-3A and Table III-2) shows a helical content indicative of coiled-coil formation. The $[\theta]_{222}$ values for the oxidized and reduced peptides were –29,700 and –20,500, respectively (Table III-1 and 2). The decrease in helical content for the reduced peptide is expected due to end fraying (Zhou *et al.*, 1992b) and the concentration dependence of the monomer-dimer equilibrium where the monomer is unfolded and the dimer folded (Zhou *et al.*, 1992b,c). In figure III-3, the reduced peptides were compared at a concentration of 100 μM. In Table III-2, data for peptide P2 are shown at 100 μM and 500 μM. The results clearly show an increase in helical content as the concentration increases (compare $[\theta]_{222}$ values of –20,500 and 26,390 for 100 μM and 500 μM, respectively). The helical content is approaching that of the disulfide-bridged P2 peptide where the helical content is concentration independent. These results indicate that, although Kif3A forms a heterodimer with Kif3B in vivo (Yamazaki *et al.*, 1995), there is no intrinsic sequence specificity in the coiled-coil region that precludes homodimer formation in the Kif3A region.

To determine the stability of the coiled-coil, peptide P2 was denatured by temperature, urea and guanidine hydrochloride in its reduced state or in its disulfide-bridged form using CD spectroscopy. The transition midpoints from temperature denaturation of the reduced and disulfide-bridged coiled-coil were 41.5°C and 81°C, respectively (Fig. III-4). The urea and GdnHCl transition midpoints of the disulfide-bridged coiled-coil were 6.7 M and 3.2 M, respectively (Table III-3). These results show that, despite the short size of the coiled-coil (P2 is 22 residues or 3 heptads), the sequence is able to form a stable homodimer similar to many other known native coiled-coils.

Table III-1: Circular dichroism data of disulfide-bridged Kif3A synthetic peptides

Peptide[a]	Number of residues[b]	$-[\theta]_{222}$ (deg.cm^2/dmol)[c]		Percent α-helix[d]		Number of calculated helical residues[e]		$[\theta]_{222}/[\theta]_{208}$[f]	
		Benign	50% TFE	Benign	50% TFE	Benign	50% TFE	Benign	50% TFE
P1	61	8950	12300	24	33	14	20	0.75	0.78
P2	22	29700	29250	94	93	21	20	1.03	0.90
P3	40	11700	15750	33	44	13	18	0.78	0.79
P4	36	20050	28100	57	81	21	29	0.96	0.91
P3/P4	40/36	17400	24300	50	69	19	26	0.94	0.90
P5	39	1200	4750	3.5	13	1	5	0.21	0.53

[a] Disulfide-bridged homostranded peptides P1, P2, P3, P4, and P5. Disulfide-bridged heterostranded peptide P3/P4. The amino acid sequence for each peptide is shown in Fig III-1.

[b] Number of residues per polypeptide chain excluding the CGG linker.

[c] The mean residue molar ellipticities at 222nm were measured at 25°C in benign buffer (0.1 M KCl, 0.05 M PO_4, pH 7). For samples containing TFE, the buffer was diluted 1:1 (v/v) with TFE.

[d] The percent helical content was calculated from the ratio of the observed $[\theta]_{222}$ value divided by the predicted molar ellipticity × 100. The predicted molar ellipticity was calculated from the equation $[\theta]_{222} = -40{,}000(1-4.6/n)$ for the chain length dependence of an α-helix (Gans *et al.*, 1991), where n is the number of residues in the peptide. A peptide of 22 residues has a predicted molar ellipticity of –31,600.

[e] The number of helical residues were calculated by multiplying the percent α-helix by the number of residues in the polypeptide chain., *e.g.*, for P2 in benign medium $29{,}700/31{,}600 \times 22$ residues = 21 α-helical residues predicted in the coiled-coil.

[f] The molar ellipticity values at 222nm and 208nm for each peptide were used to calculate the ratio $[\theta]_{222}/[\theta]_{208}$.

Interestingly, this substantial coiled-coil stability occurs despite the presence of destabilizing residues in the hydrophobic core positions "*a*" and "*d*": Lys at "*d*" (residue 356*d*) and Gly at "*d*" (residue 377*a*). These residues have been shown to destabilize coiled-coils substantially by 1.8 and 3.6 kcal/mol, respectively, compared to Ala in the hydrophobic core of model α-helical coiled-coils when substitution site was in the center of the coiled coil (Tripet *et al.*, 2000, Wagschal *et al.*, 1999a,b). However, these destabilizing residues in Kif3A are at the ends of the coiled-coil (Fig. III-1, bottom panel) and it has been shown that the contribution of these positions to stability of the coiled-coil was considerably less than internal positions (Zhou *et al.*, 1992a,b). Nevertheless, the coiled-coil sequence has 5 large hydrophobes in a row to stabilize the coiled-coil. It has been shown that coiled-coils containing as few as 5 large hydrophobes can form extremely stable coiled-coils (Su *et al.*, 1994).

Secondary structure of the charge-rich hinge region

We now addressed the question of whether the charge-rich region that follows the neck coiled-coil of Kif3A can form secondary structure. Thus, we prepared two peptides: peptide P5 (Kif3A residues 378-416), representing the highly charged region alone, and peptide P1, comprised of both the neck coiled-coil and the highly charged region (Kif3A residues 356-416) (Fig. III-1, bottom panel). These peptides were first compared in the disulfide-bridged state since it is well-known that an interstrand disulfide-bridge stabilizes coiled-coil structure and removes the concentration dependence of the monomer-dimer equilibrium (Zhou *et al.*, 1992a,b,c; Zhou *et al.*, 1993). In addition, many groups have used a Cys-Gly-Gly linker added to the N-terminus to permit disulfide

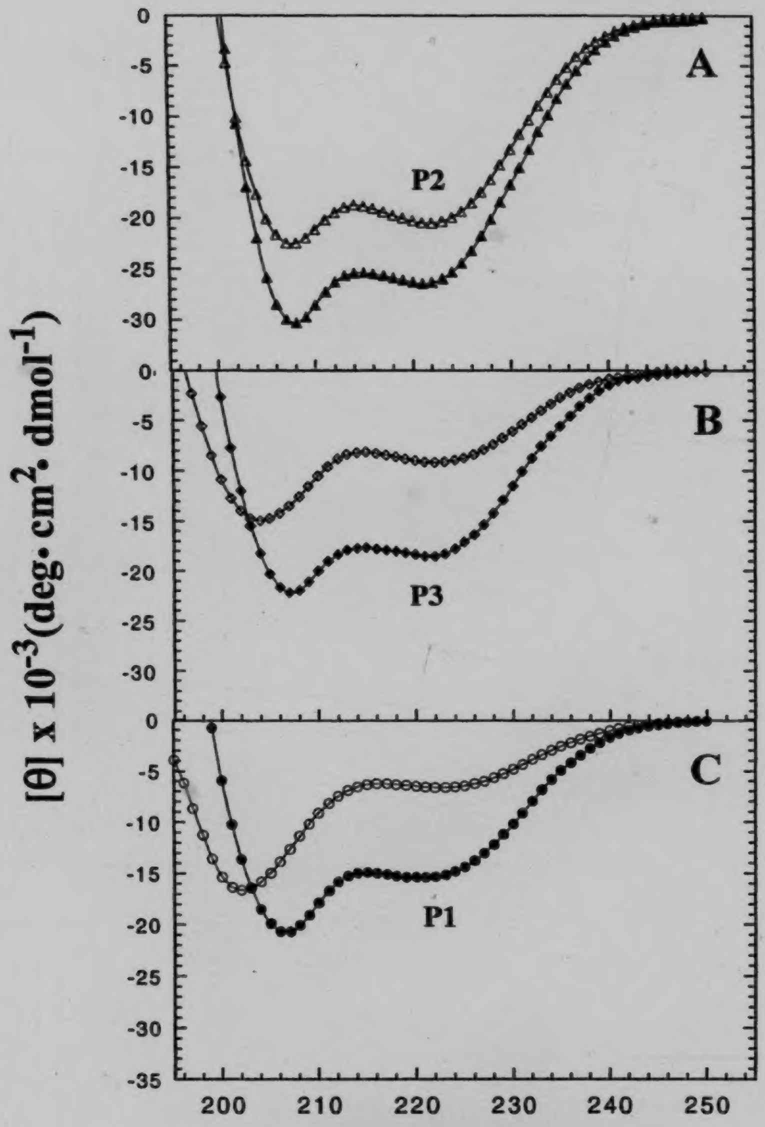

Figure III-3. Circular dichroism (CD) spectra of synthetic peptides in the absence of the disulfide-bridge. The peptides P1, P2 and P3 denote the peptide sequences shown in Fig. III-1 where the disulfide-bridge is prevented from forming by the presence of dithiothreitol (DTT). The open symbols show the CD spectrum of the peptide in benign buffer (0.1 M KCl, 0.05 M PO_4, pH 7) and closed symbols show the spectrum in the presence of 50% trifluoroethanol (TFE)-benign buffer at 25° containing 2 mM DTT.

Table III-2: Circular dichroism data of reduced Kif3A synthetic peptides

	Conc.	Number	$-[\theta]_{222}$ (deg.cm^2/dmol)[c]		Percent α-helix[d]		Number of calculated helical residues[e]		$[\theta]_{222}/[\theta]_{208}$ [f]	
Peptide[a]	μM	of residues[b]	Benign	50% TFE	Benign	50% TFE	Benign	50% TFE	Benign	50% TFE
P2	500	22	26390	--	84	--	18	--	0.99	--
P2	100	22	20500	26300	65	83	14	18	0.90	0.87
P3	100	40	9100	18500	26	52	10	21	0.73	0.83
P1	100	61	6550	15300	18	41	11	25	0.57	0.77

[a] Reduced homostranded peptides P1, P2, and P3. The amino acid sequence for each peptide is shown in Fig III-1.

[b] Number of residues per polypeptide chain excluding the CGG linker.

[c] The mean residue molar ellipticities at 222nm were measured at 25°C in benign buffer (0.1 M KCl, 0.05 M PO_4, pH 7). For samples containing TFE, the buffer was diluted 1:1 (v/v) with TFE.

[d] The percent helical content was calculated from the ratio of the observed $[\theta]_{222}$ value divided by the predicted molar ellipticity × 100. The predicted molar ellipticity was calculated from the equation $[\theta]_{222} = -40{,}000(1\text{-}4.6/n)$ for the chain length dependence of an α-helix (Gans *et al.*, 1991), where n is the number of residues in the peptide. A peptide of 22 residues has a predicted molar ellipticity of –31,600; 40 residues has a value of –35,400; 61 residues has a value of –36,980.

[e] The number of helical residues was calculated by multiplying the percent of α-helix by the number of residues in the polypeptide chain., *e.g.*, for P2 in benign medium 26,390/31,600 × 22 residues = 18.4 α-helical residues predicted in the coiled-coil.

[f] The molar ellipticity values at 222nm and 208nm for each peptide were used to calculate the ratio $[\theta]_{222}/[\theta]_{208}$.

bridge formation and to provide a flexible linker that allowed unconstrained helical alignment (O'Shea *et al.*, 1989a; Wagschal *et al.*, 1999a,b). The CD spectrum of the highly charged region alone (peptide P5) shows that the region has no secondary structure in benign medium, i.e., the spectrum is indicative of a random-coil structure (Fig. III-2B). Even in the presence of helix inducing solvent, 50% TFE, negligible α-helical structure was induced (Fig. III-2B). When this highly charged region was connected to the neck coiled-coil (peptide P1), there was no induction of α-helix in this region by the coiled-coil. In fact, the addition of the highly charged region not only decreased the molar ellipticity at 222 nm, as would be expected when adding a non-helical region to the coiled-coil (compare [θ] values of 29,700° and 8,950° for peptides P2 and P1, respectively, in benign medium; Fig. III-2C and Table III-1), but the calculated number of α-helical residues decreased to 14 compared to 21 for P2 (Table III-1). This suggests that the highly negatively charged region that follows the neck coiled-coil actually destabilizes the coiled-coil. This destabilization was confirmed by temperature denaturation studies (Fig. III-4). The T_m values for the disulfide-bridged coiled-coil and the reduced coiled-coil of peptide P2 (representing the neck coiled-coil sequence alone) were 81°C and 41.5°C, respectively. The T_m values of the disulfide-bridged and reduced peptide P1 (representing addition of the charge-rich region to the neck coiled-coil) were significantly lower than P2, i.e., 68°C and 22.6°C, respectively. Addition of 50% TFE to peptide P1, (Fig. III-2C) increases the number of α-helical residues to 20, the identical number observed for the neck coiled-coil region alone (P2) in 50% TFE (Table III-1). Similarly, peptides P1 and P3 in the reduced state at 100 μM concentration showed a reduction in the number of α-helical residues (Table III-2 and

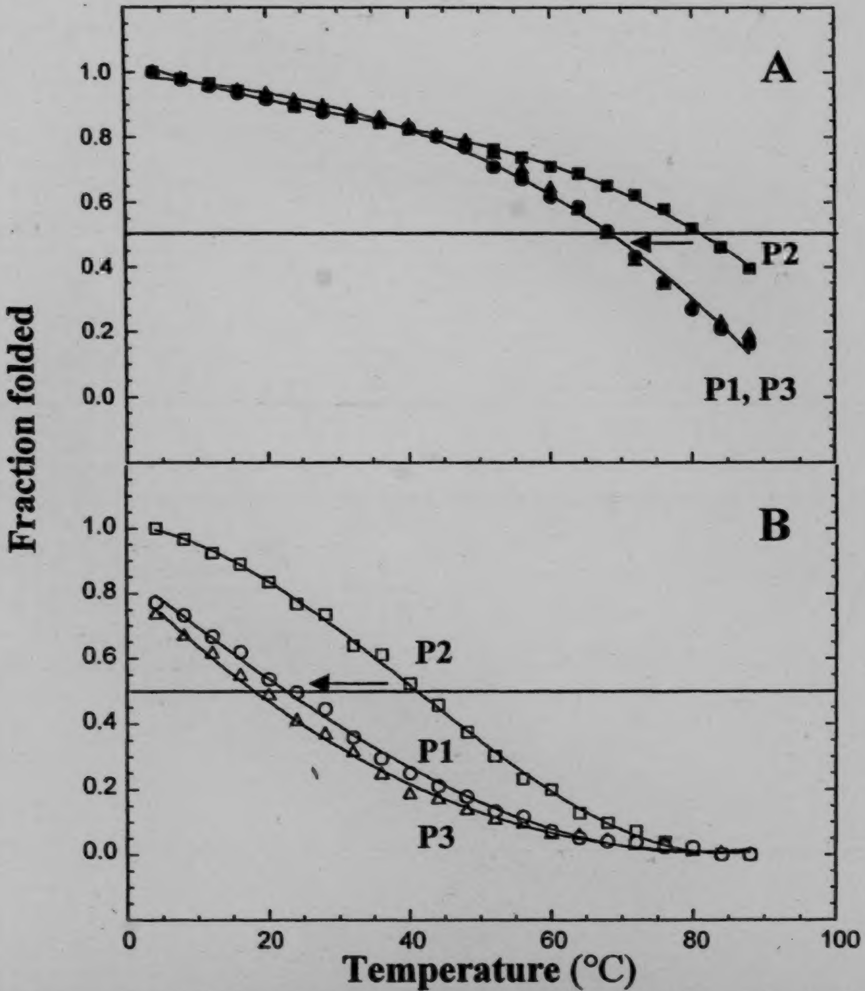

Figure III-4. Thermal denaturation of peptides P1, P2, and P3. Denaturation profiles were obtained by monitoring the ellipticity value at 222 nm for each peptide. Each peptide was incrementally heated by 2°C from 4-88°C. Reduced peptide concentration was 100 μM. The closed symbols denote the disulfide-bridged, two-stranded peptides, and the open symbols denote the peptides with the disulfide bridge reduced. P1 (circles), P2 (squares), and P3 (triangles). The arrows denote the decrease in stability by addition of highly charged regions to the coiled-coil alone (peptide P2). Peptide sequences are shown in Fig. 1. The T_m values for the reduced coiled-coils at 100 μM were P1 (23°C), P2 (41°C), P3 (18°C) and the values for disulfide-bridged coiled-coils were P1 (68°C), P2 (81°C) and P3 (68°C).

Fig. III-3) and reduced stability compared to P2 (Fig. III-4). Thus, these results clearly show that the highly charged hinge region remains unstructured in the presence of the Kif3A neck coiled coil and destabilizes the homostranded coiled-coil.

Role of charge-rich regions in dimer formation

In Kif3A, the hinge region consists of a negatively charged unit followed by a positively charged unit, while Kif3B consists of a positively charged unit followed by a negatively charged unit. In the heterodimeric complex, these charged units pair as shown in Fig. III-1, (top panel). In addition, the coiled-coil regions of Kif3A and Kif3B, though highly homologous, are different in sequence. Thus, in order to elucidate whether regions rich in charged residues can specify heterodimer formation through electrostatic attractions alone, it was decided to keep the neck coiled-coil sequence constant (Kif3A) but vary the charge-rich region that follows C-terminal to this coiled-coil and have only a single charged unit. Thus, two further peptides, P3 and P4, were synthesized, P3 containing the coiled-coil neck region of Kif3A plus the highly negatively charged region (residues 378-395 of the native sequence), while P4 contains the same coiled-coil sequence plus the highly positively charged region (residues 403-416 of the native sequence) (Fig. III-1, bottom panel). We arbitrarily chose the cut-off for the negatively charged segment of P3 at residue 395 so that this segment would have a similar length, concomitant with maximizing the number of charges, to that of the positively charged segment of P4.

The CD spectra of peptides P3 and P4 indicate that both charge extensions are not α-helical in benign medium (Fig. III-5A). The negatively charged extension on the neck

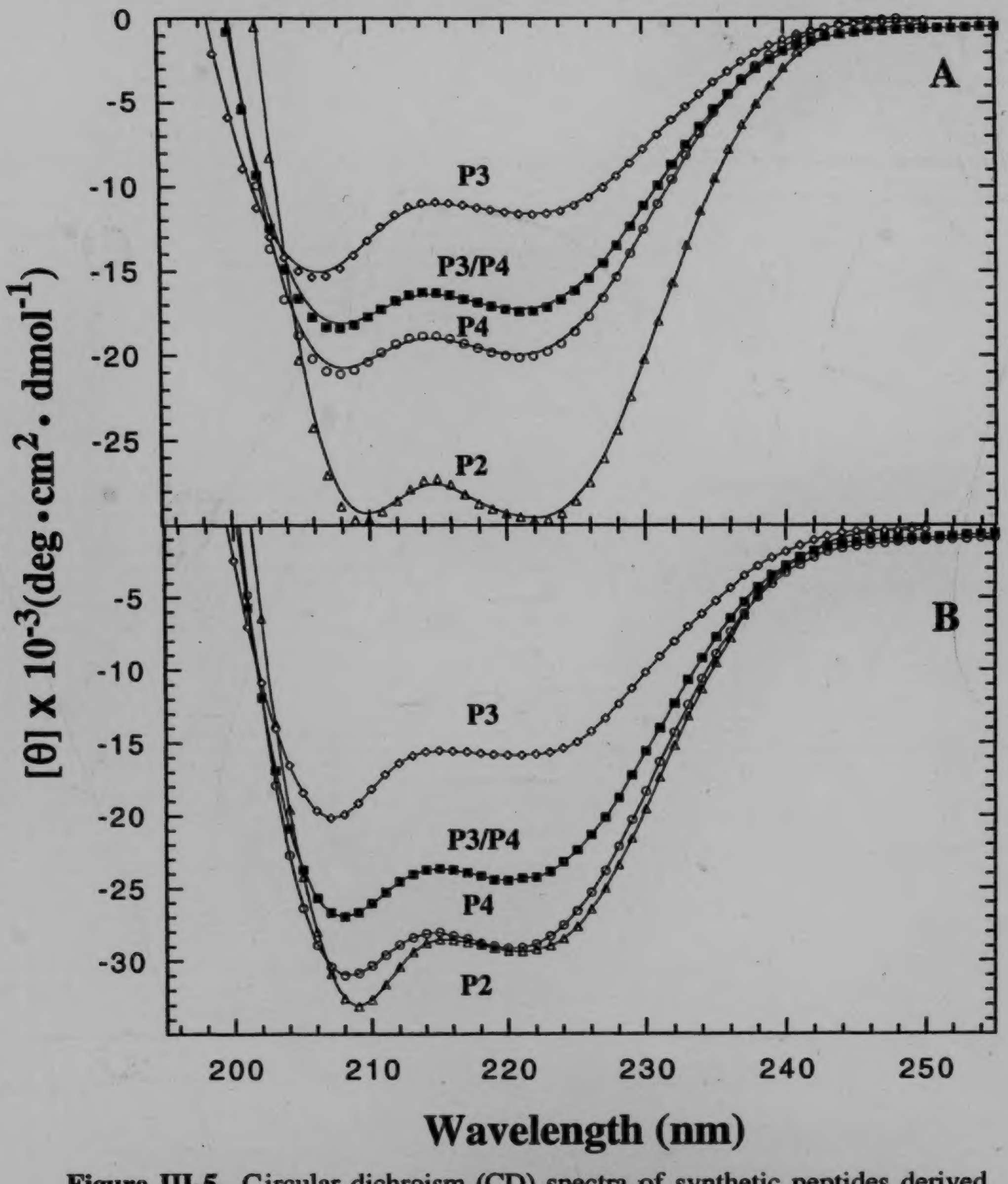

Figure III-5. Circular dichroism (CD) spectra of synthetic peptides derived from Kif3A motor protein. All peptides are disulfide-bridged two-stranded molecules, either homostranded (open symbols) or heterostranded (closed symbols). Panel A shows the peptides in benign buffer (0.1 M KCl, 0.05 M PO_4, pH 7) and Panel B shows the peptides in a 50% TFE/benign buffer at 25°C. P3 (open diamonds), P4 (open circles), P2 (open triangles) and heterostranded P3/P4 (closed squares). Peptide sequences are shown in Fig. III-1.

coiled-coil (peptide P3) decreases the molar ellipticity at 222 nm to a similar magnitude as that observed for peptide P1 (i.e., a drop to 11,700° from the 29,700° observed for P2; Fig. III-5A, Table III-1) and the number of α-helical residues was decreased to 13 in benign medium from 21 observed for the coiled-coil alone (Table III-1). Peptide P4 exhibited considerably more α-helical content than peptide P3 (20,050° for P4 compared to 11,700° for P3; Fig. III-5A, Table III-1) and contained 21 α-helical residues in benign medium, suggesting that the coiled-coil region is fully folded. These results suggest that in the homo-two-stranded coiled-coil of P3, the negative charge repulsions are very destabilizing of α-helical structure and the full folding of the coiled-coil. In contrast, the positive charge repulsions of the homo-two-stranded coiled-coil of peptide P4 have little effect on the folding of the coiled-coil region. The difference in the negatively and positively charged extensions on the coiled-coil is shown by the fact that, in the former (P3), only the coiled-coil region can be induced to fold in the presence of 50% TFE, whereas the positively charged region of P4 is inducible into α-helical structure in the presence of 50% TFE (Fig. III-5B, Table III-1). These results are in agreement with stability data shown in Fig. III-4, where the negatively charged extension on peptide P3 and its presence in peptide P1 destabilize the neck coiled-coil (compare results for P1 and P3 with those of P2) in the absence or presence of a disulfide-bridge between the individual peptide strands (Fig. III-4, Table III-3).

To determine if the charged regions C-terminal to the neck coiled-coil of Kif3A (when of opposite polarity) could specify a heterostranded peptide, we designed a redox equilibrium experiment (see Methods). Peptides P3 and P4 were oxidized to form the disulfide-bridged homo-two-stranded coiled-coils. Thus, disulfide-bridged P3 would be

Table III-3: Denaturation data for disulfide-bridged Kif3A synthetic peptides

Peptide[a]	$GdnHCl_{1/2}$[b] (M)	$Urea_{1/2}$[c] (M)	T_m[d] (°C)	$T_m$app[e] (°C)
P2	3.2	6.7	81	81
P3	2.8	3.8	68	67
P4	2.9	6.8	80	80
P3/P4	3.0	7.2	82	83

[a] Disulfide-bridged homostranded peptides, P2, P3, and P4. Disulfide-bridged heterostranded peptide P3/P4. The amino acid sequence for each peptide is shown in Fig III-1.

[b] $GdnHCl_{1/2}$ is the transition midpoint, the concentration of guanidine hydrochloride (M) required to give a 50% decrease in the molar ellipticity at 222 nm.

[c] $Urea_{1/2}$ is the transition midpoint, the concentration of urea (M) required to give a 50% decrease in the molar ellipticity at 222 nm.

[d] T_m is the observed transition midpoint in the absence of urea, the temperature (°C) at which there is a 50% decrease in the molar ellipticity at 222 nm.

[e] $T_m$app is the apparent transition midpoint in the absence of urea, obtained from extrapolation of T_m values determined in the presence of varying concentrations of urea (see Fig III-9).

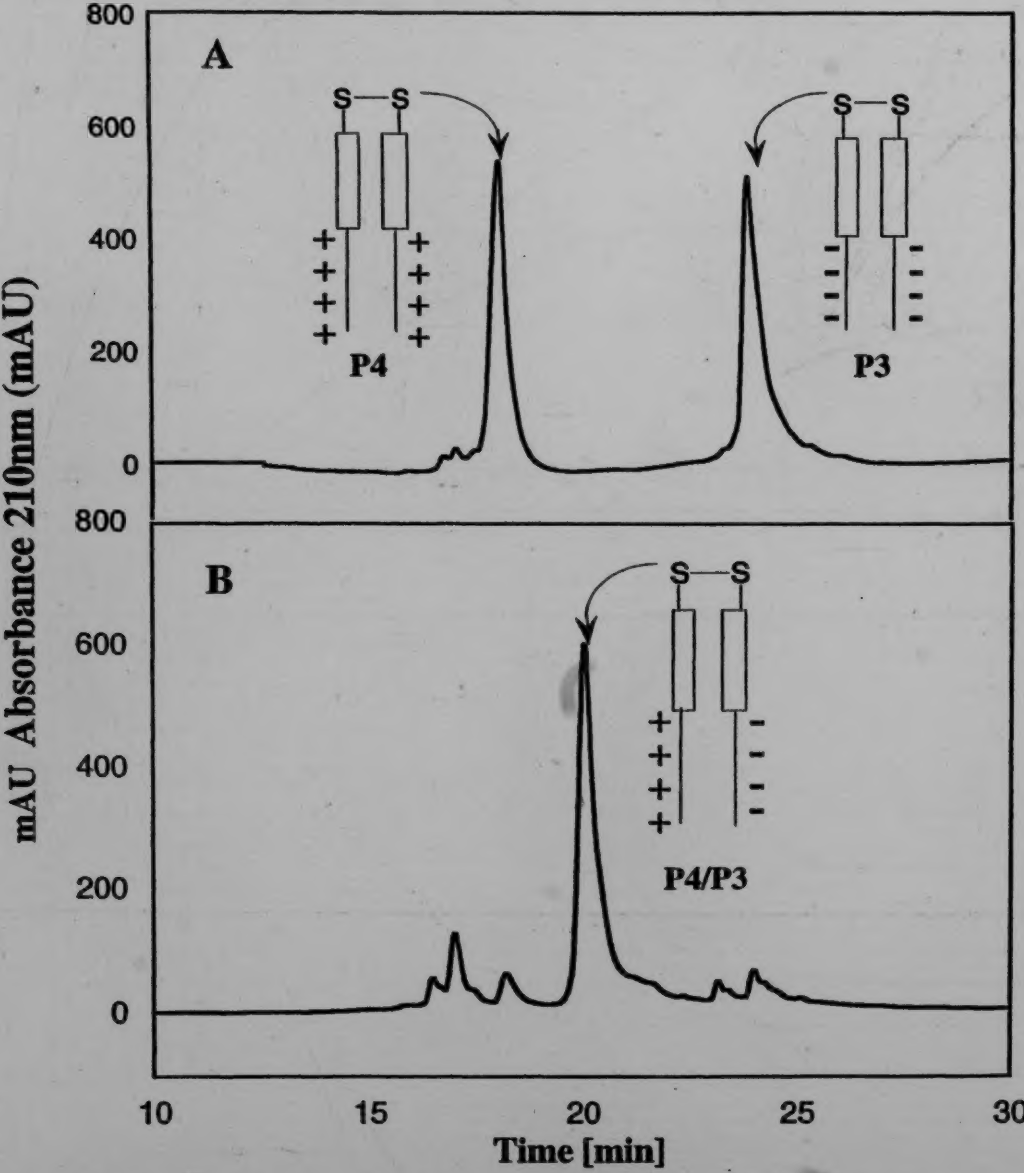

Figure III-6. RP-HPLC elution profiles of start and end points from redox experiments with oxidized P3 and P4 peptides. Panels A and B depict two time points from the redox reaction (as monitored by RP-HPLC) between the oxidized, homostranded P3 and P4 peptides. (Panel A, reaction time 0 min; Panel B, reaction time 5 min). See Methods. Peptide sequences are shown in Fig. III-1.

comprised of a coiled-coil region followed by negatively charged regions and disulfide-bridged P4 would be comprised of the coiled-coil followed by positively charged regions. These peptides were then mixed in a 1:1 ratio in the presence of a 10 times molar excess of reduced and oxidized glutathione at pH 7.0. This redox buffer allows for strand exchange and the formation at equilibrium of the most stable oxidized product. The progress of the reaction was monitored by RP-HPLC. Equilibrium was reached in 5 min. (Fig. III-6A and B) with greater than 95% formation of heterostranded peptide (reaction A, Fig. III-7). This level of reaction completeness suggests that the oppositely charged regions provide specificity and drive the exchange of peptide strands to favor the formation of the hetero-two-stranded product. Note the differences in the final equilibrium positions for the redox equilibrium experiments that involved the mixing of either P3 or P4 with P2 (reactions B and C, Fig. III-7). The formation of heterostranded products in these reactions (reactions B and C) involves only the removal of charge-charge repulsions. The final mol percent of heterostranded product is 60% in both cases. The final equilibrium position for the reaction that involved mixing P2 with N-terminally Trp-labelled P2 (P2W) yields 50% of the disulfide-bridged heterostranded peptide, (one peptide P2 and one peptide P2W; reaction D, Fig. III-7). This represents nonselective peptide exchange and would result from the random mixing of two peptides with no selectivity. Any mixture that deviates significantly from a 1:2:1 ratio of homostranded:-heterostranded:homostranded peptide implies that there is some specificity for the exchange of peptide strands to form a more thermodynamically stable product. To demonstrate that the charged attractions drive heterodimerization, we carried out the redox experiments in the presence of various concentrations of NaCl. Thus, at a

Figure III-7. The formation of oxidized, heterostranded P3/P4, P2/P3, P2/P4, and P2/P2W from redox experiments as a function of time. P2W is peptide P2 with an N-terminal tryptophan. Reaction A represents the redox results of oxidized peptides P3 and P4, (closed triangles in plot). Reactions B and C represent the redox reactions of oxidized P2 with either P3 or P4, respectively (open squares and open circles). Reaction D represents the redox reaction of peptide P2 with N-terminally labeled P2 (open diamonds). The percent heterostranded peptide was calculated by dividing the integrated area of the hetero-two-stranded HPLC peak by the total integrated area of both homo- and the heterostranded peptides for each time-point. Peptide sequences are shown in Fig. III-1.

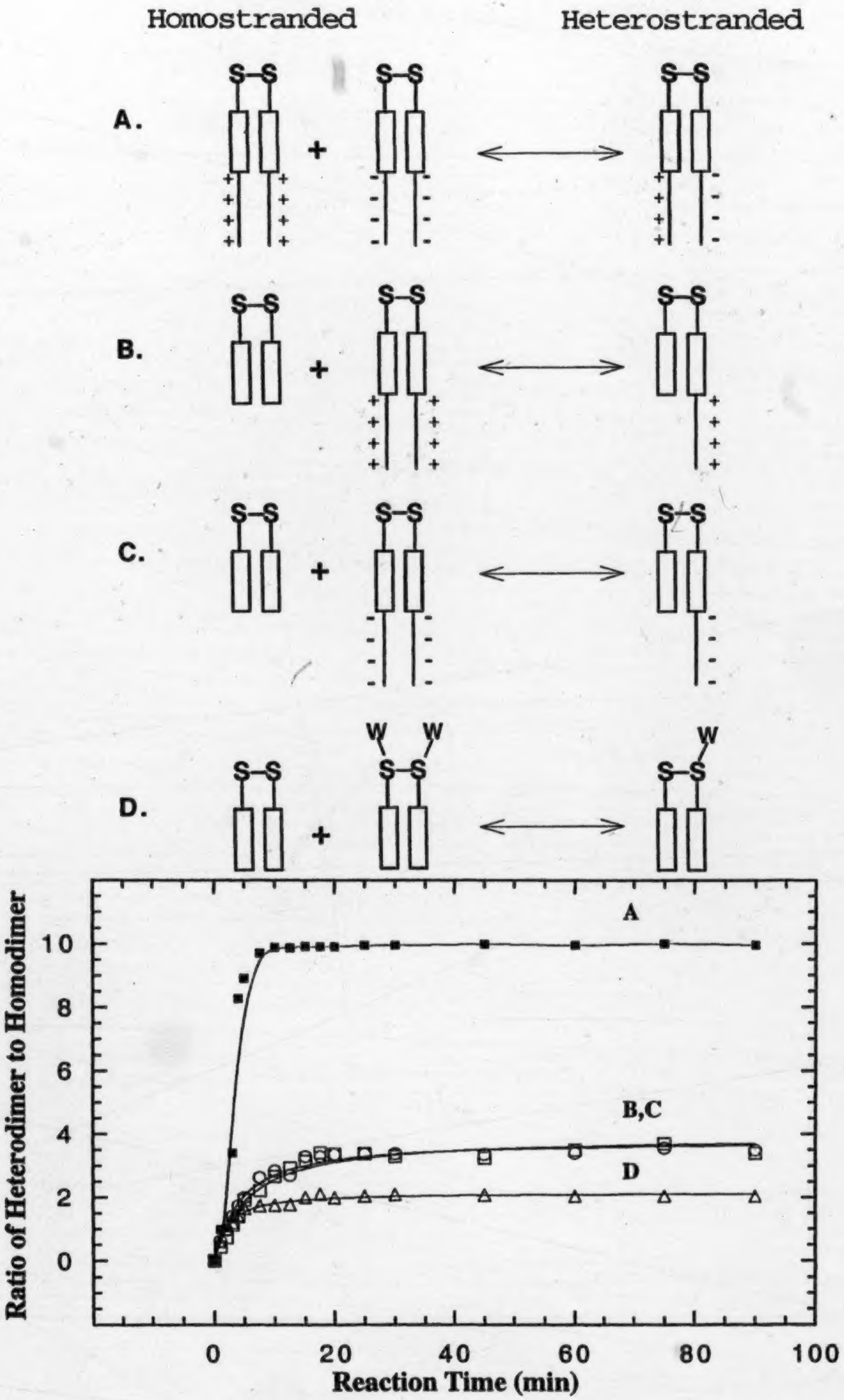
Homostranded
Heterostranded
A.
B.
C.
D.
S–S
W
+
Ratio of Heterodimer to Homodimer
Reaction Time (min)
A
B,C
D
0
2
4
6
8
10
20
40
60
80
100

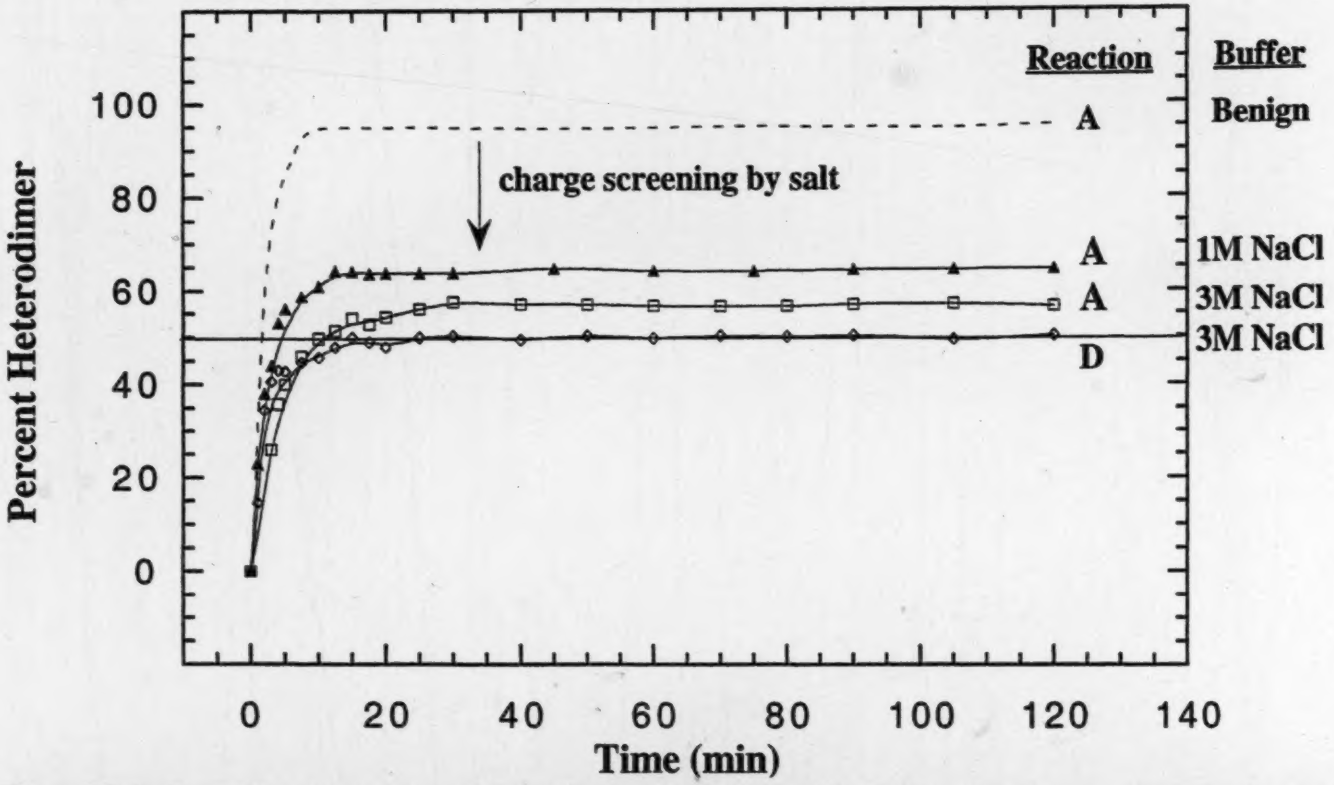

Figure III-8. Formation of heterostranded peptides in the presence of NaCl. Reaction A represents the redox results of oxidized peptides P3 and P4; dashed line is the theoretical maximum in benign medium; closed triangles, in plot, is in the presence of 1 M NaCl; open squares, in plot, is in the presence of 3M NaCl. Reaction D represents the redox reaction of peptide P2 with N-terminally Trp-labelled P2 (P2W) in the presence of 3M NaCl (open diamonds). Percent Heterostranded peptide was calculated as described in Fig. III-7.

concentration of 1M NaCl, screening of the charges on the charge-rich regions of P3 and P4 has decreased heterodimer formation to ~65% from the original 95% (Fig. III-8). A further increase in salt concentration to 3M NaCl reduces heterodimer formation even further, to a level seen for that of the oxidized P2/P3 and P2/P4 peptides in benign medium (Fig. III-7), i.e., the ratio of heterodimerization approached that for random peptide exchange [P2/Trp-labelled P2 in the absence (Fig. III-7) or presence (Fig. III-8) of 3 M NaCl].

Effect of charge-rich regions on coiled-coil stability

To assess how the stability of the Kif3A coiled-coil is affected by adding charged extensions, we denatured the α-helical structure of the neck coiled-coil using the chemical denaturants guanidine hydrochloride and urea. Since GdnHCl masks electrostatic interactions, repulsions and attractions (Monera *et al.*, 1994a), the denaturation midpoints of the disulfide-bridged homostranded peptides P2, P3 and P4 , and the disulfide-bridged heterostranded peptide P3/P4 were very similar (3.0 M ± 0.2; Table III-3), i.e., the stability results reflected the stability of the coiled-coil's hydrophobic core, which is identical in all the coiled-coil constructs (Fig. III-9A and Table III-3). Urea, an uncharged denaturant, does not mask electrostatic interactions (Monera *et al.*, 1994a) and so the stability results reflect the effect of the interactions of the charged regions on the stability of the coiled-coil (Fig. III-9 and Table III-3). The negatively charged regions destabilize the homostranded coiled-coil (compare P2, 6.7 M to P3, 3.8 M; Fig. III-9B, Table III-3), while the positively charged region has no effect on the coiled-coil stability (compare P2, 6.7 M to P4, 6.8 M; Fig. III-9B, Table III-3).

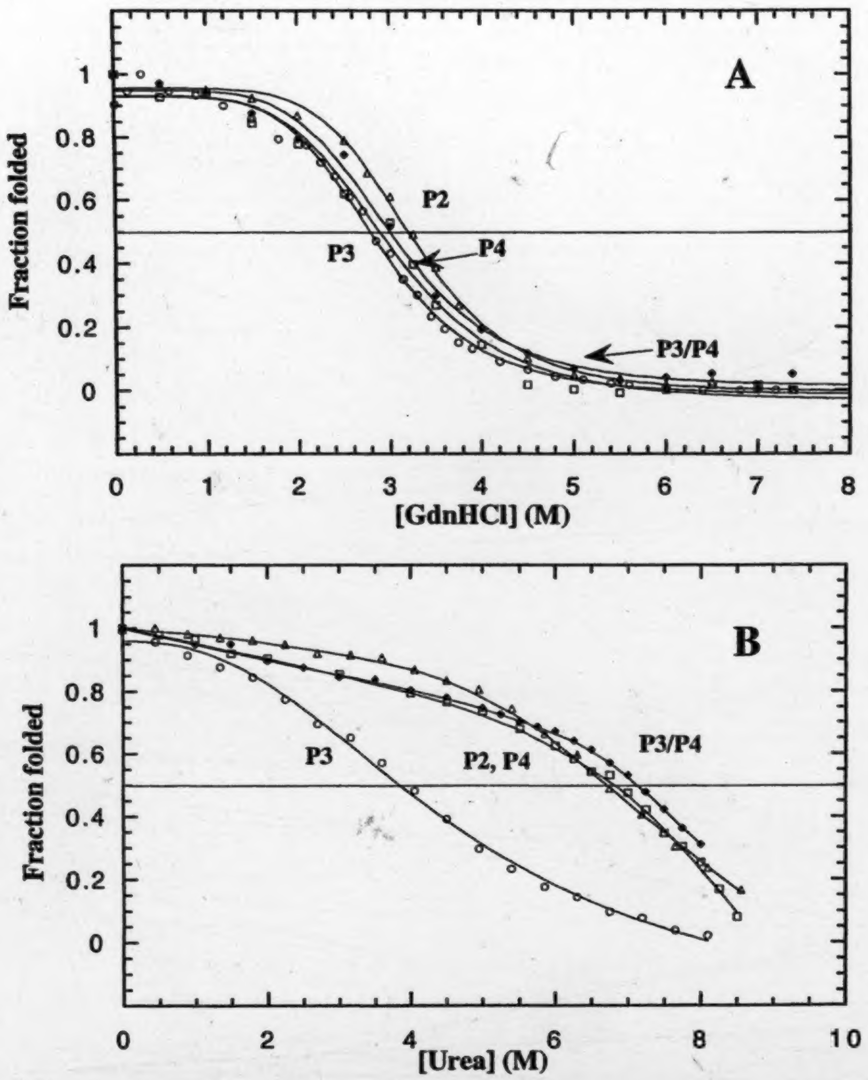

Figure III-9. Denaturation profiles of Kif3A synthetic, disulfide bridged peptides. Denaturation profiles of oxidized, Kif3A motor protein, synthetic peptides at 25°C in 0.1 M KCl, 0.05 M PO_4, pH 7 buffer with guanidine hydrochloride (Panel A) or urea (Panel B) as a denaturant. The fraction folded (f_f) of each peptide was calculated as $f_f = ([\theta] - [\theta]_u) / [\theta]_n - [\theta]_u)$, where $[\theta]$ is the observed mean residue ellipticity at 222 nm for any particular denaturant concentration and $[\theta]_n$ and $[\theta]_u$ are the mean residue ellipticities at 222 nm of the native "folded" and "unfolded" states respectively. P2 (open triangles), P3 (open circles), P4 (open squares), and heterostranded P3/P4 (closed diamonds). Peptide sequences are shown in Fig. III-1.

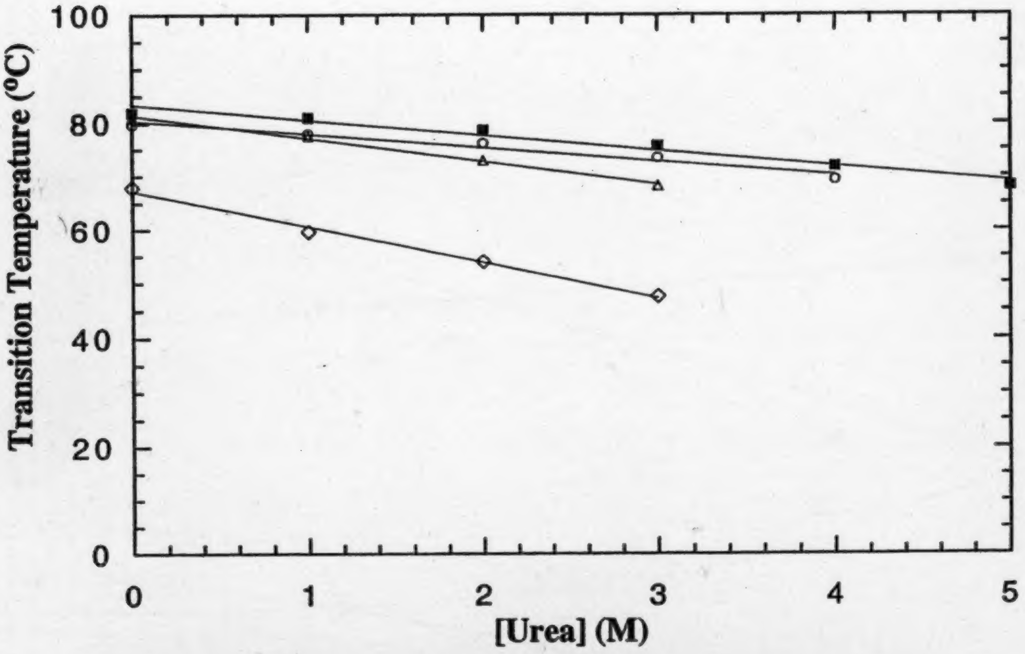

Figure III-10. Determination of apparent T_m in the absence of urea. The Kif3A synthetic, disulfide-bridged peptides were subjected to thermal denaturation in fixed concentrations of urea; the T_m values from each denaturation were plotted against urea concentration and T_m in the absence of urea was extrapolated from the acquired, T_m values in the presence of various urea concentrations. Heterostranded P3/P4 (closed squares), P4 (open circles), P2 (open triangles), and P3 (open diamonds). Peptide sequences are shown in Fig. III-1.

The hetero-two-stranded peptide (P3/P4) exhibits a coiled-coil stability ($[\text{urea}]_{1/2}$ value of 7.2 M) similar to the most stable homo-stranded peptide P4 (6.8 M). As a result of the high stability of the disulfide-bridged coiled-coils to temperature or urea denaturation, we employed a combination of physical and chemical denaturants by denaturing the coiled-coils with increasing temperature of various fixed urea concentrations. Tm and Tm app values for the peptides followed the order of stability found for the peptides using urea alone (Fig. III-10 and Table III-3). This method of temperature denaturation in the presence of various urea concentrations was carried out here for the Kif3A coiled-coils to validate this method since both temperature denaturation in the absence and presence of chemical denaturants could be performed. It is known that Kif3B is a more stable coiled-coil and the disulfide-bridged peptides of Kif3B could not be denatured by temperature alone (unpublished results). There is a significant advantage to studying the disulfide-bridged peptides in comparative stability studies since there is no concentration dependence on stability with the removal of the monomer-dimer equilibrium.

C. Discussion

We have explored the ability of oppositely charged regions to specify heterodimer formation in coiled-coils, restricting our analysis to Kif3A and studying its neck coiled-coil (residues 356-377) and its charged region (residues 378-416) (Fig. III-1). The charged region was examined by CD spectroscopy and it was found to adopt a random coil structure in the absence or presence of the coiled-coil. The negatively and positively charged regions (residues 378-395 and 403-416, respectively) were added to the C-terminus of the neck coiled-coil of Kif3A. The peptides were further linked using a disulfide bridge from the CGG flexible linker added to the N-terminus to form homo-two-stranded peptides selectively with either negatively or positively charged extensions on the C-termini of the peptide strands.

To assess the ability of the charged regions to specify heterodimer formation of a coiled-coil, we mixed disulfide bridged homo-two-stranded peptides with negatively and positively charged extensions together in redox buffer (Lavigne *et al.*, 1995; O'Shea *et al.*, 1989b). Contrary to the findings of De Marco *et al.*, 2001, where it was suggested that the charged regions were not absolutely necessary for heterodimer formation, we observed that oppositely charged regions specified the formation of a hetero-two-stranded peptide, hetero in the sense that it has one negatively charged extension and one positively charged extension on an identical sequence in the coiled-coil region (Fig. III-1, peptides 3 and 4, and Fig. III-6B). Furthermore, mixing the disulfide-bridged Kif3A neck coiled-coil together with an N-terminal tryptophan-labeled coiled-coil, led to a 1:2:1 ratio of homostranded:heterostranded:N-terminally labeled homostranded peptides, the ratio expected from a nonspecific random pairing of peptides (Fig. III-7, reaction D). The ability of the oppositely charged extensions on the C-terminus of the neck coiled-coil of the Kif3A to form preferentially a heterostranded peptide was diminished through charge screening in the presence of NaCl (Fig. III-8). Similar charge screening by salt has been described in the classic study on electrostatics by Schreiber and Fersht (1996) and Kohn *et al.* (1997).

To assess how charged extensions may affect the stability of the neck coiled-coils, we denatured the peptides in urea, a denaturant shown to reveal the effects of electrostatics on protein stability (Hagihara *et al.*, 1994; Kohn *et al.*, 1995a,b; Monera *et* *al.*, 1994b). The results indicate a decrease in the stability of the coiled-coil by the addition of negatively charged residues in the homostranded peptide. Contrary to what was expected, the addition of the positively charged region (residues 403-416) of Kif3A C-terminally to the neck coiled-coil did not affect the stability of the coiled-coil. The pairing of a negatively charged extension with a positively charged extension gave a peptide with stability similar to the homostranded peptide having positive extensions. The net charge of the coiled-coil alone at neutral pH is essentially 0. The homostranded peptide with negative extensions has a net charge of –18; the homostranded peptide with positively charged extensions has a net charge of +16; and the heterostranded molecule has a net charge of only –1. Thus, it is the electrostatic attractions that drives formation of the heterostranded molecule. Interestingly, the removal of charge-charge repulsions (either negatively charged or positively charged) had little effect on heterodimerization (Fig. III-7, reactions B and C). That is, it is the electrostatic attractions that drive the specificity of heterodimerization, not the removal of positive or negative charge-charge repulsions.

In accordance with the postulate of Rashid *et al.* (1995) we see that complementary charged regions can specify hetero-two-stranded coiled-coil formation. However, our results suggest that it is not through the destabilization of the homodimers relative to the heterodimer; for while the pairing of negatively charged regions led to a decreased stability in the homostranded Kif3A neck region, the pairing of positively charged regions did not. In fact, the addition of the positively charged regions had little effect on stability of the coiled-coil (Table III-3). The heterostranded coiled-coil has not lost any stability and, indeed, has a stability similar to that of the most stable homodimeric coiled-coil, i.e., formation of the heterostranded coiled-coil maintains stability similar to that of the most stable homostranded molecule (Table III-3) and the unstructured oppositely charge regions drive specificity. The same phenomenon has been observed for the Fos-Jun heterodimeric coiled-coil. The Fos-Jun heterodimer was shown to form to the exclusion of homodimers. The stability of the heterodimeric coiled-coil Fos-Jun was shown to be similar to the stability of the Jun homodimer, the most stable homodimer (O'Shea *et al.*, 1989b). The major difference between these two systems is that in the Fos-Jun coiled-coil, control of specificity is within the coiled-coil sequence, whereas here unstructured charged regions outside the coiled-coil sequence are responsible for heterodimer formation.

Lysine residues have been shown to destabilize coiled-coils through electrostatic repulsions at the dimer interface (*e* and *g* positions) of the coiled-coil (Monera *et al.*, 1994b; Zhou *et al.*, 1994). The positively charged region of Kif3A is outside the coiled-coil, does not adopt any structure in benign conditions and does not show any effect on stability, suggesting that unstructured positively charged regions are not repulsive, unlike negatively charged unstructured regions. It is possible that the 4-carbon aliphatic side-chain of lysine provides a counteractive nonspecific hydrophobic force that negates the repulsive force of the side-chain ε-amino group or simply allows the positively charged groups to remain at a greater distance from each other.

The results of De Marco *et al.* (2001), using truncated mutants of Xklp3A and Xklp3B (highly homologous in the neck-hinge region to MmKif3A and MmKif3B) showed in a co-translation experiment in an *in vitro* reticulocyte system (complex formation was tested by immunoprecipitation with antibodies) that no heterodimers were observed unless the C-terminal four heptads of the stalk (in the region of residues ~570 to 598) distant from the neck coiled-coil region were present. Their interpretation of their results was that the charged regions and neck coiled-coil do not have any significant role in heterodimer formation. However, to clarify further the heterodimerization and function of the constructs described by De Marco *et al.* (2001), it will be necessary to express individually and purify *in vitro* the individual molecules and truncated constructs for biophysical and structural analysis in detail. Although we cannot explain their results at this time, it is extremely clear from the studies reported here that the neck coiled-coil in Kif3A can form an autonomous folded coiled-coil on its own or in the presence of the charged extensions and that these oppositely charged extensions can drive heterodimer formation when these regions are studied in solution independently from the complete protein. It is also conceivable that other interactions in the native protein (*e.g.* head and/or stalk regions) could modulate the interactions identified with the short peptides in this study to provide greater control of heterodimerization. Thus, the neck coiled-coil with the charged hinge region, unidentified interactions in the head region and the C-terminal region in the stalk identified by De Marco *et al.* (2001) are all essential and could work in concert to control/modulate heterodimerization.

CHAPTER IV

An investigation into the effects of highly charged regions on the stability of the neck region coiled-coil of kinesin-like motor protein Kif3B[2]

A. Introduction

Along with actin and intermediate filaments, microtubules comprise the cytoskeleton of eukaryotic cells. Intracellular transport occurs along these filamentous structures, with unconventional myosins using the actin based skeleton, and dynein and kinesin using microtubules. Conventional kinesin has been characterized and has been shown to be composed of two heavy chains and two light chains (Bloom et al., 1988; Kuznetsov et al., 1988; Hirokawa et al., 1989). Another protein in the kinesin superfamily of proteins to be completely characterized was found to be a heterotrimeric complex composed of two motor subunits with microtubule activated ATPase activity and an accessory protein (Wedaman et al., 1996). This heterotrimeric protein was termed Kinesin-II but is also called the Kif3 complex where Kif represents the kinesin family (Yamazaki et al., 1996).

Cole et al. (1993) began the sequence identification and characterization for the subunits of the Kif3 complex, isolated from sea urchin. The 85kDa subunit was fully sequenced, and termed spKRP85 for *Strongylocentrotus purpuratus* **K**inesin **R**elated **P**rotein-85kDa. The heterotrimeric complex was shown to move in the anterograde direction on microtubules (Cole et al., 1993). Kondo et al. (1994) reported a mouse analogue, Kif3A for **K**inesin **F**amily. In 1995, Rashid et al. published the sequence of the 95kDa subunit found in sea urchin, and Yamazaki et al. published the sequence of Kif3B. In the following year, the accessory proteins in sea urchin and mouse were sequenced and reported (Wedaman et al., 1996; Yamazaki et al., 1996). These proteins have since been named KAPs for **K**inesin-like **A**ssociated **P**roteins.

---

[2] A version of this chapter has been submitted for publication: Chana, MS, Tripet, BP, Mant, CT, and Hodges, RS. (2002). *Journal of Protein Science*, In Submission.

Upon analysis of the spKRP85/95 and Kif3A/B motor subunits, it was noted that the NH_2 termini (approximately residues 1-350) were likely to comprise a motor domain similar to conventional kinesin, based on sequence homology. The NH_2 terminal domains were predicted to be separated from the small globular COOH terminal domains by a central α-helical segment thought to form a coiled-coil similar to the one shown for conventional kinesin (de Cuevas et al., 1992). A stalk-like structure similar to that seen in conventional kinesin was noted for the Kif3A/B complex in electron micrographs (Yamazaki et al., 1995). See Fig. IV-1 for a schematic of the structure of the kinesin-like Kif3A/Kif3B heterodimer.

From sequence analysis, it appeared that spKRP85 and Kif3A were orthologues, having a 73% homology along their full lengths, and it was predicted that spKRP95 would be the orthologue to Kif3B (Rashid et al., 1995). It is interesting to note that while spKRP85 has 699 amino acids, Kif3A is comprised of 701, while both spKRP95 and Kif3B were originally reported to have 742 amino acids, with the extra residues found at the COOH termini (Rashid et al., 1995; Yamazaki et al., 1995).

Within the same organism, spKRP85 was found to have 52% identity with the full-length spKRP95, and 73% within the motor region. Kif3A and Kif3B were found to have 47% identity along their full length and 61% in their motor regions. Interestingly, in the similarity profiles between spKRP85 and spKRP95 or Kif3A and Kif3B, a small portion of the sequence was found to have strikingly low homology. This region was located between the putative neck coiled-coil and coiled-coil stalk domain and had dramatically low probability for α-helix formation (Cole et al., 1993; Rashid et al., 1995; Yamazaki et al., 1995). These regions in spKRP85/Kif3A had a cluster of negatively charged amino acids, 11 and 13, respectively. This negatively charged segment was followed by a segment of positively charged amino acids, 9 for both proteins. This region of sequence disparity in spKRP95/Kif3B was found to begin with a stretch of positively charged amino acids, 8 in each protein, followed by a segment of negatively charged amino acids, 11 and 14, respectively.

It was postulated that these complementary charged regions could help the motor subunits form spKRP85/95 and Kif3A/B heterodimers through the destabilization of homodimers, and stabilization of heterodimers through electrostatic attractions (Rashid et al., 1995).

DeMarco et al. (2001) demonstrated the necessity for the C-terminal coiled-coil region in the stalk domain (region 515-597 of Xklp3A and region 515-592 of Xklp3B) to form heterodimers and that heterodimers could form between the C-terminal regions of the stalk in the absence of the highly charged regions and neck coiled-coil (approximately 350-415). Recently, Chana et al. (2002) showed that the neck coiled-coil in Kif3A can form an autonomous folded coiled-coil on its own or in the presence of the charged extensions and that these oppositely charged extensions can drive heterodimer formation when these regions are studied in solution independent of the complete protein. Thus, it seems reasonable to assume that the neck coiled-coil with the charged hinge region and the C-terminal region in the stalk could both be essential and work in concert to control/modulate heterodimerization.

To lend further support to the importance of the neck coiled-coil and charged extensions in heterodimerization, the present study was designed to: (1) show that the predicted Kif3B neck coiled-coil region (residues 351-372) would form an autonomous folding unit and compare its stability to the Kif3A coiled-coil; (2) identify whether there is structure in the charged hinge region of Kif3B (residues 373-411); (3) determine whether negatively and positively charged extensions can affect the stability of the putative Kif3B coiled-coil neck region in a similar manner to Kif3A; (4) show whether electrostatics specify heterodimerization even when the two strands of the coiled-coil are identical and (5) determine whether coiled-coil stability can affect the rate at which the oppositely charged extensions can drive the formation of the heterostranded peptide when the strands of the coiled-coil are identical.

B. Results

Folding of the predicted neck coiled-coil region of Kif3B

As a first step toward characterizing the biophysical properties of the neck region of Kif3B and the putative role of its coiled-coil and hinge region, it was necessary to determine whether the putative neck coiled-coil-forming sequence of Kif3B would form a two-stranded α-helical coiled-coil in the absence of the rest of the Kif3B molecule (Fig. IV-1). In this regard, we chose to study a series of disulfide-bridged two-stranded peptides (Fig. IV-2) to remove the concentration dependency of the monomer/dimer equilibrium found in non-crosslinked peptides. The peptides shown in Fig. IV-2 were synthesized and subsequently analyzed by circular dichroism spectroscopy (CD).

Peptide P7 (Fig. IV-2), representing the putative neck coiled-coil region (residues 351-372), showed a CD spectrum (Fig. IV-3A) characteristic of a folded α-helical coiled-coil with a high molar ellipticity value, double minima at 208 nm and 222 nm and an α-helical content of 87%, giving 19 calculated α-helical residues out of 22 (Table IV-1) (Gans et al.,1991). In addition, the peptide appeared to be fully folded in benign medium, since there was no change in the molar ellipticity value at 222 nm when the helix inducing solvent, trifluoroethanol (TFE), was added. The $[\theta]_{222}/[\theta]_{208}$ ratio greater than 1.0 is a value used to characterize coiled-coils in benign medium and this value decreases to ~0.90 in the presence of the helix-inducing solvent TFE (Lau et al., 1984a). Although TFE stabilizes the helical structure of the individual strands of a coiled-coil, it denatures tertiary and quaternary structure, i.e., the coiled-coil is dissociated to single-stranded α-helices as was clearly demonstrated by high-performance size-exclusion chromatography of coiled-coils (Lau et al., 1989a, b; Monera et al., 1993; Zhou et al., 1992 a, b; Mant et al., 1997). The value observed for the $[\theta]_{222}/[\theta]_{208}$ ratio for the disulfide-bridged Kif3B peptide, P7, was 1.05 in benign medium and 0.89 in the presence of 50% TFE (Table IV-1). Kif3B forms a heterodimer with Kif3A in vivo (Yamazaki et al., 1995), yet we observe in vitro that Kif3B's neck region forms a homo-stranded coiled-coil. Thus, there appears to be no intrinsic sequence specificity in the Kif3B neck coiled-coil region that precludes its homodimer formation.

Secondary structure of the charge-rich hinge region

We then addressed the question whether the charge-rich region that follows the neck coiled-coil region of Kif3B has any secondary structure. We prepared two disulfide-bridged two-stranded peptides, peptide P10 (Kif3B residues 373-411) which represents the highly charged region on its own, and peptide P6, which contains the coiled-coil and the highly charged region together (Kif3B residues 351-411) (Fig. IV-2, top panel). The

CD spectrum of the highly charged region alone showed no apparent secondary structure and the spectrum is indicative of a random-coil (Fig. IV-3B). Even in the presence of helix inducing solvent, 50% TFE, very little α-helical structure could be induced (Fig. IV-3B). When this highly charged region was connected to the C-terminus of the neck coiled-coil, there was no increase in α-helix over that observed for the coiled-coil alone. In fact, addition of the highly charged region decreased the molar ellipticity at 222nm. This is to be expected when residues in a non-helical conformation are added to the coiled-coil region. The calculated number of α-helical residues decreased from 19 in peptide P7 to 17 in peptide P6 in benign medium (Table IV-1). This suggests that the highly positively charged region that follows the coiled-coil does not significantly affect the coiled-coil. The spectra in Fig. IV-3C represent the additivities of the absorption spectra for the peptides in panels A and B. Thus, the peptide appears to have a folded α-helical section and an unfolded random coil section.

Role of oppositely charged regions in dimer formation

To determine how the oppositely charged unstructured extensions, when added C-terminally to the neck coiled-coil of Kif3B, would affect the structure, stability and heterodimerization of the coiled-coil, we prepared peptides P8 and P9 (Fig. IV-2 top panel). We linked the peptides by the N-terminal cysteine residues to create disulfide-bridged homo-two-stranded P8 and P9 peptides as well as hetero-two-stranded P8/P9. The results of our circular dichroism (CD) analysis are presented in Fig. IV-4. The CD spectrum of peptide P9 suggests that the negatively charged extension is not helical in benign medium (Fig. IV-4A) which is evident by the loss in the overall molar ellipticity value for P9 compared to P7. However, the extension does not appear to decrease the

Figure IV-1. Top Panel shows a schematic of the kinesin-like heterodimeric motor protein (Kif3A/Kif3B). This protein consists of two different polypeptide chains Kif3A and Kif3B which resemble conventional kinesin heavy chains. Each polypeptide chain contains an N-terminal globular motor domain, followed by a potential neck coiled-coil region, a highly charged hinge region, a coiled-coil stalk region and the C-terminal tail region (which binds to an accessory unit, the so-called kinesin associated protein KAP). The middle panel compares the putative neck coiled-coil regions of Kif3B and Kif3A. The regions of the sequence that are identical are boxed. The **a** and **d** positions denote the hydrophobic core positions of the heptad repeat **abcdefg** that form the coiled-coil. The (...) show the interactions between **a** and **a′** and **d** and **d′** in the heterodimeric coiled-coil. The lower panel shows the hinge region that follows the coiled-coil sequence in Kif3A and Kif3B. The positively charged and negatively charged regions are boxed.

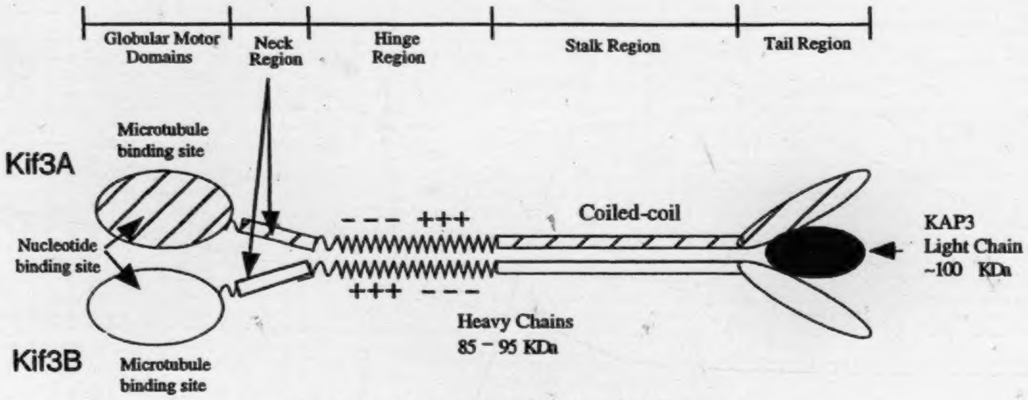
Globular Motor Domains
Neck Region
Hinge Region
Stalk Region
Tail Region
Kif3A
Microtubule binding site
Nucleotide binding site
--- +++
+++ ---
Coiled-coil
KAP3 Light Chain ~100 KDa
Heavy Chains 85 – 95 KDa
Kif3B
Microtubule binding site

Kinesin-like Kif3A/Kif3B Heterodimer

Putative Neck Coiled-coil Region

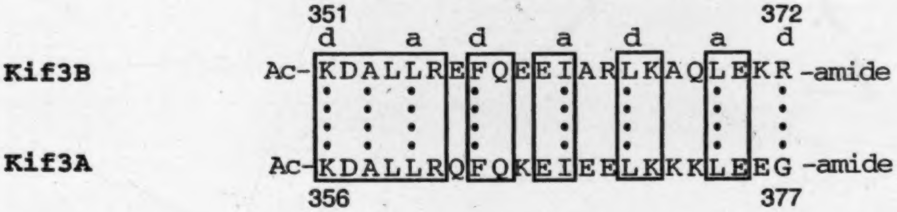
351
372
d a d a d a d
Kif3B
Ac-KDALLREFQEEIARLKAQLEKR-amide
Kif3A
Ac-KDALLRQFQKEIEELKKKLEEG-amide
356
377

Hinge Region

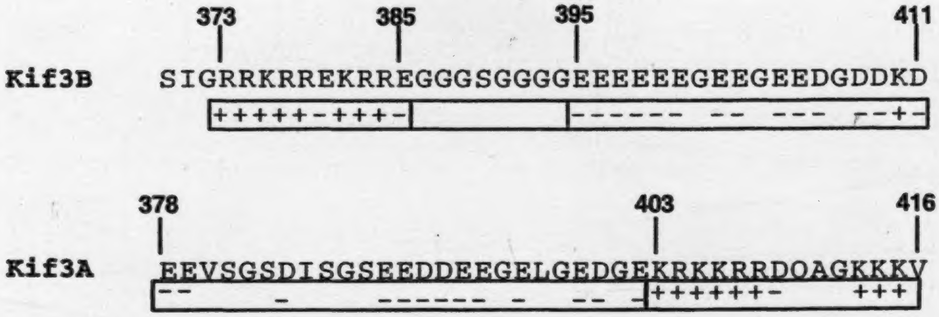
373
385
395
411
Kif3B
SIGRRKRREKRREGGGSGGGEEEEEEGEEGEEDGDDKD
+++++-+++-
------ -- --- --+-
378
403
416
Kif3A
EEVSGSDISGSEEDDEEGELGEDGEKRKKRRDQAGKKKV
-- - ------ - -- -
++++++- +++

Figure IV-2. Amino acid sequences of the Kif3B and Kif3A peptides used in this study. P6-P10 are Kif3B peptides and P2 to P4 are Kif3A peptides described previously (Chana et al., 2002). The boxed regions below the peptide sequences denote the predicted coiled-coil region and the highly negatively charged and positively charged regions. The negatively charged residues and positively charged residues are indicated by a (-) or (+) sign, respectively. CGG represents a flexible linker added N-terminally to each peptide. Ac- denotes N^{α}-acetyl and –amide denotes C^{α}-amide. All of the synthetic peptides are aligned to the native sequence except P9, which consists of the coiled-coil region 351-372 combined with the negatively charged region 394-411, deleting the positively charged and glycine spacer region 373-393.

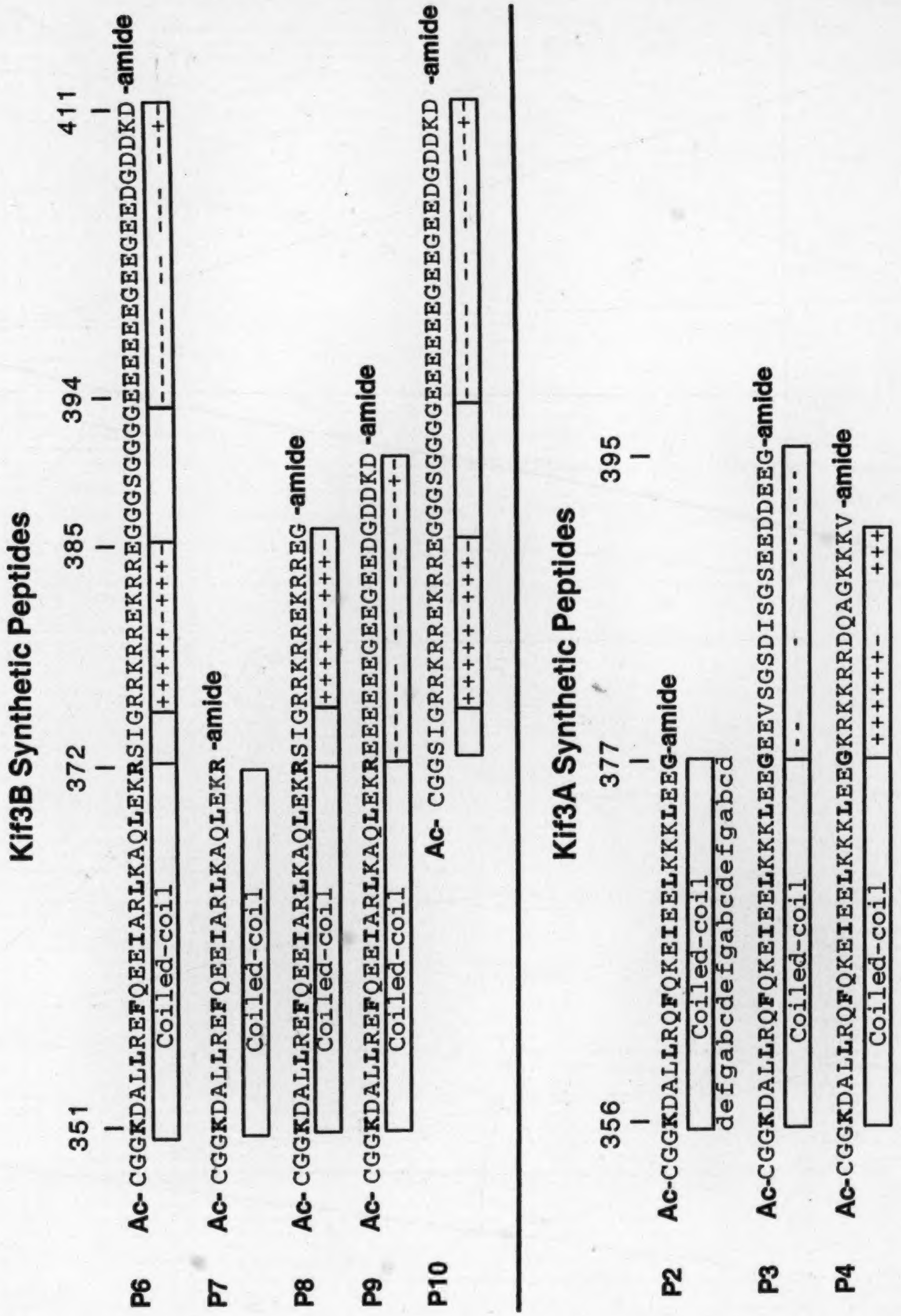
Kif3B Synthetic Peptides
351
372
385
394
411
P6 Ac- CGGKDALLREFQEEIARLKAQLEKRSIGRRKRREKRREGGGSGGGGEEEEEEGEEGEEDGDDKD -amide
Coiled-coil
+++++-+++-
------ -- --- --+-
P7 Ac- CGGKDALLREFQEEIARLKAQLEKR -amide
Coiled-coil
P8 Ac- CGGKDALLREFQEEIARLKAQLEKRSIGRRKRREKRREG -amide
Coiled-coil
+++++-+++-
P9 Ac- CGGKDALLREFQEEIARLKAQLEKREEEEEEGEEGEEDGDDKD -amide
Coiled-coil
------ -- --- --+-
P10 Ac- CGGSIGRRKRREKRREGGGSGGGGEEEEEEGEEGEEDGDDKD -amide
+++++-+++-
------ -- --- --+-
Kif3A Synthetic Peptides
356
377
395
P2 Ac-CGGKDALLRQFQKEIEELKKKLEEG-amide
Coiled-coil
defgabcdefgabcdefgabcd
P3 Ac-CGGKDALLRQFQKEIEELKKKLEEGEEVSGSDISGSEEDDEEG-amide
Coiled-coil
-- - ------
P4 Ac-CGGKDALLRQFQKEIEELKKKLEEGKRKKRRDQAGKKKV -amide
Coiled-coil
++++++- +++

Figure IV-3. Circular dichroism (CD) spectra of synthetic peptides. CD spectra of disulfide-bridged two-stranded peptides in benign buffer (0.1 M KCl, 0.05M PO_4,pH 7) (open symbols) and in the presence of 50% trifluoroethanol (TFE) –benign buffer (closed symbols) at 25^{O}C. Panel A (peptide P7), Panel B (peptide P10), and Panel C (peptide P6). The peptide sequences are shown in Fig IV-1.

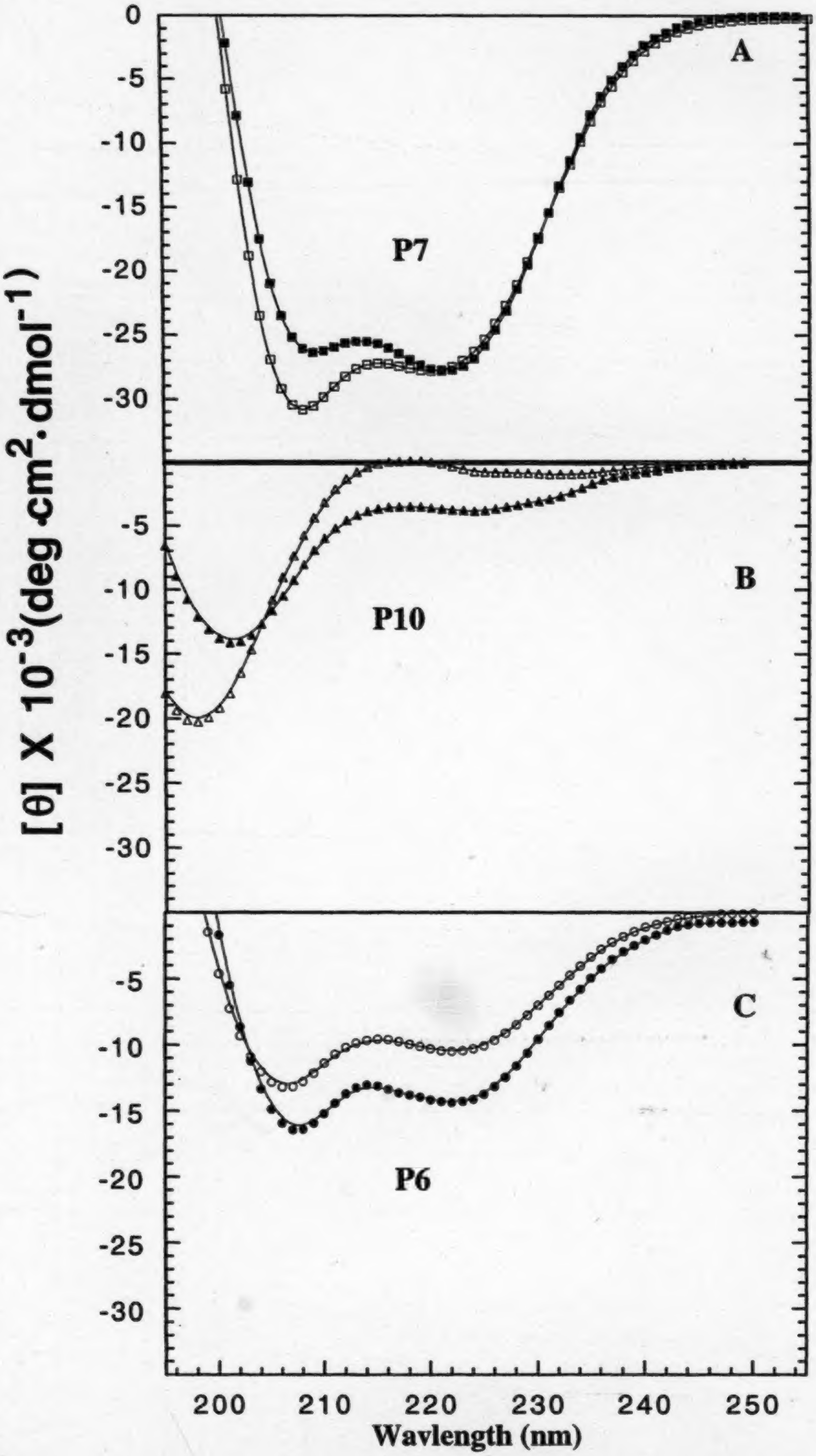
[θ] X 10^{-3}(deg·cm^2·dmol^{-1})
A
P7
B
P10
C
P6
0
-5
-10
-15
-20
-25
-30
200
210
220
230
240
250
Wavlength (nm)

Table IV-1: Circular dichroism data of Kif3B synthetic peptides

	number	$-[\theta]_{222}$ (deg·cm^2/dmol)[c]		% α-helix[d]		Number of calculated helical residues[e]		$[\theta]_{222}/[\theta]_{208}$[f]	
Peptide[a]	of Residues[b]	benign	50% TFE	benign	50% TFE	benign	50% TFE	benign	50% TFE
P6	61	10350	14350	28	39	17	24	0.83	0.90
P7	22	27500	27500	87	87	19	19	1.05	0.89
P8	36	22000	29350	63	84	23	30	0.93	0.90
P9	40	16800	18800	47	53	19	21	0.86	0.83
P8/P9	40/36	20000	23550	57	67	22	25	0.93	0.88

[a] Disulfide-bridged homostranded peptides P6, P7, P8, and P9. Disulfide-bridged heterostranded peptide P8/P9. The amino acid sequence for each peptide is shown in Fig IV-2.

[b] Number of residues per polypeptide chain.

[c] The mean residue molar ellipticities at 222nm were measured at 25°C in benign buffer (0.1 M KCl, 0.05 M PO_4, pH 7). For samples containing TFE, the buffer was diluted 1:1 (v/v) with TFE.

[d] The percent helical content was calculated from the ratio of the observed $[\theta]_{222}$ value divided by the predicted molar ellipticity × 100. The predicted molar ellipticity was calculated from the equation $[\theta]_{222} = -40 \times 10^3 \times (1\text{-}4.6/n)$ for the chain length dependence of an α-helix (Gans et al., 1991), where n is the number of residues in the peptide. A peptide of 22 residues has a predicted molar ellipticity of –31,600.

[e] The number of helical residues was calculated by multiplying the % α-helix by the number of residues in the polypeptide chain., e.g., for P7 in benign medium 27,500/31,600 × 22 residues = 19 α-helical residues predicted in the coiled-coil.

[f] The molar ellipticity values at 222nm and 208nm for each peptide were used to calculate the ratio $[\theta]_{222}/[\theta]_{208}$.

number of helical residues in the coiled-coil since the number of calculated helical residues, 19, is the same for the coiled-coil peptides P7 and P9 (Table IV-1). In contrast, the positively charged extension on P8 actually increases the helical content slightly since the number of calculated helical residues is 23 compared to 19 for peptide P7 (Table IV-1). This small increase in the number of α-helical residues is probably due to the removal of end effects. It is obvious that both charged extensions on the coiled-coil are mainly unstructured since the molar ellipticity decreases for P8 and P9 or P8/P9 relative to P7 (Fig. IV-4A). As shown in Fig. IV-4A, the spectrum of the hetero-stranded disulfide-bridged molecule P8/P9 is representative of the additivity of the spectra of the individual homo-stranded peptides P8 and P9.

To examine whether the charged regions could be induced into α-helical structure, when C-terminus to the coiled-coil, we determined the spectra of peptides P7, P8, P9 and P8/P9 in the presence of 50% TFE. As shown in Table IV-1 and Fig. IV-4C, further helical structure is induced in P8, P9 and P8/P9 compared to the same peptides in benign buffer. The induction of α-helical structure in the presence of 50% TFE for the positively charged extension is significantly greater than for the negatively charged extension (P8 and P9, Table IV-1). This can be explained by the higher helical propensity of the Lys and Arg residues in the positively charged extension versus the Glu and Asp residues in the negatively charged extension (Zhou et al., 1994). Interestingly, in the formation of the heterostranded peptide P8/P9, where the charge extensions are oppositely charged, these potential attractions have no significant effect on the number of helical residues in the coiled-coil in benign medium (Table IV-1).

Figure IV-4. Circular dichroism spectra of synthetic peptides derived from Kif3B. The peptides in panels A and C are the disulfide-bridged two-stranded molecules, either homostranded (open symbols) or heterostranded (closed symbols). Panels B and D are the reduced peptides of the same peptides shown in panels A and C. Panels A and B are the peptides in benign buffer (0.1M KCl, 0.05M PO_4, pH7) and panels C and D are the peptides in 50% TFE/benign buffer at 25°C. P7 (open circles), P8 (open squares), P9 (open triangles), P8/P9, heterostranded peptide (closed squares). Heterostranded sequences are shown in Fig IV-1.

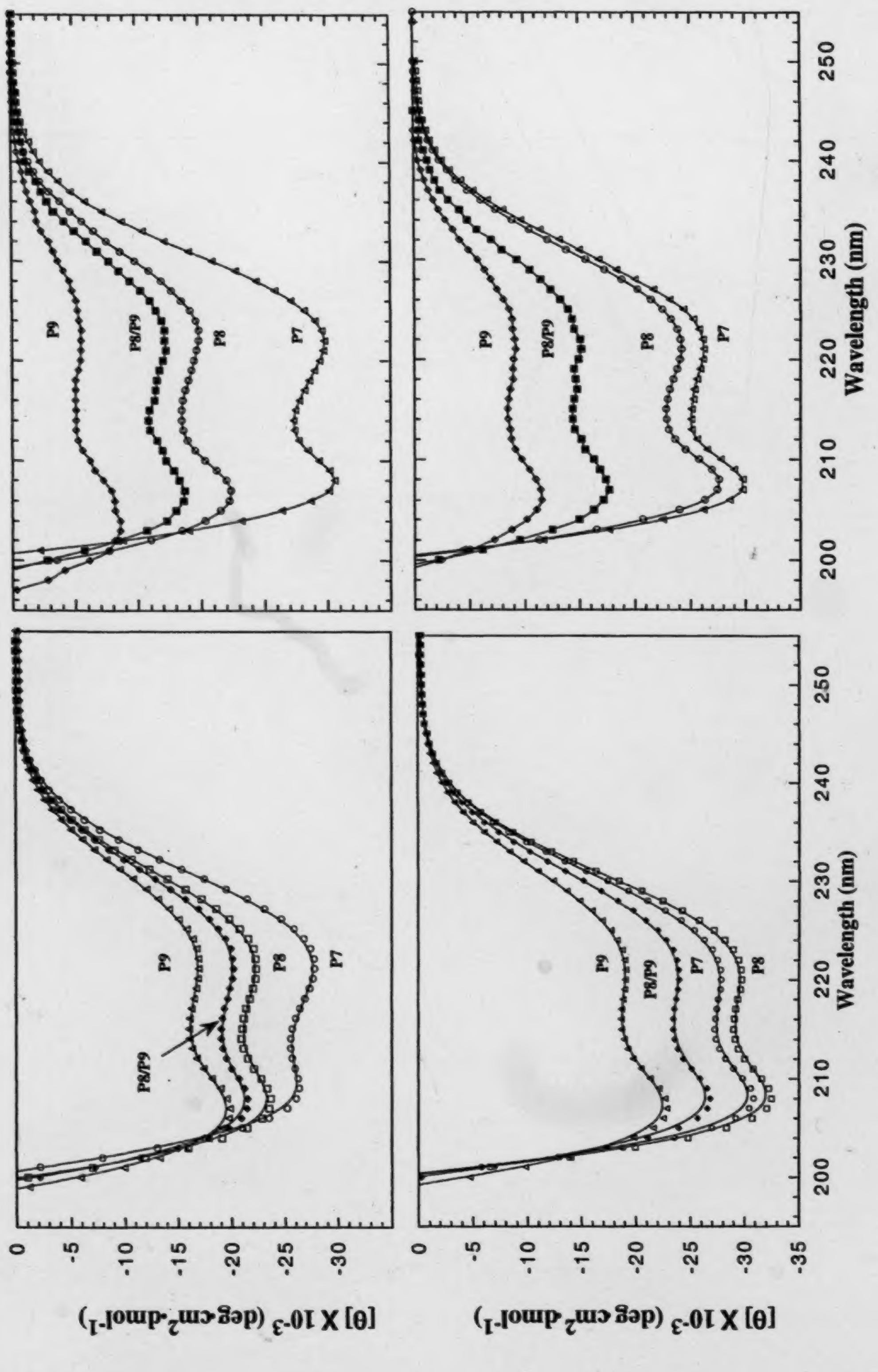
P9
P8/P9
P8
P7
P9
P8/P9
P8
P7
P8/P9
P9
P8
P7
P9
P8/P9
P7
P8
200
210
220
230
240
250
Wavelength (nm)
0
-5
-10
-15
-20
-25
-30
-35
[θ] X 10-3 (deg·cm2·dmol-1)

To assess how the stability of the Kif3B coiled-coil is affected by adding charged extensions, we denatured the α-helical structure of Kif3B's coiled-coil using the chemical denaturants guanidine hydrochloride and urea. Since GdnHCl masks electrostatic interactions, repulsions and attractions (Monera et al., 1994), it was not unexpected that the denaturation midpoints were essentially identical (~3.9M), with the stability results reflecting the stability of the coiled-coil's hydrophobic core, which is identical in all the coiled-coil constructs (Fig. IV-5A and Table IV-2). Urea, an uncharged denaturant, does not mask electrostatic interactions and so the stability results reflect the contribution of interactions of the charged regions to the stability of the coiled-coil. As observed in Fig. IV-5B and Table IV-2, the negatively charged regions destabilize the homostranded coiled-coil (compare $\text{urea}_{1/2}$ values for P7, 8.9M to P9, 6.9M, Table IV-2), while the positively charged region has little if any effect on coiled-coil stability (compare $\text{urea}_{1/2}$ values for P7, 8.9M to P8, 8.7M, Table IV-2). The hetero-two-stranded peptide P8/P9 in which electrostatic attractions have replaced the electrostatic repulsions of the negatively charged regions in P9 exhibits stability ($\text{urea}_{1/2}$ value of 8.5M) similar to the most stable homo-stranded peptide P8.

To characterize further the effects of the charged regions on the coiled-coil of Kif3B, we reduced the peptides so that they were no longer covalently linked through a disulfide bond. We denatured the peptides in the presence of excess DTT with increasing concentrations of urea or increasing temperature (Fig. IV-6A and B respectively). Though the overall stability of the reduced, unlinked peptides decreases relative to the disulfide-bridged peptides (compare P7ox, $\text{urea}_{1/2}$ value of 8.9M to P7red, $\text{urea}_{1/2}$ value of 3.1M; Table IV-2), the relative stabilities, whether reduced or oxidized, between peptides

P9 and P7, and P8 and P8/P9 are similar (Table IV-2). The relative order of stabilities of the peptides (reduced or oxidized) are P7, P8 and P8/P9 >>> than P9. The negatively charged regions, when placed adjacent to the coiled-coil, decrease the stability of the coiled-coil, while the positively charged regions do not.

To ascertain whether there was any difference between the oxidized and reduced peptides structurally, we collected the CD data of the reduced peptides (Fig. IV-4, panels B and D; Table IV-3). The α-helical content of the reduced peptides is less than that of the oxidized peptides due to the concentration dependence of the monomer to dimer equilibrium. At the concentration of 90 μM, the $[\theta]_{222}$ value is less for all peptides in benign medium or in the presence of TFE, though the relative order remains the same for the disulfide-bridged or reduced peptides (compare panels A and B in benign medium or panels C and D in 50% TFE; Fig. IV-4, Tables IV-1 and IV-3.)

Similar to the oxidized peptides, the negatively charged extensions of P9 are not helical, and the effect on the α-helical content is substantial at this concentration, where the reduced peptide has only 6 calculated helical residues while the oxidized coiled-coil has 19 in benign medium.

Stability of the neck coiled-coil Kif3B with Kif3A

To understand the effect of coiled-coil stability on the rate of heterodimerization by the oppositely charged regions we first compared the stabilities of the coiled-coils alone (Kif3A and Kif3B). The results show that the coiled-coil of Kif3B's neck region is more stable than that of Kif3A (Fig IV-7). Surprisingly, Kif3A and Kif3B have high sequence homology (Fig IV-1) and very little difference in their hydrophobic **a** and **d** residues, which constitute the hydrophobic core of the two-stranded coiled-coil. The only

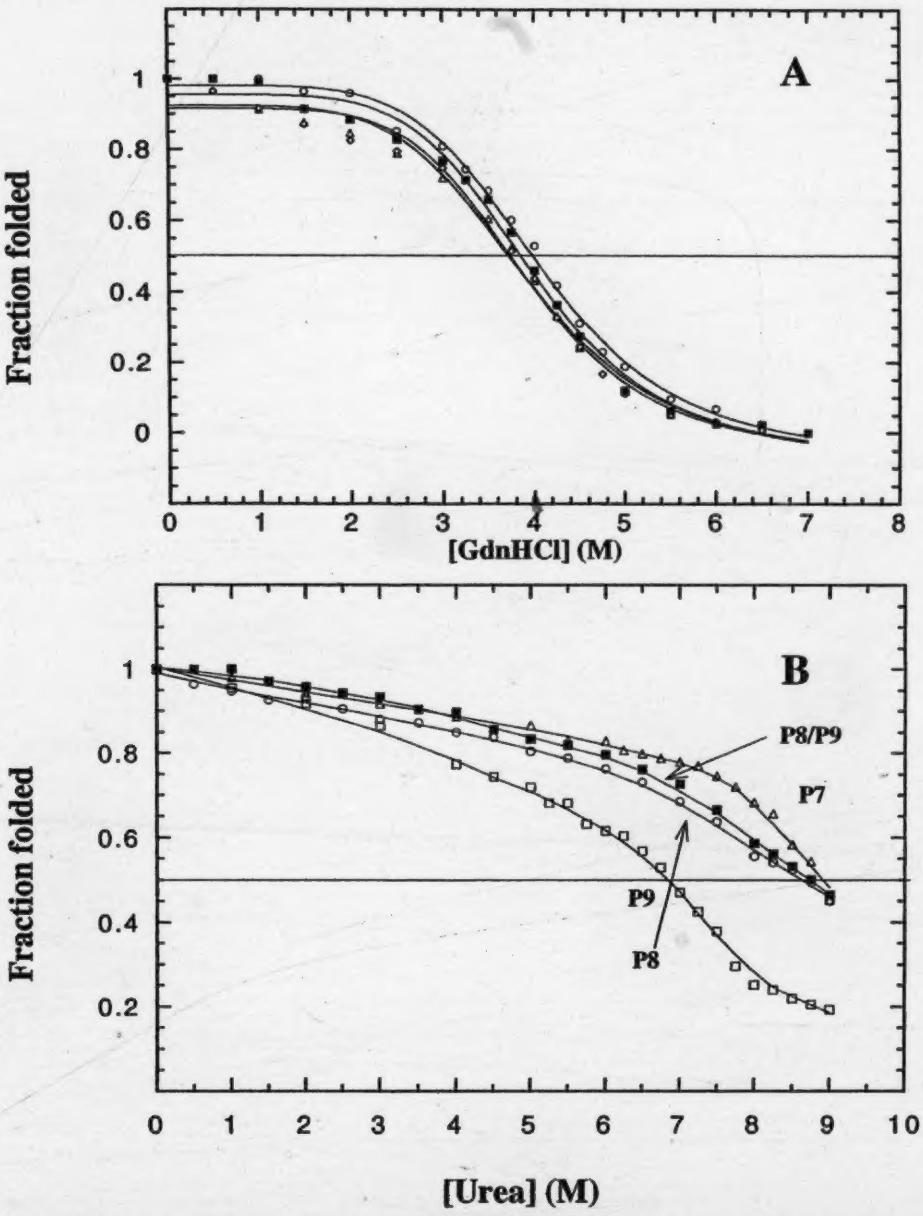

Figure IV-5. Denaturation profiles of Kif3B synthetic, disulfide-bridged peptides. Denaturation profiles of oxidized, Kif3B synthetic peptides at 25°C in 0.1M KCl, 0.05M PO_4, pH 7 buffer with guanidine hydrochloride (Panel A) or urea (Panel B) as a denaturant. P7 (open triangles), P8 (open circles), P9 (open squares), and heterostranded P8/P9 (closed squares). Peptide sequences are shown in Fig IV-1.

Table IV-2: Denaturation data for Kif3B synthetic peptides

	Oxidized		Reduced	
Peptide[a]	$GdnHCl_{1/2}$[b] (M)	$Urea_{1/2}$[c] (M)	T_m[d] (°C)	$Urea_{1/2}$[e] (M)
P7	3.7	8.9	46	3.1
P8	3.9	8.7	44	3.1
P9	3.7	6.9	29	1.4
P8/P9	3.9	8.5	46	3.1

[a] Disulfide-bridged homostranded peptides, P7, P8, and P9. Disulfide-bridged heterostranded peptide P8/P9. The amino acid sequences for each peptide is shown in Fig IV-2.

[b] $GdnHCl_{1/2}$ is the concentration of guanidine hydrochloride (M) required to give a 50% decrease in the molar ellipticity at 222 nm.

[c] $Urea_{1/2}$ is the concentration of urea (M) required to give a 50% decrease in the molar ellipticity at 222 nm.

[d] T_m is the temperature required to give a 50% decrease in the molar ellipticity at 222 nm for the reduced peptides in benign medium (100mM KCl, 50mM PO_4, at pH 7.2mM DTT).

[e] $Urea_{1/2}$ is the concentration of urea (M) required to give a 50% decrease in the molar ellipticity at 222 nm for the reduced peptides.

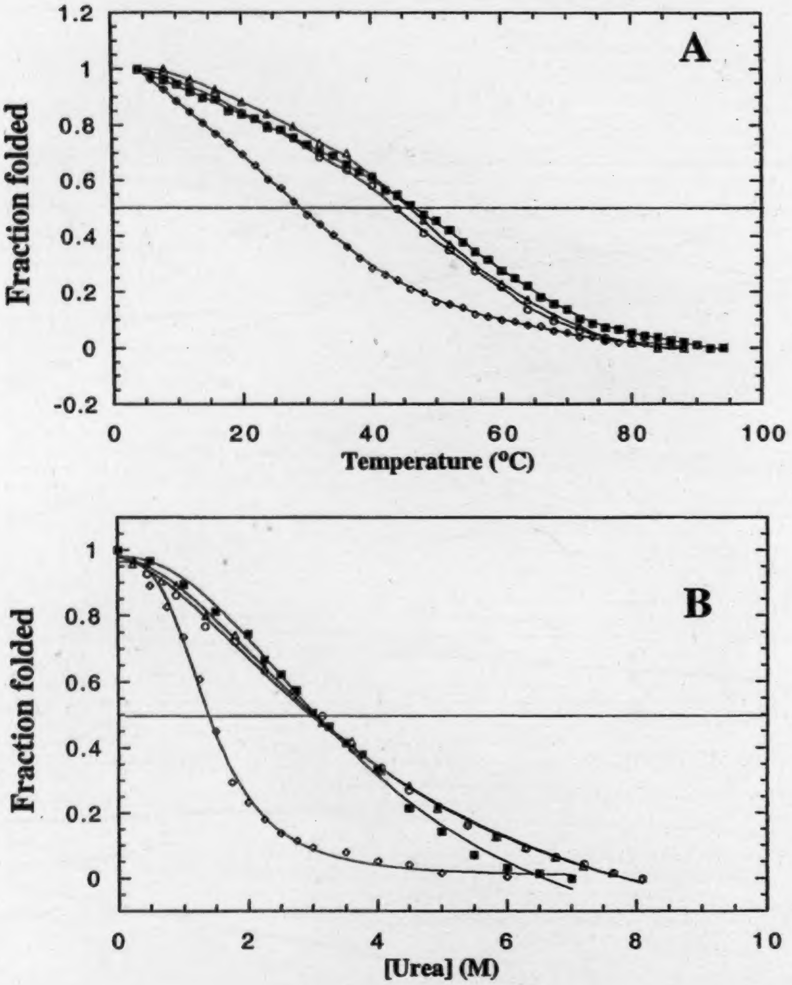

Figure IV-6. Denaturation of reduced Kif3B peptides. Panel A depicts the thermal denaturation of the reduced two-stranded α-helical coiled-coil peptides. Panel B shows the urea denaturation for the reduced peptides. Reduced peptides were denatured in 0.1M KCl, 0.05M PO_4, 2mM DTT, pH 7 buffer with urea. The fraction folded (f_f) of each peptide was calculated as $f_f = ([\theta] - [\theta]_u) / ([\theta]_n - [\theta]_u)$, where $[\theta]$ is the observed mean residue molar ellipticity at 222 nm for any particular denaturant concentration and $[\theta]_n$ and $[\theta]_u$ are the mean residue ellipticities at 222nm of the native "folded" and "unfolded" states, respectively. Peptide P7 (open triangles), P8 (open circles), P9 (open squares), and peptide P8/P9 (closed squares).

difference in the **a** and **d** positions is the C-terminal **d** position which has Arg in Kif3B and Gly in Kif3A. Tripet et al. (2000) have shown that the differences in the contribution of these residues to stability (if the substitutions were made in the center of the coiled-coil) could account for only 0.7 kcal/mol in favor of Kif3B. It has also been shown that the **a** and **d** positions at the ends of the coiled-coil contribute less to stability relative to the internal positions (approximately 1/3) (Zhou et al., 1992 a, b). Thus, this change would not be expected to account for the stability difference observed in Fig. IV-7. We summed the α-helical propensity values at positions **b**, **c**, **e**, **f** and **g** for Kif3A and Kif3B sequences. The difference between Kif3A and Kif3B was 2.2 kcal/mol using the values for single-stranded α-helices (Zhou et al., 1994) or 1.2 kcal/mol when corrected for coiled-coils (Kwok et al., 1999). Though electrostatic interactions (intra- and interchain) can make major contributions to the stability of coiled-coils (Kohn et al., 1995 a,b, 1997, 1998; Zhou et al., 1993, 1994), there is only one possible difference observed between Kif3A and Kif3B that would favor the higher stability of Kif3B, that is, an i to i′ + 2 (**e** to **g′**) interchain electrostatic repulsion between Lys residues at 371(**e**) and 373(**g′**) in Kif3A. It has been shown by Kohn et al. (1995a) that Glu residues at positions **e** and **g′** (i to i′ + 2) do not lead to destabilization. Similarly, O'Shea et al. (1991) concluded that the bulky hydrophobes at position **d** hinder side-chains in the i to i′ + 2 orientation from interacting to form Lys-Glu salt bridges. Thus, the difference in stability between Kif3A and Kif3B (Fig. IV-7) could be accounted for by the combined effects of differences in the hydrophobic cores at position **d** and differences in helix propensity at positions **b**, **c**, **e**, **f** and **g**.

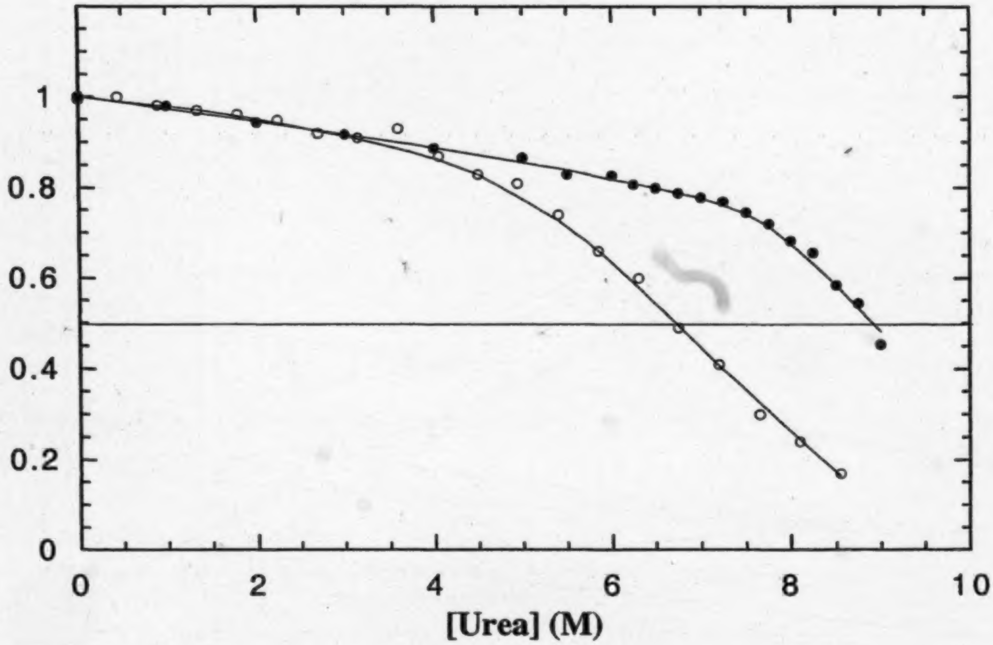

Figure IV-7. Peptide stabilities. The above panel shows the difference in the stabilities between oxidized P7 and P2 as determined by urea denaturation. The fraction folded (f_f) of each peptide was calculated as $f_f = ([\theta] - [\theta]_u) / ([\theta]_n - [\theta]_u)$, where $[\theta]$ is the observed mean residue molar ellipticity at 222 nm for any particular denaturant concentration and $[\theta]_n$ and $[\theta]_u$ are the mean residue ellipticities at 222 nm of the native "folded" and "unfolded" states, respectively. Peptide P7 (closed circles), P2 (open circles).

Table IV-3: Circular dichroism data of reduced Kif3B synthetic peptides

		$-[\theta]_{222}$ (deg·cm^2/dmol)[c]		% α-helix[d]		Number of calculated helical residues[e]		$[\theta]_{222}/[\theta]_{208}$[f]	
Peptide[a]	number of Residues[b]	benign	50% TFE	benign	50% TFE	benign	50% TFE	benign	50% TFE
P7	22	24750	26000	78	82	17	18	0.97	0.87
P8	36	14800	24150	42	69	15	25	0.88	0.88
P9	40	5500	9000	16	25	6	10	0.76	0.82
P8/P9	40/36	12200	15150	35	43	13	16	0.92	0.88

[a] Reduced peptides P7, P8, and P9 and P8/P9. The amino acid sequence for each peptide is shown in Fig IV2.

[b] Number of residues per polypeptide chain.

[c] The mean residue molar ellipticities at 222nm were measured at 25°C in benign buffer (0.1 M KCl, 0.05 M PO_4, pH 7, 2mM DTT). For samples containing TFE, the buffer was diluted 1:1 (v/v) with TFE.

[d] The percent helical content was calculated from the ratio of the observed $[\theta]_{222}$ value divided by the predicted molar ellipticity × 100. The predicted molar ellipticity was calculated from the equation $[\theta]_{222} = -40 \times 10^3 \times (1\text{-}4.6/n)$ for the chain length dependence of an α-helix (Gans et al., 1991), where n is the number of residues in the peptide. A peptide of 22 residues has a predicted molar ellipticity of –31,600.

[e] The number of helical residues was calculated by multiplying the % α-helix by the number of residues in the polypeptide chain., e.g., for reduced P7 in benign medium 24,600/31,600 × 22 residues = 17 α-helical residues predicted in the coiled-coil. The 50% TFE values reflect the maximum helical residues that can be formed at a 90 μM concentration.

[f] The molar ellipticity values at 222nm and 208nm for each peptide were used to calculate the ratio $[\theta]_{222}/[\theta]_{208}$.

Selective heterodimer formation

As described above, we have established the differences between Kif3A and Kif3B's neck coiled-coil stabilities and compared the effects of adding negatively and positively charged extensions to the C-terminus. We now wished to determine if there would be a difference in the results of redox equilibrium experiments between oxidized peptides P3 and P4 (the neck coiled-coil of Kif3A with, respectively, a negatively or positively charged extension added C-terminally) and oxidized peptides P8 and P9 (the neck coiled-coil of Kif3B with, respectively, a positively or negatively charged extension added C-terminally) (Fig. IV-2). The results show that the redox equilibrium state is reached more slowly for oxidized peptides P8 and P9 forming the heterostranded molecule P8/P9 (Fig. IV-8). We attribute this slower rate to the greater stability of Kif3B's neck coiled-coil. Thus, the rate of peptide strand exchange will depend upon the stability of the coiled-coils. At a fixed concentration, a more stable coiled-coil will dissociate less frequently (Ozeki et al., 1991), since the folded dimer is in equilibrium between its fully folded and unfolded states.

Since the redox equilibrium experiments for mixing oxidized peptides P3 and P4 or mixing oxidized peptides P8 and P9 led to the formation of the hetero-two-stranded peptide P3/P4 or P8/P9, respectively, the charged regions of Kif3A and Kif3B clearly have the ability to drive heterodimer formation when the coiled-coil strands are identical (Fig. IV-8).

Figure VI-8. The formation of oxidized heterostranded peptides of Kif3A coiled-coil (P3/P4) and of Kif3B coiled-coil (P8/P9) from the corresponding disulfide-bridged homostranded peptides during redox equilibrium experiments. The bottom panel depicts the different rates of formation of the heterostranded peptides of Kif3A (open triangles) and Kif3B (open circles).

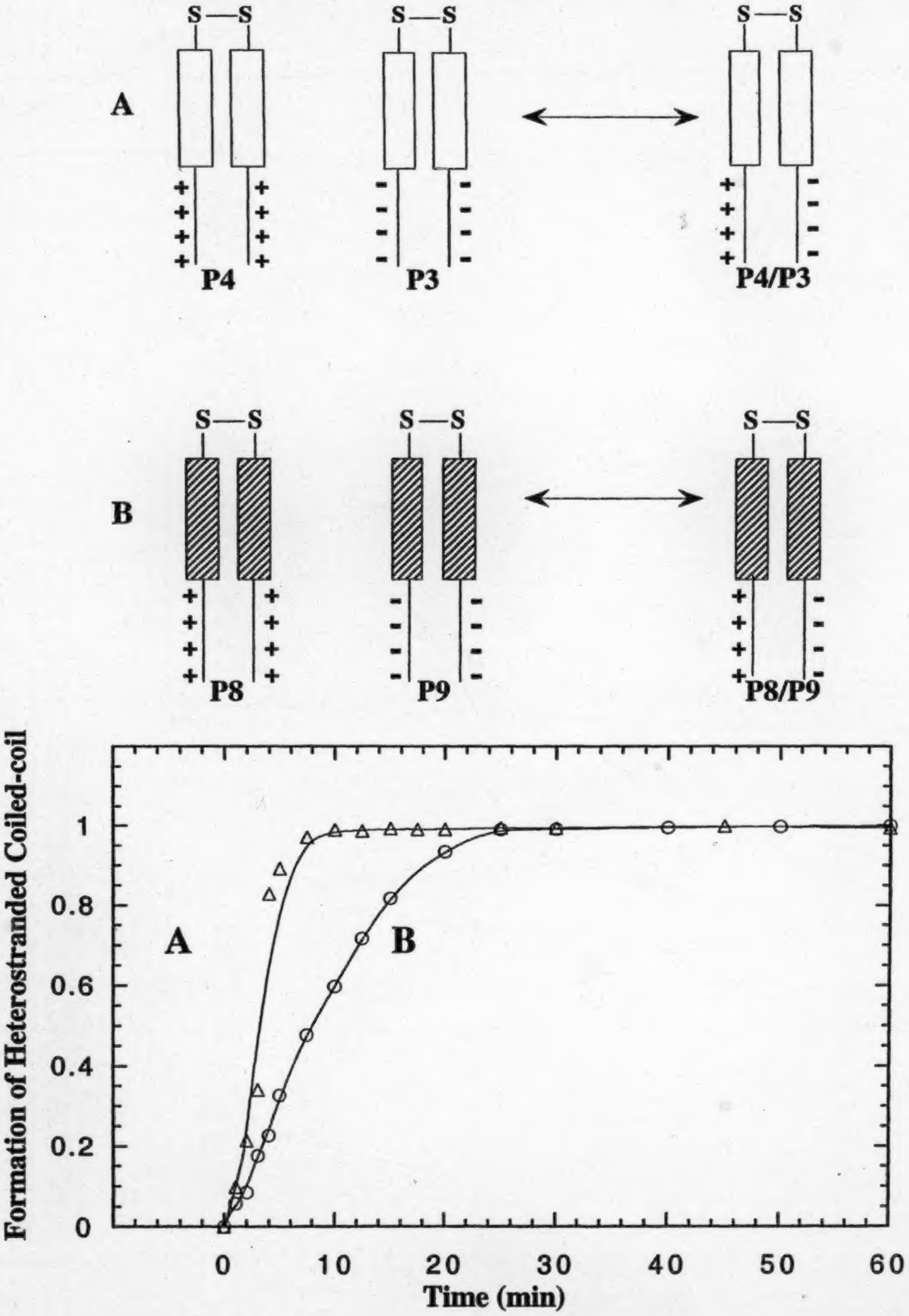
A
S—S
P4
P3
P4/P3
B
P8
P9
P8/P9
Formation of Heterostranded Coiled-coil
Time (min)
0
0.2
0.4
0.6
0.8
1
10
20
30
40
50
60

C. Discussion

Our investigation into the predicted neck coiled-coil and highly charged region of the Kif3B motor protein has led us to conclude that the neck region (residues 351-372; Fig. IV-2, top panel) can form a coiled-coil (Fig. IV-3A). In its oxidized state this region formed 19 helical residues out of a possible 22 (Table IV-1). The inability of the coiled-coil to form the full 22 helical residues can be explained by fraying of the coiled-coil at its C-terminus (Zhou et al., 1992). Based on the behavior of Kif3B's neck coiled-coil in aqueous medium and 50% trifluoroethanol, we could conclude that the peptide was fully folded and the maximum number of residues that could be helical had indeed adopted that secondary structure when the peptide was covalently linked through a disulfide bond (Fig. IV-3A and Table IV-1).

We next investigated whether the highly charged region of Kif3B, complementary to the charged region in Kif3A, can adopt an ordered secondary structure in solution. Our results, based on circular dichroism spectroscopy, indicated that on its own, and when located C-terminally on Kif3B's neck coiled-coil, the highly charged region of Kif3B does not form any organized secondary structure (Fig. IV-3B and IV-3C).

We found that there was a large difference in stability between the neck coiled-coil of Kif3B and the complementary neck coiled-coil region of Kif3A, where the coiled-coil of Kif3B was more stable (Fig. IV-7), even with the high sequence homology between Kif3A and Kif3B (Fig. IV-1, middle panel). The major contributor to the stability of any fold is thought to be the burial of hydrophobes away from the aqueous environment (Dill, 1990; Pace et al., 1996). The differences in stability between the coiled-coils of Kif3A and Kif3B can be explained by a combination of the contribution of residues at position **a** (Arg 372 in Kif3B and Gly 377 in Kif3A), α-helical propensity differences at positions **b**, **c**, **e**, **f** and **g** throughout the coiled-coil, and possibly the occurrence of an i to i′ + 2 electrostatic repulsion of Lys residues at positions 371 and 373 in Kif3A (Fig. IV-1).

It has been predicted that the complementary charged regions found on the motor subunits of the heterotrimeric motor proteins could lead to destabilization of homodimers and stabilization of heterodimers (Rashid et al., 1995). To monitor how the charged region of Kif3B could affect coiled-coil stability, the positively and negatively charged segments of the charged region were individually added to the C-terminus of Kif3B's neck coiled-coil, producing peptides P8 and P9 (Fig. IV-2). We linked the peptides with a disulfide-bridge to produce homostranded peptides P8 and P9 and heterostranded peptide P8/P9. Peptide P8/P9 is considered heterostranded, even though the coiled-coil strands are identical, because one chain has a positively charged C-terminal segment, while the other chain has a negatively charged C-terminal segment. The repulsive effect of the negatively charged region in P9 had no effect on the number of calculated α-helical residues in the neck region's coiled-coil (Table IV-1). However, the negatively charged regions did dramatically destabilize the coiled-coil (Table IV-2). In comparison, placing the positive extensions C-terminally (P8) led to no loss in stability of the coiled-coil (Table IV-2). This result was surprising considering we would have expected repulsions between the positively charged residues and destabilization of the coiled-coil as observed with the negatively charged extensions. However, the long side-chains of the lysine residues may allow the charged ε-amino groups to be appropriately distant from each other, causing minimal repulsive interactions and thus having little effect on the stability of the coiled-coil. In contrast, the shorter side-chains of glutamic acid residues do not allow the negatively charged groups to distance themselves from the polypeptide backbone, resulting in destabilization of the coiled-coil. Peptide P8/P9, which has oppositely-charged extensions, should show electrostatic attractions between the strands; however, these interactions did not enhance the stability of this construct compared to the coiled-coil alone (P7) or the stability of the homostranded coiled-coil with positively charged extensions (P8) (Table IV-2). In contrast, peptide P8/P9 was dramatically more stable than the homostranded peptide with negatively charged extensions (P9) (Table IV-2). Thus, as shown by our redox experiments (Fig. IV-8), it seems that the electrostatic attractions between the unstructured regions drive specificity for heterodimerization, rather than playing the role of enhancing stability. We found that both positively and negatively charged segments of Kif3B's highly charged regions were required to be located C-terminally to the neck coiled-coil to drive the almost exclusive formation (95%) of heterostranded peptide. Thus, the two oppositely charged regions seem to attract each other leading to the formation of heterostranded product similar to that observed with the Kif3A coiled-coil (Chana et al., 2002).

It is interesting that the positively charged extension is found C-terminally on the more stable coiled-coil, Kif3B. This extension had no effect on the stability of the Kif3B coiled-coil (urea$_{1/2}$ value of 8.7M for P8 compared to the Kif3B coiled-coil alone, P7, with a urea$_{1/2}$ value of 8.9M). On the other hand, the negatively charged extension is located C-terminally on the less stable coiled-coil, Kif3A. This extension dramatically destabilized the Kif3A coiled-coil (urea$_{1/2}$ value of 3.8M for P3 compared to the Kif3A coiled-coil alone, P2, with a urea$_{1/2}$ value of 6.7M). The net result is that this situation enhances the stability difference between the Kif3B and Kif3A molecules (urea$_{1/2}$ value of 8.7M for P8 and 3.8M for P3 relative to that of the coiled-coils alone, 8.9M for P7 and 6.7M for P2), which allows a greater driving force for heterodimerization between Kif3A and Kif3B proteins. Thus, over all, electrostatic attractions seem to be important for specificity of heterodimer formation while maintaining the stability of the heterodimer equivalent to the most stable homodimer.

Electrostatic interactions in large numbers or in clusters have been suggested to play unique roles in proteins. For example, it has been reported that electrostatic networks could contribute to thermostability of thermophilic proteins through resilience rather than rigidity, whereby ionic networks can increase the kinetic barrier to unfolding so that instead of increased hydrophobic packing in the core, individual structured elements in a protein are linked together through an extensive ion-pairing network. Thus, if sections of a protein come apart, they will be drawn back together by electrostatic forces (Aguilar, 1997). In addition, Schreiber and Fersht (1996) have shown that long-range electrostatic forces can accelerate the interaction of two molecules (faster than diffusion) to form an initial encounter. Thus, as occurs in the present study, the electrostatic bias leads to the law of mass action favoring the folding of the heterodimeric complex in the absence of any significant difference in stability of the heterodimer versus the most stable homodimer.

Chapter V

Stability and specificity of heterodimer formation for the neck regions of the motor proteins Kif3A and Kif3B[3]

A. Introduction

Conventional kinesin has been characterized and has been shown to be composed of two heavy and two light chains (Bloom et al., 1988; Kuznetsoz et al., 1988; Hirokawa et al., 1989). The second protein in the kinesin superfamily of proteins to be completely characterized was found to be a heterotrimeric complex composed of two motor subunits with microtubule activated ATPase activity and an accessory protein (Wedaman et al., 1996). This heterotrimeric protein was termed Kinesin-II but is also called the Kif3 complex, where Kif represents kinesin family (Yamazaki et al., 1996).

The sequence identification and characterization for the subunits of the Kif3 complex, isolated from sea urchin, have been completed. The 85kDa subunit was the first to be characterized and was termed spKRP85 for *Strongylocentrotus purpuratus* **K**inesin **R**elated **P**rotein-85kDa (Cole et al., 1993). The characterization of the mouse protein homologue Kif3A has also been reported (Kondo et al., 1994). In 1995, the sequence of the 95kDa subunit found in sea urchin, termed spKRP95, was published (Rashid et al., 1995), it was followed by the sequence publication of its mouse homologue, Kif3B (Yamazaki et al., 1995). The accessory proteins in sea urchin and mouse were sequenced and reported in 1996 (Wedaman et al., 1996; Yamazaki et al., 1996). These proteins have since been named KAPs for **K**inesin-like **A**ssociated **P**roteins.

---

[3] A version of this chapter is in preparation for submission to the Journal of Biological Chemistry.

Upon analysis of the spKRP85/95 and Kif3A/B motor subunits, it was noted that the NH_2 termini (approximately residues 1-350) were likely, based on sequence homology, to comprise a motor domain similar to conventional kinesin. The NH_2 terminal domains were predicted to be separated from the small globular COOH terminal domains by a central α-helical segment thought to form a coiled-coil similar to the one shown for conventional kinesin (de Cuevas et al., 1992). A similar stalk-like structure as seen for conventional kinesin was noted for the Kif3A/B complex in electron micrographs (Yamazaki et al., 1995).

From sequence analysis, it appeared that spKRP85 and Kif3A were orthologues, having a 73% homology along their full lengths. Similarly, it was predicted that spKRP95 would be the orthologue to Kif3B (Rashid et al., 1995). It is interesting to note that while spKRP85 has 699 amino acids, Kif3A is comprised of 701, while both spKRP95 and Kif3B were originally reported to have 742 amino acids, with the extra residues found at the COOH termini.

Within the same organism, spKRP85 was found to have 52% sequence identity with the full-length spKRP95, and 73% within the motor region. Kif3A and Kif3B were found to have 47% sequence identity along their full length and 61% in their motor regions. Interestingly, in the similarity profiles between spKRP85/Kif3A and spKRP95/Kif3B, a small portion of sequence was found to have strikingly low homology. This region was found located in the predicted coiled-coil stalk domain, but had low probability for α-helix formation (Cole et al., 1993; Rashid et al., 1995; Yamazki et al., 1995). When these regions were further scrutinized it was noted that spKRP85/Kif3A had a stretch of amino acids that had a number of negatively charged amino acids closely spaced side-by-side (11 and 13 negatively charged amino acids in spKRP85 and Kif3A, respectively). This negatively charged segment was found to be followed by a segment of positively charged amino acids (9 in both proteins). This region of sequence disparity in spKRP95/Kif3B was found to begin with a stretch of positively charged amino acids (8 in each protein) followed by a segment of negatively charged amino acids (11 and 14, respectively, in spKRP95 and Kif3B) (Fig. V-1). It was postulated that these complementary charged regions in the hinge region could help the motor subunits form spKRP85/95 and Kif3A/B heterodimers through the destabilization of homodimers, and stabilization of heterodimers through electrostatic attractions (Rashid et al., 1995). It was also noted that polar and charged residues were found in the stalk region **a** and **d** positions of the coiled-coil (Rashid et al., 1995). The **a** and **d** positions are classically reserved for hydrophobic residues in a coiled-coil (Hodges et al., 1972), and it was predicted that the formation of heterodimers would prevent electrostatic repulsions in the hydrophobic core of the coiled-coil stalk region of the homodimeric proteins (8). Support for the possible role of **a** and **d** positions in the stalk region in heterodimer formation has been bolstered by a recent study (De Marco et al., 2001), where the ability of the C-terminal heptads of the stalk domain to form heterodimers was demonstrated.

In our efforts to characterize the neck region coiled-coil and complementary charged regions (hinge region; Fig. V-1) of the motor proteins Kif3A and Kif3B, we have analyzed the ability of each neck region to form a coiled-coil on its own (Chana et al., 2002a,b). Furthermore, in recent studies, we focused on the effects of complementary charged regions on the formation of the homodimeric coiled-coils of Kif3A and Kif3B (Chana et al., 2002a,b). That is, the coiled-coil segment was homodimeric but, with oppositely charged regions attached, the molecules were heterostranded. We demonstrated that the negatively charged segments of both Kif3A and Kif3B charged regions, when attached directly to the neck region coiled-coils, destabilized their respective neck region coiled-coils, while, in contrast, the positively charged segments did not affect the stability of the coiled-coil neck regions. Furthermore, it was shown that a negative and positive charged extension was required to specify heterostranded peptide formation in the presence of identical coiled-coil sequences.

In the present study, we are examining the formation of heterodimeric molecules of Kif3A and Kif3B, where both the coiled-coil regions and the charged segments represent the sequences found in native Kif3A and Kif3B. These results allowed us to determine the role of the complementary charged regions in determining the specificity and stability of the heterodimeric Kif3A/Kif3B coiled-coil.

B. Results

Secondary structure of the complementary charged regions of Kif3A and Kif3B

The complementary charged regions we have investigated are those of Kif3A (residues 378-416) and Kif3B (residues 373-411). We synthesized two peptides to represent these regions (P5 and P10, respectively) (Fig. V-1). CD analysis of the peptides showed that, on their own and mixed equally at a 1:1 ratio, they did not adopt any regular secondary structure (Fig. V-2A). Interestingly, when the peptides were linked by a disulfide bond at the N-terminus using a flexible CGG linker, they still did

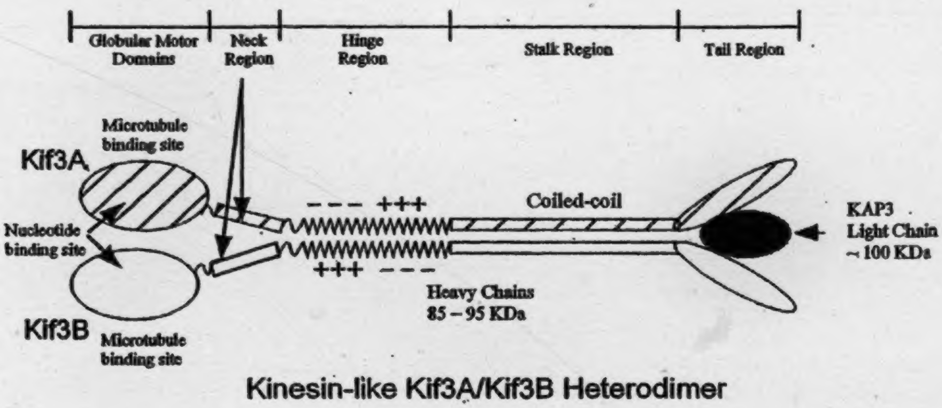
Globular Motor Domains
Neck Region
Hinge Region
Stalk Region
Tail Region
Microtubule binding site
Kif3A
Nucleotide binding site
--- +++
Coiled-coil
KAP3 Light Chain ~100 KDa
+++ ---
Heavy Chains 85 – 95 KDa
Kif3B
Microtubule binding site

Kinesin-like Kif3A/Kif3B Heterodimer

Protein	Peptide name	Res. #	Complementary Charge-Rich Regions
Kif3A Charged Region	**P5**	(378-416)	**Ac–**CGGEEVSGSDISGSEEDDEEGELGEDGEKRKKRRDQAGKKKV**-amide** -- - ------ - -- - | ++++++- +++
Kif3B Charged Region	**P10**	(373-411)	**Ac–**CGGSIGRRKRREKRREGGGSGGGGEEEEEEGEEGEEDGDDKD**-amide** +++++-+++- | | ------ -- --- --+-

Figure V-1. Top panel shows a schematic of the kinesin-like heterotrimeric motor protein Kif3A/Kif3B/KAP3. This protein consists of two different polypeptide chains, Kif3A and Kif3B, which resemble conventional kinesin heavy chains. Each polypeptide chain contains a N-terminal globular motor domain, followed by a potential neck coiled-coil region, a highly charged hinge region, a coiled-coil stalk region and the C-terminal tail region (which binds to an accessory unit, the kinesin-like associated protein KAP3). Bottom panel shows the amino acid sequences of the complementary charged regions in Kif3A and Kif3B. Shown are the charged regions, residues 378-416 and 373-411, which comprise the nonhomologous regions of Kif3A and Kif3B, respectively. The charged region of Kif3A begins with negatively charged amino acids followed by positively charged amino acids; the analogous region in Kif3B begins with a positively charged region followed by a glycine spacer and then a negatively charged region. CGG represents a flexible linker added N-terminally to each peptide. Ac- denotes N$^{\alpha}$-acetyl and –amide denotes C$^{\alpha}$-amide.

not adopt any detectable, regular secondary structure. Thus, the oxidized (disulfide-linked) peptides P5 and P10 showed a random coil spectrum (Fig. V- 2B). The oxidized heterostranded peptide P5/P10 also showed a spectrum characteristic of a random coil peptide (Fig. V-2B).

Folding of neck region coiled-coil

We now characterized the neck region coiled-coil of Kif3A/B to show that the heterostranded neck region coiled-coil does indeed form a coiled-coil in the absence of the rest of the molecule. Peptide P2 (Kif3A residues 356-377) and peptide P7 (Kif3B residues 351-372) were synthesized (Fig. V-3, top and bottom panels) and analyzed by CD spectroscopy. The CD spectrum of disulfide-bridged P2/P7 (Fig. V-4A) was characteristic of a fully folded α-helical coiled-coil, based upon the following characteristics: high molar ellipticity value in benign medium, double minima at 208 nm and 222 nm, and a maximum at 190 nm; an α-helical content of 100% and 22 calculated α-helical residues out of 22 (Table V-1); the addition of 50% TFE did not increase the α-helical content (determined at 222 nm) (Table V-1); the $[\theta]_{222}/[\theta]_{208}$ ratio in benign medium (1.05) is characteristic of coiled-coils, i.e., >1.0 (Lau et al., 1984b) and this value decreased to 0.86 in the presence of the helix-inducing solvent TFE. Although TFE stabilizes the helical secondary structure, it denatures tertiary and quaternary structure, i.e., the coiled-coil is dissociated to single-stranded α-helices as was clearly demonstrated by high-performance size-exclusion chromatography of coiled-coils (Monera et al., 1993; Lau et al.,1984a,b; Zhou et al., 1992a,b; Mant et al., 1997) oxidized heterostranded peptide P2/P7 is compared with the spectra of the oxidized homostranded peptides P2 and P7. The flexible Cys-Gly-Gly linker was used to link peptides P2 and P7 to ensure

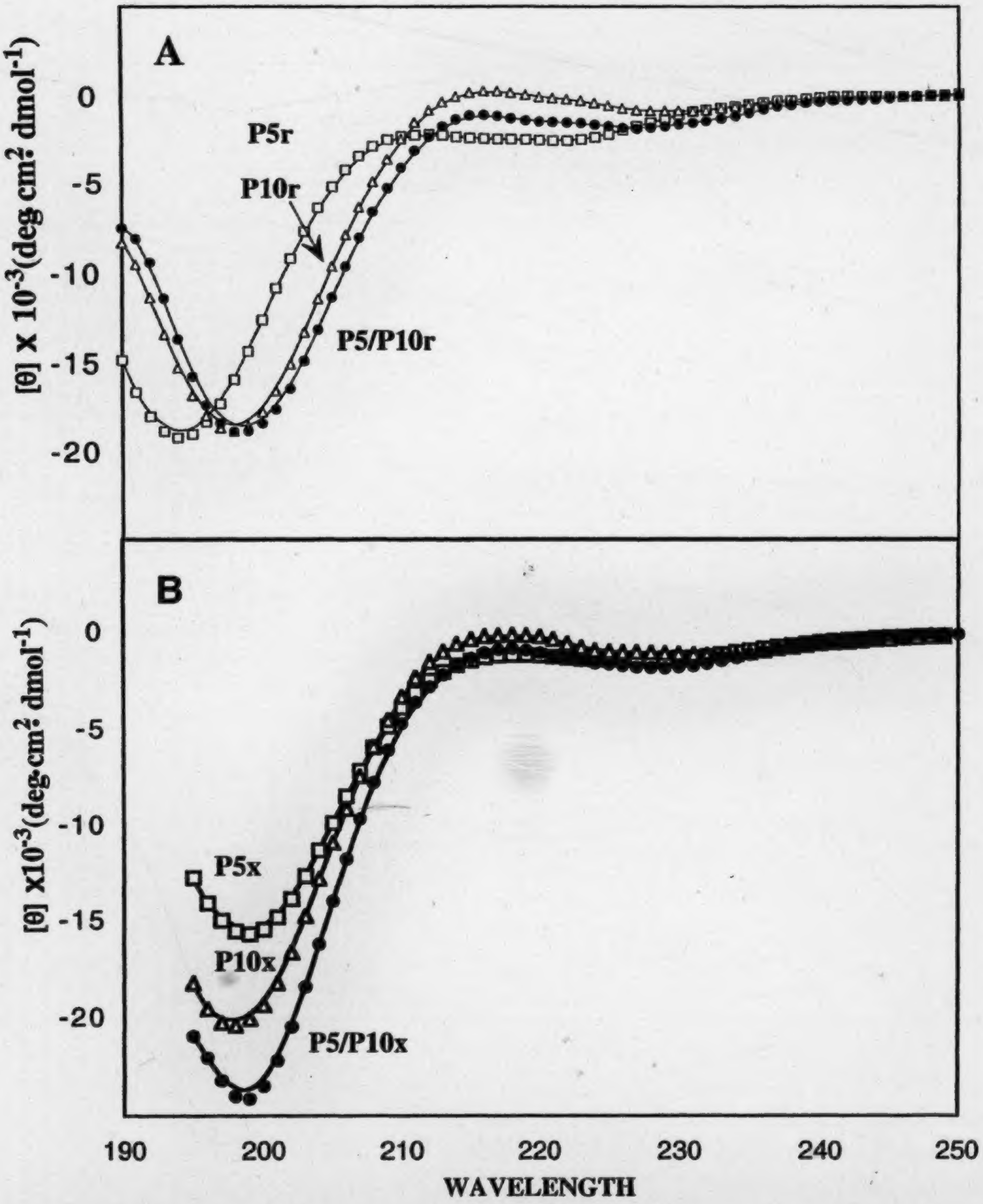

Figure V-2. Circular dichroism (CD) spectra of the complementary charged regions. Panel A depicts the random coil spectra of the non-linked (reduced) peptides denoted P5r, P10r and P5 mixed P10 (1:1) denoted P5/P10r. Panel B shows the random coil spectra of the disulfide bridged (oxidized) homostranded peptides denoted P5x, P10x and the heterostranded peptide P5/P10x. P5 open squares, P10 open triangles, and P5/P10 closed circles. The peptide sequences are shown in Fig V-3.

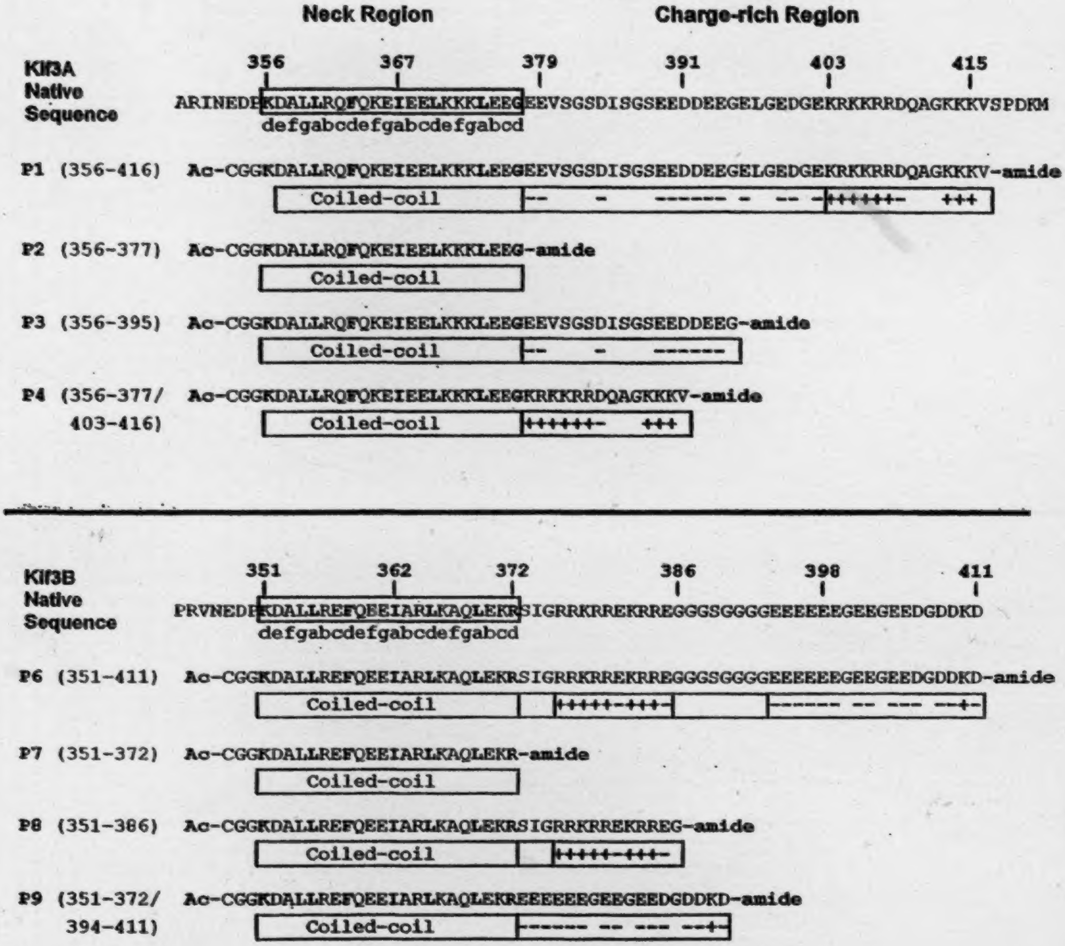
Neck Region
Charge-rich Region
Kif3A Native Sequence
356
367
379
391
403
415
ARINEDEKDALLRQFQKEIEELKKKLEEGEEVSGSDISGSEEDDEEGELGEDGEKRKKRRDQAGKKKVSPDKM
defgabcdefgabcdefgabcd
P1 (356-416)
Ac-CGGKDALLRQFQKEIEELKKKLEEGEEVSGSDISGSEEDDEEGELGEDGEKRKKRRDQAGKKKV-amide
Coiled-coil
-- - ------ - -- -
++++++- +++
P2 (356-377)
Ac-CGGKDALLRQFQKEIEELKKKLEEG-amide
Coiled-coil
P3 (356-395)
Ac-CGGKDALLRQFQKEIEELKKKLEEGEEVSGSDISGSEEDDEEG-amide
Coiled-coil
-- - ------
P4 (356-377/ 403-416)
Ac-CGGKDALLRQFQKEIEELKKKLEEGKRKKRRDQAGKKKV-amide
Coiled-coil
++++++- +++
Kif3B Native Sequence
351
362
372
386
398
411
PRVNEDPKDALLREFQEEIARLKAQLEKRSIGRRKRREKRREGGGSGGGEEEEEEGEEGEEDGDDKD
defgabcdefgabcdefgabcd
P6 (351-411)
Ac-CGGKDALLREFQEEIARLKAQLEKRSIGRRKRREKRREGGGSGGGEEEEEEGEEGEEDGDDKD-amide
Coiled-coil
+++++-+++-
------ -- --- --+-
P7 (351-372)
Ac-CGGKDALLREFQEEIARLKAQLEKR-amide
Coiled-coil
P8 (351-386)
Ac-CGGKDALLREFQEEIARLKAQLEKRSIGRRKRREKRREG-amide
Coiled-coil
+++++-+++-
P9 (351-372/ 394-411)
Ac-CGGKDALLREFQEEIARLKAQLEKREEEEEEGEEGEEDGDDKD-amide
Coiled-coil
------ -- --- --+-

Figure V-3. Amino acid sequences of the Kif3A and Kif3B peptides used in this study. The native mouse Kif3A and Kif3B sequences, residues 356-416 and 351-411, are shown above the synthetic peptides prepared for this study. The open box around the native sequence indicates the predicted neck α-helical coiled-coil region. The heptad repeat of the coiled-coil is denoted by abcdefg, where positions a and d are typically the non-polar residues (shown in bold) involved in the 3-4 hydrophobic repeat. The boxed regions below the peptide sequences denote the predicted coiled-coil region and the highly negatively charged and positively charged regions. The negatively charged residues and positively charged residues are indicated by a (-) or (+) sign, respectively. CGG represents a flexible linker added N-terminally to each peptide. Ac- denotes N^{α}-acetyl and –amide denotes C^{α}-amide. All of the synthetic peptides are aligned to the native sequence except peptides P4 and P9, which consist of their respective coiled-coil regions, residues 356-377 and 351-372, respectively, combined with the positively charged region, residues 403-416, and the negatively charged region, residues 394-411, respectively.

that we were exclusively analyzing the heterostranded peptide. The values observed by CD spectroscopy for the heterostranded and homostranded peptides are shown in Table V-1. The heterostranded peptide shows an increased α-helical content and complete folding compared to the two homostranded peptides.

Role of complementary charged regions in dimer formation

The neck region coiled-coil and complementary charged regions of Kif3A and Kif3B (peptide P1 and P6, respectively) are comprised of residues 356-416 and 351-411, respectively (Fig. V-3). To understand the role of charged regions on specificity and stability of the heterodimeric coiled-coil, we synthesized a series of peptides derived from these sequences (Fig. V-3). The top panel of Fig. V-3 shows the native sequence taken from Kif3A; the neck region coiled-coil-forming residues are boxed in the native sequence and depicted by a box beneath each of the synthetic peptides. The residues found in the hydrophobic **a** and **d** positions are shown in bold. The individual charged extensions added C-terminally are depicted by the boxes containing – and + signs, representing the charged amino acids. Similarly, the bottom panel shows the native Kif3B and derived peptide sequences.

In our previous studies, we showed the need for both positively and negatively charged regions to be present in order to specify the formation of heterostranded peptide (Chana et al., 2002a), and that the stability of the coiled-coil could affect the rate of heterostranded peptide formation when the starting peptides were homostranded (Chana et al., 2002b). In the present study, the results of redox equilibrium experiment (see Methods) showed that the presence of charged extensions C-terminal to the coiled-coil-forming sequences can specify the formation of a truly heterodimeric coiled-coil (Fig. V-

Figure V-4. Comparison of hetero-two-stranded coiled-coil with homo-two-stranded coiled-coil neck regions. Panel A depicts the CD spectra of the 3 heptad coiled-coils for the neck regions of Kif3A/Kif3B, Kif3A, and Kif3B (peptides P2/P7, P2 and P7 respectively). Panel B depicts the relative stabilities of the neck region coiled-coils in guanidine hydrochloride. Panel C depicts the relative stabilities of the neck region coiled-coils for the homo- and hetero-two-stranded peptides in urea. Homostranded Kif3A neck region, P2, (open circles), homostranded Kif3B neck region, P7, (open squares), heterostranded Kif3A/Kif3B neck region, P2/P7, (closed triangles). Peptide sequences are shown in Fig V-3.

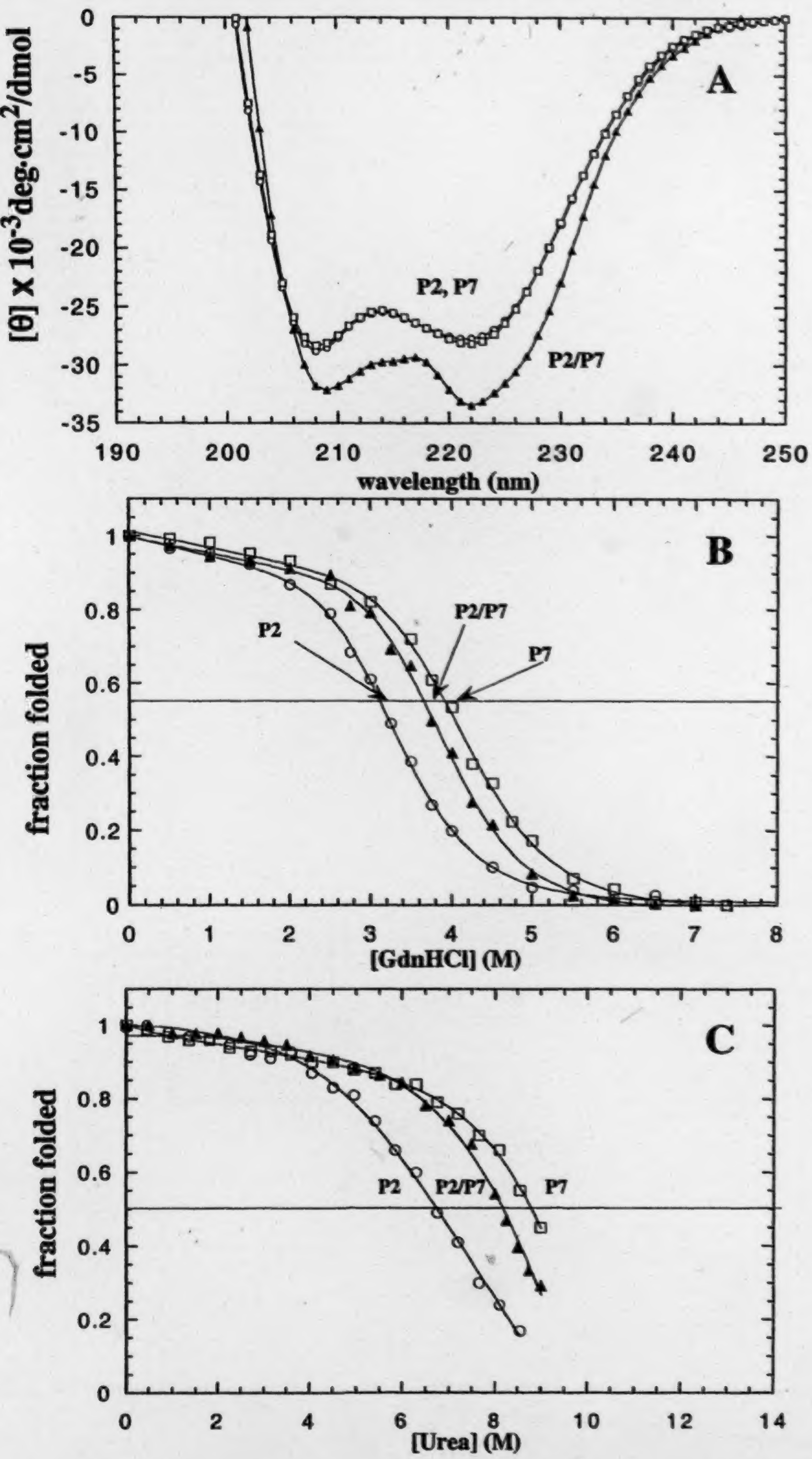
A
[θ] x 10^-3 deg·cm^2/dmol
0
-5
-10
-15
-20
-25
-30
-35
190
200
210
220
230
240
250
wavelength (nm)
P2, P7
P2/P7
B
fraction folded
1
0.8
0.6
0.4
0.2
0
0
1
2
3
4
5
6
7
8
[GdnHCl] (M)
P2
P2/P7
P7
C
fraction folded
1
0.8
0.6
0.4
0.2
0
0
2
4
6
8
10
12
14
[Urea] (M)
P2
P2/P7
P7

Table V-1: Circular dichroism data of synthetic peptides

Peptide[a]	number of Residues[b]	$-[\theta]_{222}$ (deg·cm^2/dmol)[c]		% α-helix[d]		Number of calculated helical residues[e]		$[\theta]_{222}/[\theta]_{208}$[f]	
		benign	50% TFE	benign	50% TFE	benign	50% TFE	benign	50% TFE
P2	22	27700	28750	88	91	19	20	0.96	0.86
P7	22	28150	28300	89	90	20	20	0.99	0.86
P2/P7	22/22	33450	31750	100	100	22	22	1.05	0.86

[a] Disulfide-bridged homostranded peptides P2 and P7. Disulfide-bridged heterostranded peptide P2/P7. The amino acid sequence for each peptide is shown in Fig. V-3.

[b] Number of residues per polypeptide chain.

[c] The mean residue molar ellipticities at 222nm were measured at 25°C in benign buffer (0.1 M KCl, 0.05 M PO_4, pH 7). For samples containing TFE, the buffer was diluted 1:1 (v/v) with TFE.

[d] The percent helical content was calculated from the ratio of the observed $[\theta]_{222}$ value divided by the predicted molar ellipticity × 100. The predicted molar ellipticity was calculated from the equation $[\theta]_{222} = -40 \times 10^3 \times (1-4.6/n)$ for the chain length dependence of an α-helix (Gans et al., 1991), where n is the number of residues in the peptide. A peptide of 22 residues has a predicted molar ellipticity of –31,600.

[e] The number of helical residues was calculated by multiplying the percent α-helix by the number of residues in the polypeptide chain., e.g., for reduced P7 in benign medium 27,700/31,600 × 22 residues = 19 α-helical residues predicted in the coiled-coil.

[f] The molar ellipticity values at 222nm and 208nm for each peptide were used to calculate the ratio $[\theta]_{222}/[\theta]_{208}$.

5, reactions A, B, C). Notice that the presence of two segments of complementary charged regions C-terminal to the coiled-coils behave similarly (Fig. V-5, reaction A) to one segment of complementary charge (Fig. V-5, reactions B and C) in specifying heterostranded coiled-coil formation. The absence of charged regions leads to the formation of only 50% heterodimer, a value expected for random exchange of polypeptide strands (Fig. V-5, reaction D), that is, no specificity for heterodimer formation. In this study, we tested the ability of the complementary charged region found in Kif3A and Kif3B to specify formation of heterostranded coiled-coil in the presence of 3M NaCl (Fig. V-6). We see that in redox buffer (O'Shea et al., 1989; Lavigne et al., 1995) containing 3M NaCl there was a decreased ability of the charged regions to contribute to the formation of heterostranded coiled-coil, producing only ~60% (Fig. V-6) heterostranded coiled-coil product instead of the original 95% (Fig. V-5). The percentage of heterostranded coiled-coil formed approaches the amount formed by random mixing of the coiled-coils without charged extensions in 3M NaCl (Fig. V-6, reaction D).

Effect of complementary charged regions on coiled-coil stability

To assess how the stability of the heterostranded coiled-coil is affected by adding complementary charged extensions in comparison to the homostranded coiled-coils of Kif3A and Kif3B, that have repulsive charged extensions, we denatured the α-helical structure of the neck coiled-coil using the chemical denaturants GdnHCl and urea. Since GdnHCl masks electrostatic interactions, repulsions and attractions (Monera et al., 1994a), the denaturation midpoints of the disulfide-bridged homostranded peptides P2

Figure V-5. The formation of oxidized, heterostranded P1/P6, P3/P8, P4/P9, and P2/P7 from redox experiments as a function of time. Reaction A represents the redox results of oxidized peptides P1 and P6, (closed triangles in plot). Reactions B and C represent the redox reactions of oxidized P3 with P8 and P4 with P9, respectively (open diamonds and open squares). Reaction D represents the redox reaction of peptide P2 with P7, (open circles). The percent heterostranded peptide was calculated by dividing the integrated area of the hetero-two-stranded HPLC peak by the total integrated area of both the homo- and heterostranded peptides for each time-point. Peptide sequences are shown in Fig V-3.

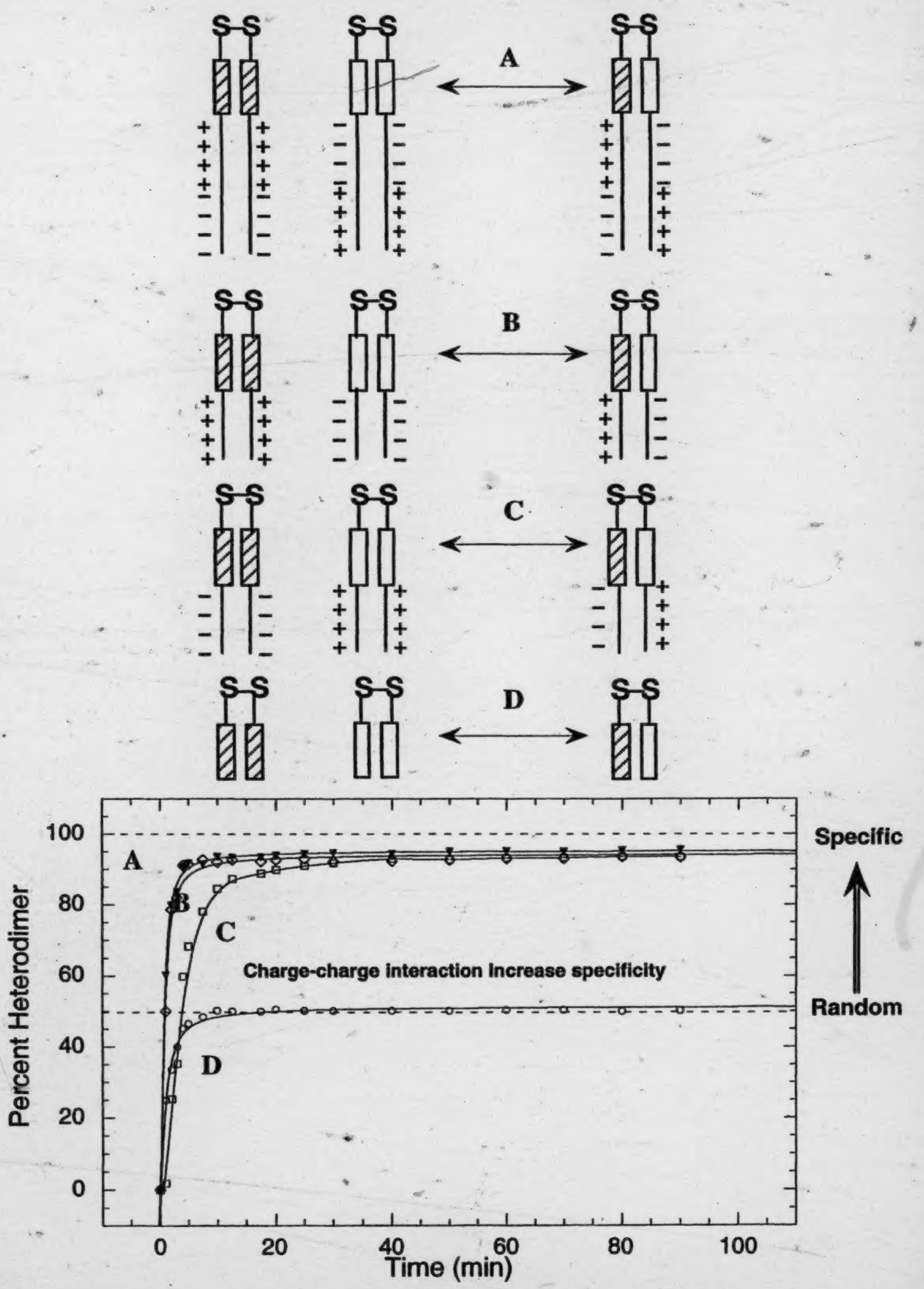
S-S
A
B
C
D
+
−
100
80
60
40
20
0
Percent Heterodimer
0
20
40
60
80
100
Time (min)
Charge-charge interaction increase specificity
Specific
Random

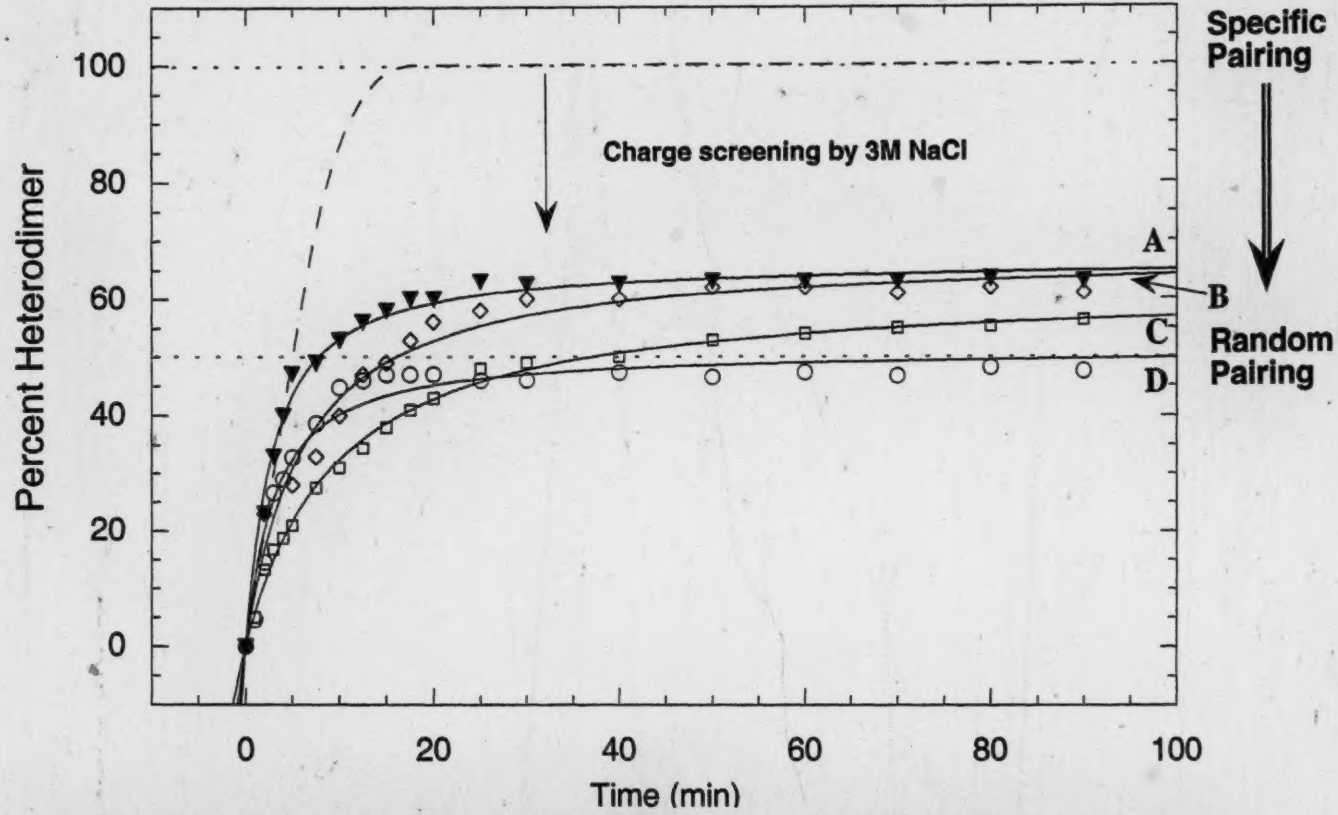

Figure V-6. Formation of heterostranded peptides in the presence of NaCl. The dashed line is the theoretical maximum in benign medium. Reaction A represents the redox results of oxidized peptides P1 and P6 (closed triangles). Reaction B represents the result of mixing oxidized peptides P3 and P8 (open diamonds). Reaction C is the result of mixing oxidized peptides P4 and P9 (open squares). Reaction D is the result of mixing oxidized peptides P2 and P7 (open circles). Percent heterostranded peptide was calculated as described for Fig V-5.

and P7 and the disulfide-bridged heterostranded peptide P2/P7 will be a reflection of the stability of the coiled-coils' hydrophobic cores (Fig. V-4B; Table V-2A). The denaturation midpoint value of the heterostranded peptide P2/P7 (3.6M) is approximately intermediate between the values for the homostranded peptides (P2, 3.1M and P7, 3.9M; Fig. V-4B; Table V-2A). Urea, an uncharged denaturant, does not mask electrostatic interactions (Monera et al., 1994a) and so the stability results will reflect the combined effect of the hydrophobic interactions in the hydrophobic core and the effect of charged regions on the stability of the coiled-coil. Since there are no charged extensions on peptides P2 and P7, the denaturation midpoints of these coiled-coils in urea will reflect the stabilities of the coiled-coils alone and this serves as our control experiment. Again the stability of the heterostranded P2/P7 coiled-coil (8.1M; Fig. V-4C; Table V-2A) is approximately intermediate between the values of the two homostranded coiled-coils, P2 and P7 (P2, 6.7M and P7, 8.8M; Fig. V-4C; Table V-2A).

For peptides with only one segment of the complementary charged region added C-terminally to the coiled-coil-forming sequences, peptides P3 and P8, we expect a relative stability pattern in GdnHCl between the homostranded and heterostranded peptides to be similar to the stability pattern for the coiled-coils alone, since, as noted above, GdnHCl masks electrostatic interactions. The stability of the heterostranded P3/P8 in GdnHCl, was slightly higher than the expected midpoint (3.5M; Fig. V-7A; Table V-2B, compared to a theoretical 3.3M). The denaturation midpoint values of the homostranded peptides P3 and P8 in GdnHCl were 2.8M and 3.7M, respectively (Fig. V-7A and Table V-2B). In urea, where the effects of the charged region interactions can be observed, it would be expected that the value for the heterostranded peptide would not lie

Table 2A: Denaturation data for synthetic coiled-coil peptides

	Oxidized	
Peptide[a]	$GdnHCl_{1/2}$[b] (M)	$Urea_{1/2}$[c] (M)
P2	3.1	6.7
P7	3.9	8.8
P2/P7	3.6	8.1

Table 2B: Denaturation data for synthetic peptides with one charge segment

	Oxidized	
Peptide[a]	$GdnHCl_{1/2}$[b] (M)	$Urea_{1/2}$[c] (M)
P3	2.8	3.9
P8	3.7	8.2
P3/P8	3.5	7.6

Table 2C: Denaturation data for synthetic peptides with both charge segments

	Oxidized	
Peptide[a]	$GdnHCl_{1/2}$[b] (M)	$Urea_{1/2}$[c] (M)
P1	2.7	3.9
P6	3.6	8.0
P1/P6	3.1	7.8

[a] Disulfide-bridged homostranded peptides, P7, P8, and P9. Disulfide-bridged heterostranded peptide P8/P9. The amino acid sequence for each peptide is shown in Fig. V-1.

[b] $GdnHCl_{1/2}$ is the concentration of guanidine hydrochloride (M) required to give a 50% decrease in the molar ellipticity at 222 nm.

[c] $Urea_{1/2}$ is the concentration of urea (M) required to give a 50% decrease in the molar ellipticity at 222 nm.

intermediate between the values of the two homostranded peptides. In fact, the hetero-two-stranded peptide (P3/P8) exhibited a coiled-coil stability (urea$_{1/2}$ value of 7.6M) closer to the most stable homostranded peptide P8 (8.2M; Fig. V-7B; Table V-2B). A urea denaturation midpoint value that came half way between the values of the two homostranded-peptides (3.9M and 7.6M) would be 5.8M. The heterostranded peptide is considerably more stable than the homostranded peptide P3 (compare urea$_{1/2}$ values of 7.6M and 3.9M, respectively).

Lastly, for the peptides that incorporate the full length charged region found in Kif3A and Kif3B, peptides P1 and P6 (Fig. V-3), the GdnHCl midpoint value of the heterostranded P1/P6 (3.1M; Fig. V-8A; Table V-2C) appeared to come between the GdnHCl midpoint values for the homostranded peptides P1 and P6 (2.7M and 3.6M, respectively). In urea, we see that the heterostranded peptide (P1/P6) again exhibited a stability (urea$_{1/2}$ value of 7.8M) similar to the most stable homostranded peptide P6 (8.0M; Fig. V-8B, Table V-2C). The heterostranded peptide P1/P6 is substantially more stable than the homostranded peptide P1 (compare urea$_{1/2}$ values of 7.8M and 3.9M respectively).

C. Discussion

We have explored the ability of oppositely, complementary charged regions to specify heterodimer formation in the neck region coiled-coil found in the heterotrimeric motor protein complex Kif3A/Kif3B/KAP3. The complementary charged regions alone (residues 378-416 and 373-411 for Kif3A and Kif3B, respectively) were examined by CD spectroscopy and they were found to adopt a random coil structure by themselves and

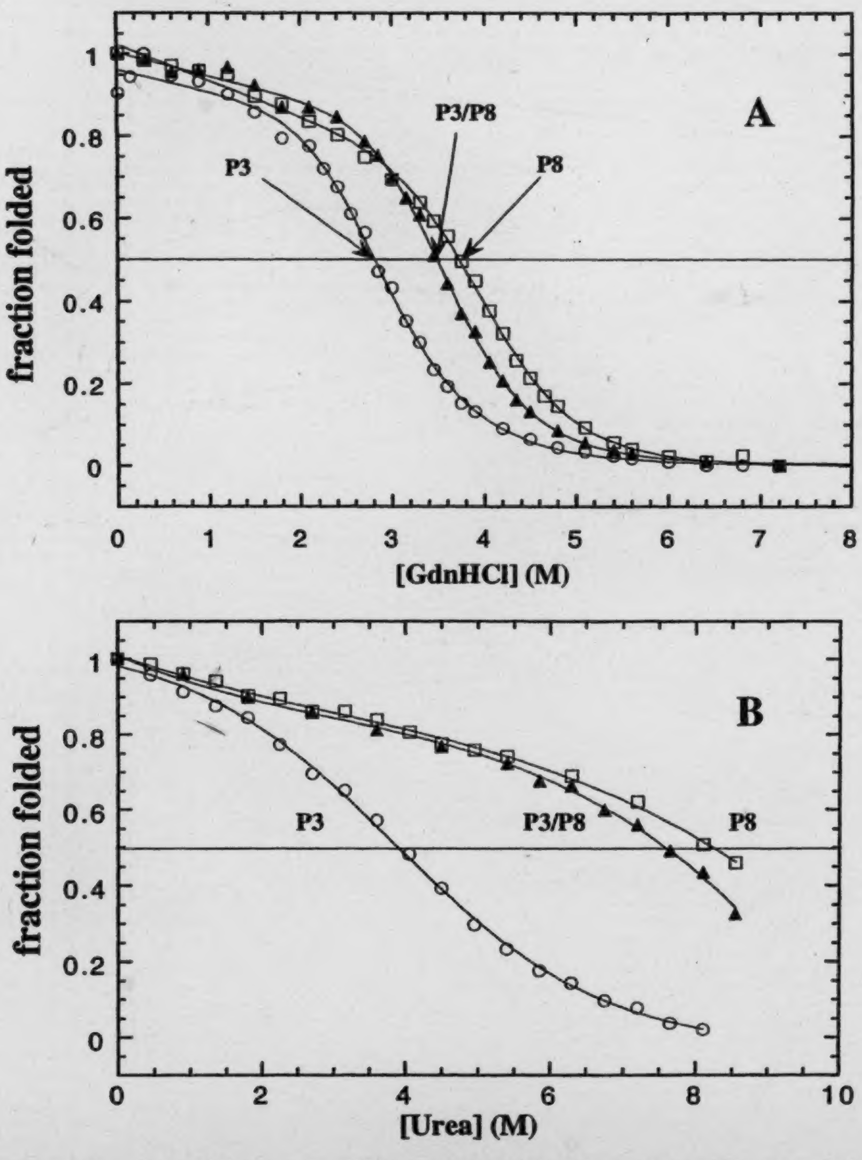

Figure V-7. Comparison of stabilities of oxidized peptides P3, P8, and P 3/P8: coiled-coils with the first segment of the complementary charged region. Panel A depicts the relative stabilities, in guanidine hydrochloride, for homostranded peptide P3, heterostranded peptide P3/P8, and homostranded peptide P8. The peptides are comprised of the neck region coiled-coils with the first segment from the complementary charged regions found in Kif3A and Kif3B (Fig V-3) added C-terminally. Panel B depicts the relative stabilities of peptides P3, P3/P8, and P8 in urea. Homostranded peptides P3 and P8 (open circles and open squares, respectively); heterostranded peptide P3/P8 (closed triangles). Peptide sequences are shown in Fig V-3.

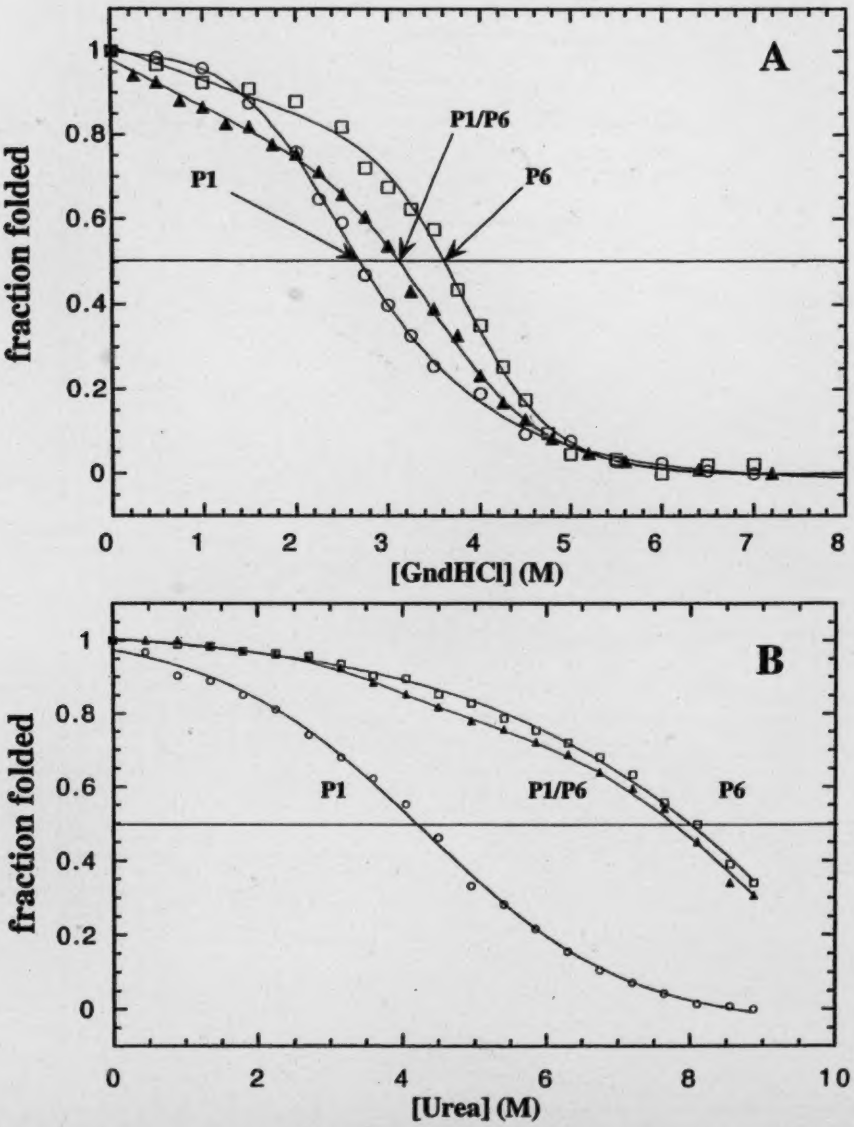

Figure V-8 Comparison of stabilities of oxidized peptides P1, P6, and P1/P6: coiled-coils with both segments of complementary charged residues. Panel A depicts the relative stabilities of the coiled-coil neck regions for homostranded P1, heterostranded P1/P6, and homostranded P6 in guanidine hydrochloride. The peptides are comprised of the coiled-coils with the full complementary charged regions (Fig V-3) added C-terminally. Panel B depicts the stabilities of the peptides in urea. Homostranded peptides P1 and P6 (open circles and open squares, respectively); heterostranded peptide P1/P6 (closed triangles). Peptide sequences are shown in Fig V-3.

when mixed together in a 1:1 ratio. Peptides, including the neck coiled-coil and the complementary charged regions (residues 356-416 and 351-411 for Kif3A and Kif3B, respectively) were studied in their disulfide-bridged form (CGG linker added to the N terminus) either as homo-two-stranded peptides or hetero-two-stranded peptides. To assess the ability of the complementary charged regions to specify heterodimer formation of a coiled-coil, we mixed disulfide-bridged homo-two-stranded Kif3A and Kif3B peptides with their respective charged regions attached, in redox buffer (O'Shea et al., 1989; Lavigne et al., 1995). Contrary to recent findings (De Marco et al., 2001), where it was suggested that the charged regions were not necessary for heterodimer formation, we observed that oppositely charged regions specified the formation of a hetero-two-stranded peptide (Fig. V-3 and Fig. V-5, reactions A, B, C). Furthermore, mixing the disulfide-bridged Kif3A neck coiled-coil together with the disulfide-bridged Kif3B neck coiled-coil led to a 1:2:1 ratio of Kif3A homostranded: Kif3A/B heterostranded: Kif3B homostranded peptides, the ratio expected from a nonspecific random pairing of peptides (Fig. V-5 reaction D). The ability of the complementary charged extensions on the C-terminus of the neck coiled-coil of the two proteins to form preferentially a heterostranded peptide was diminished through charge screening in the presence of NaCl (Fig. V-6). Similar charge screening by salt has been reported elsewhere (Schreiber et al., 1996; Kohn et al., 1997).

To assess how complementary charged extensions may affect the stability of the heterodimeric neck coiled-coils in comparison to the homodimeric coiled-coils, we denatured the peptides in urea, a denaturant shown to reveal the effects of electrostatics on protein stability (Hagihara et al., 1994; Kohn et al., 1995a,b; Monera et al., 1994b).

The results indicate that for the neck region coiled-coils alone, the heterodimeric coiled-coil made up of the neck regions of both Kif3A and Kif3B has an intermediate stability between the homodimeric neck coiled-coils (Fig. V-4C, Table V-2A). With complementary charged regions added to the C-terminus of the heterodimeric neck region coiled-coil, the stability of the coiled-coil is increased relative to the intermediate stability position and is similar to the stability of the more stable homodimeric neck region of Kif3B (Fig. V-7B, Table V-2C).

In accordance with the original postulate (Rashid et al., 1995) for the functional role of the complementary charged regions in the Kif3 complex, we see that complementary charged regions can specify hetero-two-stranded coiled-coil formation. However, the results of this study and our previous investigations (Chana et al., 2002a,b) show the effects of the charged extensions on the stability of the coiled-coil regions. Thus, the pairing of negatively charged regions directly C-terminus to the coiled-coil led to a dramatic decrease in stability of the homostranded Kif3A neck region, while the pairing of positively charged regions did not decrease the stability of homostranded Kif3B neck region (compare Table V-2A and V-2B) (Chana et al., 2002a,b). Interestingly, adding a second and oppositely-charged segment to the single charged extension already present in either Kif3A or Kif3B had no effect on the stability of the coiled-coil (Table V-2B, V-2C). The heterostranded coiled-coil with complementary charged C-terminal extensions maintained essentially the same stability as the most stable homodimeric coiled-coil in urea (Table V-2C). The unstructured, oppositely and complementary charged regions seem to drive specificity. Perhaps in the full-length molecule, the negatively charged segment of the Kif3A charged region functions to destabilize its homodimeric neck region while the negatively charged segment of the Kif3B charged region functions to destabilize its homodimeric stalk region. The positively charged regions of Kif3A and Kif3B lie in between the neck and stalk coiled-coil regions, do not adopt any structure in benign conditions, and do not exhibit any effect on neck coiled-coil stabilities, suggesting that unstructured positively charged regions are not repulsive, unlike negatively charged unstructured regions.

The results of a previous study (De Marco et al., 2001), which makes use of truncated mutants of Xlklp3A and Xlklp3B (*Xenopus laevis* kinesin-like protein subunits 3A and 3B), homologous to the neck and highly charged regions of Kif3A and Kif3B, respectively, demonstrated the ability of the C-terminal heptads of the stalk domain to form heterodimers. It was shown that heterodimers could form between the C-terminal regions of the stalks in the absence of the highly charged regions (De Marco et al., 2001). When the investigators used full-length XlKlp3A protein, and a C-terminally truncated XlKlp3B (and vice-versa) protein that still had the complementary charged region present, they were not able to detect heterodimers, but this can be explained by their results pertaining to the C-terminal region of the stalk. Thus, these investigators found that there was a distinct need for the C-terminal portion of the stalk domain in order for the two proteins to bind together so that they could be immunoprecipitated. Hence, the inability of the investigators' C-terminally truncated mutants to form heterodimers with a full length partner does not preclude the importance of the complementary charged regions described in the present study in heterodimer formation. The complementary charged regions may simply be one component in a two-component system that favors heterodimer formation. The C-terminal heptads of the stalk could be important for binding and specificity, while the complementary charged regions next to the neck coiled-coil could further increase binding specificity. These two regions could work in concert to control/modulate heterodimer formation.

Chapter VI

Future Investigations

Kinesin-like proteins:

Structural investigations of the kinesin neck region have demonstrated the existence of a stable two-stranded α-helical coiled-coil. Since many other members of the kinesin superfamily are predicted to contain similar coiled-coil regions, our future work has taken the direction of establishing the presence of these structures and their thermodynamic stability. Following are examples of results we would generate from studying the kinesin family of proteins.

The discovered kinesin-like proteins have been identified as either N, M, or C-type depending on where their motor domains are located [Vale and Fletterick, 1997], The vast array of kinesin-like proteins have been grouped and organized into a kinesin-superfamily, and the various kinesin proteins homologous among different organisms have been grouped under the title of KifX, where X is a number and Kif stands for kinesin superfamily [Miki et al., 2001]. Among the N-type Kif proteins there are many sub-classes, denoted N-1, N-2 . . .N-11 sub-classes (Fig. VI-1). We have analyzed the neck regions of a number of N-type kinesins from the different sub-classes (Fig. VI-2A,B) and have aligned them based on their β-linker regions found in the neck region of the proteins. From this type of alignment, one can see that the Kif proteins in the sub-types N-1 to N-5 have a very similar structural motif in their neck regions (Fig. VI-2A). The neck regions are thought to comprise the β-linker and α-helical coiled-coil that follows

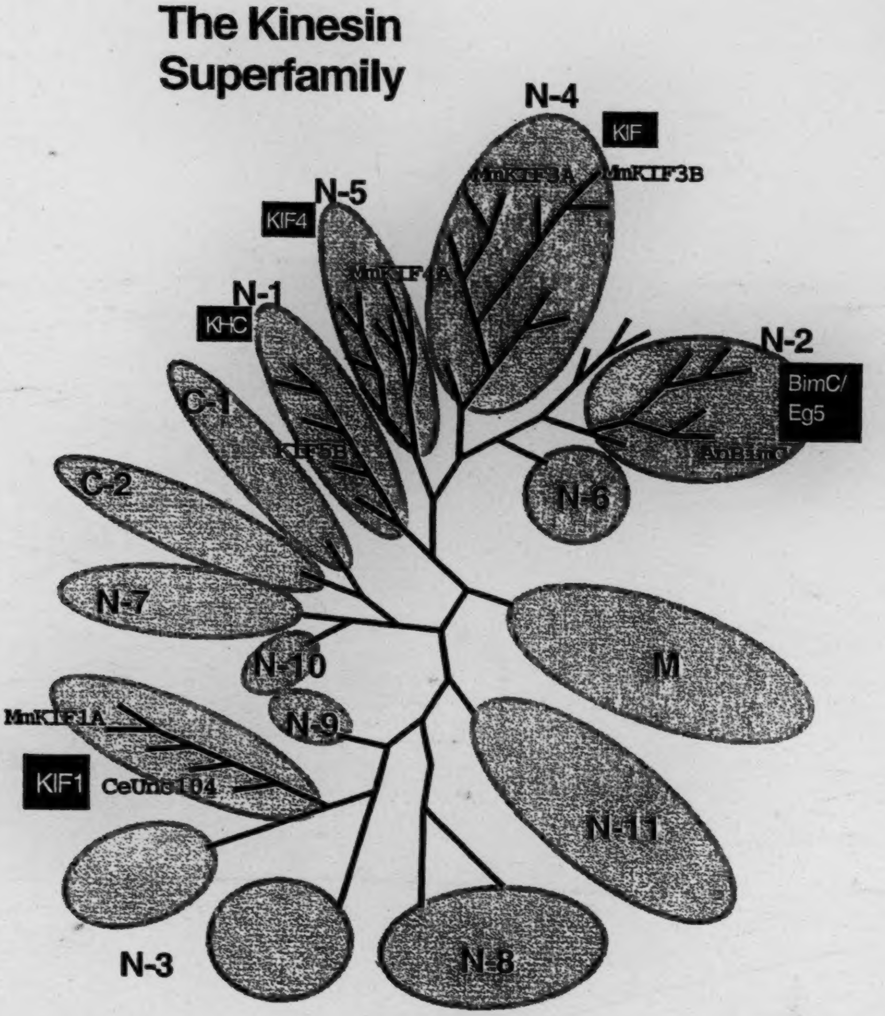
The Kinesin Superfamily
N-4
KIF
MmKIF3A
MmKIF3B
N-5
KIF4
MmKIF4A
N-1
KHC
C-1
KIF5B
N-2
BimC/Eg5
AnBimC
N-6
C-2
N-7
N-10
M
MmKIF1A
N-9
KIF1
CeUnc104
N-11
N-3
N-8

Figure VI-1. The un-rooted kinesin superfamily tree depicts the three types of kinesin motors, N, M, and C. The motors differ in the placement of the motor region so the N-type kinesins have their motor domains located N-terminally, the M-type in the middle, and the C-type C-terminally in the protein. The N-type are further divided into sub-types, N-1, N-2, N-3, etc. Each of the sub-types represents different kinesin families; some family names are indicated in the darkened boxes. Proteins that are listed for the N-sub-types: N-1, N-2, N-3, N-4, and N-5 were analyzed in the present study. This tree was modified from Miki et al., (2001) and was created by comparing the homology among the motor domains of the proteins.

immediately afterward. The formation of a coiled-coil in the neck region of conventional kinesin has been demonstrated [Morii et al., 1997; Tripet et al., 1997] for human kinesin, which is analogous to MmKif5B. Figure VI-2A also represents the regions we have predicted to form α-helical coiled-coils in the Kif proteins. It is clear that not all of the sequences are predicted to have coiled-coils, but all seem to have a β-linker region with a level of relatedness (Fig. VI-2B). To determine whether the regions predicted to form α-helices would form coiled-coil structures, we synthetically prepared the sequences shown in bold in figure VI-2A and are further depicted in figure VI-3. To determine whether the putative neck coiled-coil forming sequences of the listed N-type kinesin-like proteins (Fig. VI-3) were able to form autonomously folded two-stranded α-helical coiled-coils, the peptides representing the neck coiled-coils of XlEg5, AnBimC, MmKif1A, Ceunc104, MmKif3A, MmKif3B, and MmKif4 were synthesized (Fig. VI-3). The circular dichroism spectra (Fig. VI-4A) show a characteristic α-helical pattern, with double minima at 208 nm and 222 nm. The 222nm/208nm ratios were calculated where a ratio > 1.0 typically indicates a fully folded two-stranded peptide population [Lau et al., 1984b]. The 222nm/208nm ratio values (Table VI-1) are <1.0 for the synthesized peptides, indicating that the peptides are in a state of flux between the two-stranded coiled-coil, and single-stranded random coil states [Tripet et al., 1997]. The spectra determined in the presence of 50% trifluoroethanol, a helix inducing solvent, shows that the peptides were not fully folded in benign medium since a greater amount of helicity was induced as is shown by the increase in the absolute values of the 222nm molar ellipticity values for the peptides (Fig. VI-4B, Table VI-1).

Figure VI-2. Alignment of *Mus Musculus* kinesin family motor proteins (Kif) by the beta-linker neck regions. Capital letters are those residues that were aligned using the DALIGN algorithm, which aligns sequences based on segment similarity. The light gray boxes depict the β-linker region in the necks for these molecules. The dark gray boxes represent known and predicted α-heilx forming regions. Those sequences shown in bold have been shown to form two-stranded α-helical coiled-coils with the exception of MmKif4, see text. Secondary structure predictions were done using "Stable Coil," a program designed to predict the location and stability of alpha-helical coiled-coil conformations within protein sequences (www.pence.ca/stablecoil/). The letters **a** and **d** above each N-type family's sequences represent the **a** and **d** positions of the heptad repeat denoted **abcefg**.

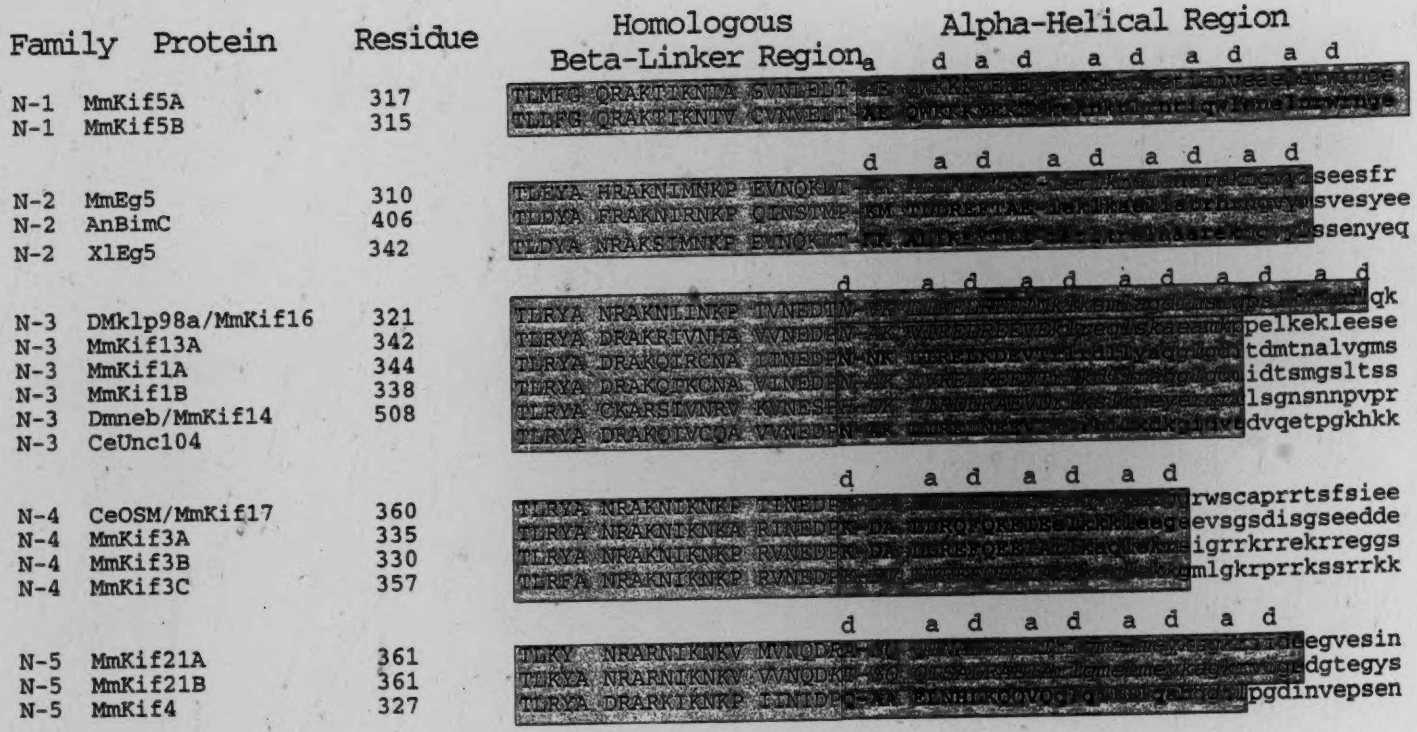
Family
Protein
Residue
Homologous Beta-Linker Region
Alpha-Helical Region
N-1 MmKif5A 317 TLMFG QRAKTIKNTA SVNLELT
N-1 MmKif5B 315 TLLFG QRAKTIKNTV CVNVELT AE
N-2 MmEg5 310 TLEYA HRAKNIMNKP EVNQKLT seesfr
N-2 AnBimC 406 TLDYA FRAKNIRNKP QINSTMP svesyee
N-2 XlEg5 342 TLDYA NRAKSIMNKP EVNQKLT ssenyeq
N-3 DMklp98a/MmKif16 321 TLRYA NRAKNLINKP TVNEDTN qk
N-3 MmKif13A 342 TLRYA DRAKRIVNHA VVNEDPN pelkekleese
N-3 MmKif1A 344 TLRYA DRAKQIRCNA IINEDPN tdmtnalvgms
N-3 MmKif1B 338 TLRYA DRAKQIKCNA VINEDPN idtsmgsltss
N-3 Dmneb/MmKif14 508 TLRYA CKARSIVNRV KVNESPH lsgnsnnpvpr
N-3 CeUnc104 TLRYA DRAKQIVCQA VVNEDPN dvqetpgkhkk
N-4 CeOSM/MmKif17 360 TLRYA NRAKNIKNKP IINEDP rwscaprrtsfsiee
N-4 MmKif3A 335 TLRYA NRAKNIKNKA RINEDPK evsgsdisgseedde
N-4 MmKif3B 330 TLRYA NRAKNIKNKP RVNEDPK igrrkrrekrreggs
N-4 MmKif3C 357 TLRFA NRAKNIKNKP RVNEDP mlgkrprrkssrrkk
N-5 MmKif21A 361 TLKY NRARNIKNKV MVNQDRA egvesin
N-5 MmKif21B 361 TLKYA NRARNIKNKV VVNQDKT dgtegys
N-5 MmKif4 327 TLRYA DRARKIKNKP IINIDPQ pgdinvepsen
a d a d a d a d a d

Fig. VI-2A. Sequence alignment of kinesin-like protein neck regions, N1-N5

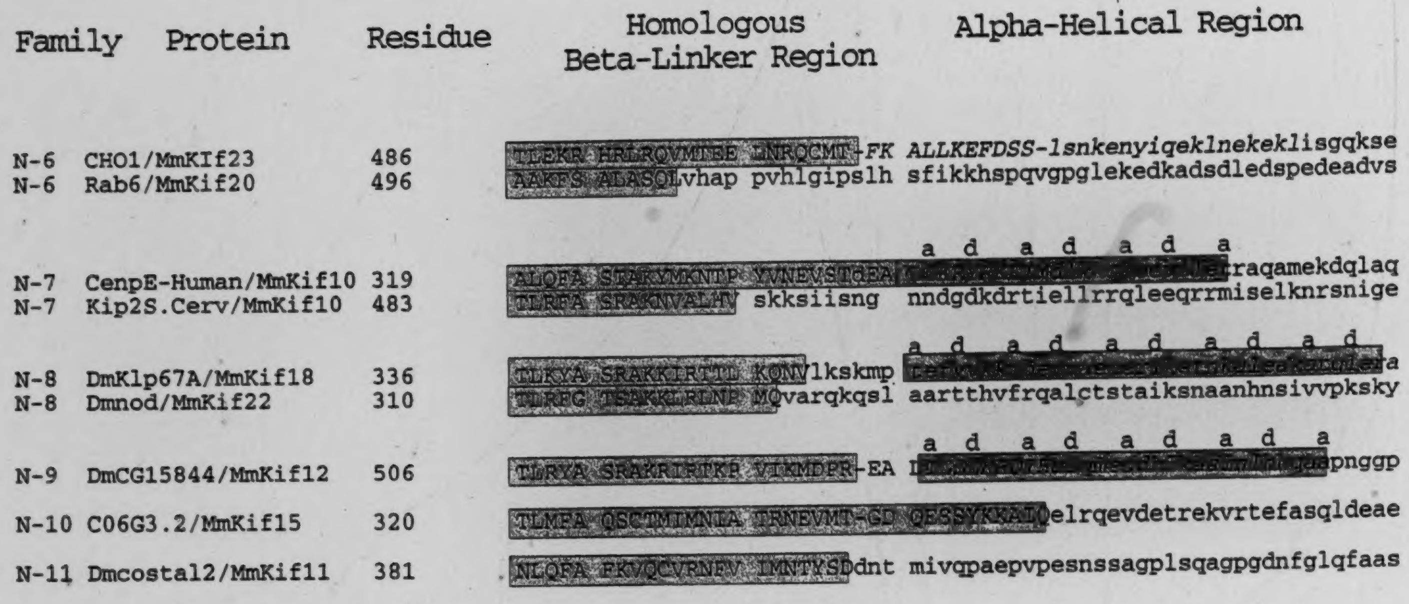

Family	Protein	Residue	Homologous Beta-Linker Region	Alpha-Helical Region
N-6	CHO1/MmKIf23	486	TLEKR HRLRQVMTEE LNRQCMT-*FK*	*ALLKEFDSS-lsnkenyiqeklnekekl*isgqkse
N-6	Rab6/MmKif20	496	AAKFS ALASQLvhap pvhlgipslh	sfikkhspqvgpglekedkadsdledspedeadvs
				a d a d a d a
N-7	CenpE-Human/MmKif10	319	ALQFA STAKYMKNTP YVNEVSTDEA	[illegible]raqamekdqlaq
N-7	Kip2S.Cerv/MmKif10	483	TLRFA SRAKNVALHV skksiisng	nndgdkdrtiellrrqleeqrrmiselknrsnige
				a d a d a d a d a d
N-8	DmKlp67A/MmKif18	336	TLKYA SRAKKIRTTL KQNVlkskmp	[illegible]a
N-8	Dmnod/MmKif22	310	TLRFG TSAKKLRLNP MQvarqkqsl	aartthvfrqalctstaiksnaanhnsivvpksky
				a d a d a d a d a
N-9	DmCG15844/MmKif12	506	TLRYA SRAKRIRTKP VIKMDPR-EA	[illegible]pnggp
N-10	C06G3.2/MmKif15	320	TLMFA QSCTMIMNIA TRNEVMT-GD QESSYKKAIQ	elrqevdetrekvrtefasqldeae
N-11	Dmcostal2/MmKif11	381	NLQFA FKVQCVRNFV IMNTYSDdnt	mivqpaepvpesnssagplsqagpgdnfglqfaas

Fig. VI-2B. Sequence alignment of kinesin-like protein neck regions, N6-N11

Class	Protein	Residue	Peptide sequence
N-2	XlEg5	364	Ac-**K**KAL**I**KE**Y**TEE**I**ER**L**KRE**L**AT**A**REK -amide
N-2	AnBimC	428	Ac-**K**MTL**L**RE**F**TAE**I**EK**L**KAE**L**IA**T**RHR -amide
N-3	MmKif1A	366	Ac-**N**NKL**I**RE**L**KDEVTR**L**RDL**L**YA**Q**-amide
N-3	CeUnc104	358	Ac-**N**AKL**I**RE**L**NEE**V**IK**L**RHI**L**KD**K**GIDVT-amide
N-4	MmKif3A	356	Ac-**K**DAL**L**RQ**F**QKE**I**EE**L**KKK**L**EE**G**-amide
N-4	MmKif3B	351	Ac-**K**DAL**L**RE**F**QEE**I**AR**L**KAQ**L**EK**R**-amide
N-5	MmKif4	349	Ac-**Q**AAE**L**NH**L**KQQ**V**QQ**L**QIL**L**LQ**A**H-amide
			defg**a**bc**d** **a** **d** **a** **d**

Figure VI-3. Amino acid sequences of the synthetic peptides for the putative coiled-coil forming sequences in the listed N-type kinesin superfamily proteins used in this study. Shown are the sub-class and protein names for each of the peptides. The residue number for where each peptide begins in the native protein is listed. The heptad repeat of the putative coiled-coils are denoted **abcdefg**, where positions **a** and **d** are the non-polar residues (shown in bold) involved in the 3-4 hydrophobic repeat. Ac- denotes Na-acetyl and –amide denotes Ca-amide.

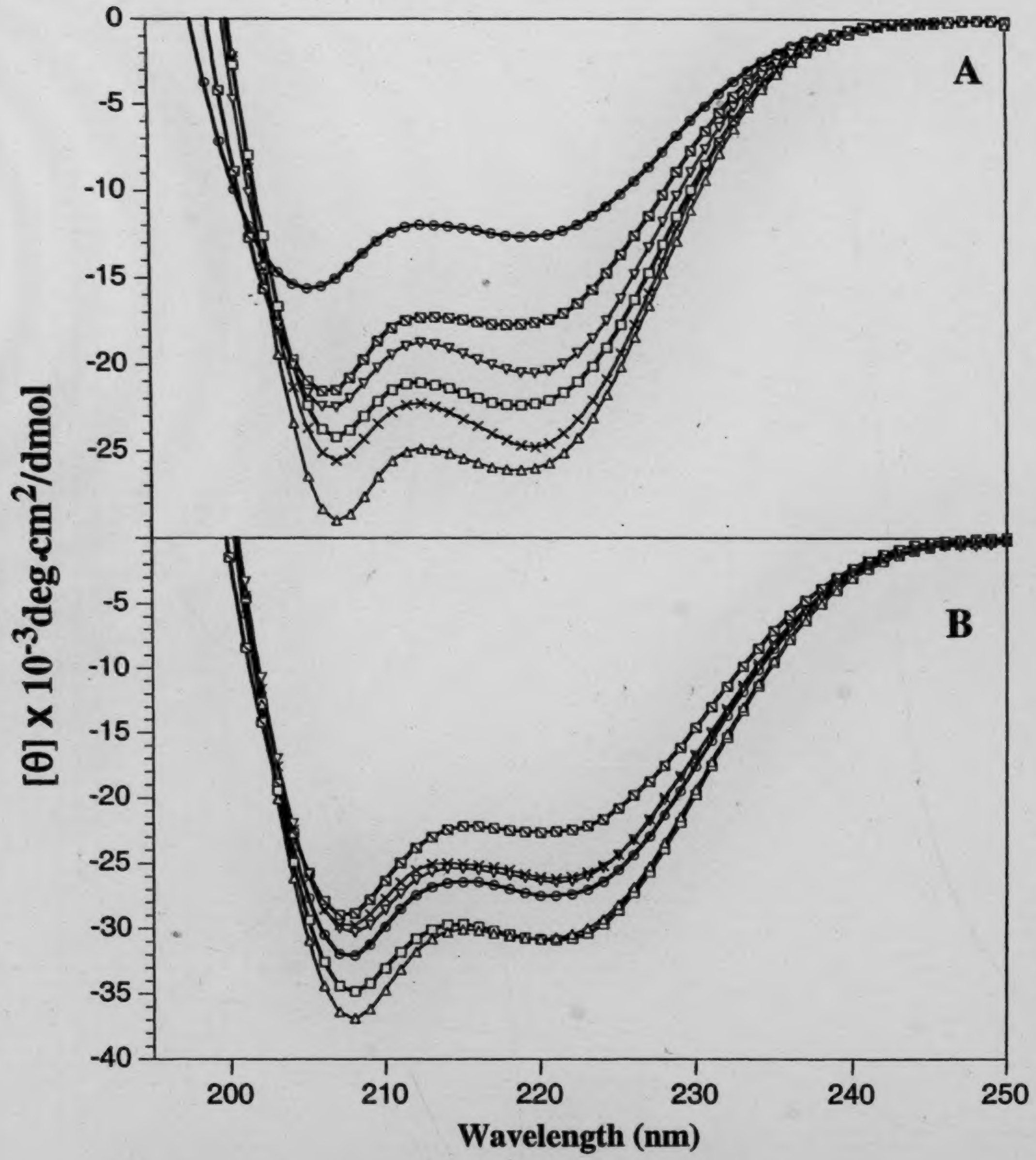

Figure VI-4. The circular dichroism spectra of the synthetic peptides. Panel A shows the peptides in benign medium (0.1M KCl, 0.05M PO_4, 2mM DTT, pH 7) and Panel B shows the peptides in 50% trifluroethanol/benign buffer at 25°C. AnBimC (circles), CeUnc104, (hatched squares), XlEg5 (squares), MmKif3A (downward triangle), MmKif3B (crosses), and MmKif1A (upward triangles).

Table VI-1: Circular dichroism data of reduced, synthetic peptides from N-type kinesin superfamily protiens

		$-[\theta]_{222}$ (deg·cm^2/dmol)[c]		% α-helix[d]		# of calculated helical residues[e]		$[\theta]_{222}/[\theta]_{208}$[f]	
Peptide[a]	# of Residues[b]	benign	50% TFE	benign	50% TFE	benign	50% TFE	benign	50% TFE
AnBimC	25	12600	27250	39	83	10	21	0.84	0.85
CeUnc104	27	17550	22550	53	68	14	18	0.82	0.78
XlEg5	25	22270	30750	68	94	17	24	0.92	0.88
MmKif1A	22	25950	30550	82	97	18	21	0.90	0.83
MmKif3A	22	20450	26400	65	83	14	18	0.91	0.87
MmKif3B	22	24750	26000	78	82	17	18	0.97	0.87

[a] Reduced peptides AnBimC CeUnc104, XlEg5, MmKif1A, MmKif3A, MmKif3B. The amino acid sequence for each peptide is shown in Fig. VI-3.

[b] # of residues per polypeptide chain.

[c] The mean residue molar ellipticities at 222nm were measured at 25°C in benign buffer (0.1 M KCl, 0.05 M PO_4, pH 7, 2mM DTT). For samples containing TFE, the buffer was diluted 1:1 (v/v) with TFE.

[d] The % helical content was calculated from the ratio of the observed $[\theta]_{222}$ value divided by the predicted molar ellipticity X 100. The predicted molar ellipticity was calculated from the equation $[\theta]_{222} = 40 \times 10^3 \times (1\text{-}4.6/n)$ for the chain length dependence of an α-helix [Gans et al., 1991], where n is the number of residues in the peptide. A peptide of 22 residues has a predicted molar ellipticity of –31,600.

[e] The # of helical residues wa calculated by multiplying the % α-helix by the # of residues in the polypeptide chain., e.g., for reduced MmKif1A in benign medium, 25,950/31,600 x 22 residues = 18 α-helical residues predicted in the coiled-coil. The 50% TFE values reflect the maximum helical residues that can be formed at a 90μM concentration.

[f] The molar ellipticity values at 222nm and 208nm for each peptide were used to calculate the ratio $[\theta]_{222}/[\theta]_{208}$.

To assess the stability of the coiled-coil forming peptides, MmKif1A, MmKif3B, XlEg5, Ceunc104, and AnBimC, we denatured the α-helical structure of the peptides using guanidine hydrochloride, a denaturant shown to disrupt secondary and quaternary structures in proteins [Monera et al., 1994a] (Fig. VI-5A). The most stable coiled-coil was the neck region of MmKif1A with a $GdnHCl_{1/2}$ of 2.4M while the weakest was that of AnBimC with a $GdnHCl_{1/2}$ of 0.6M. The stability values for the peptides are shown in Table VI-2. The differences in the core residues between the coiled-coils of MmKif1A and AnBimC are an Ile to Leu substitution in an **a** position, a Leu to a Phe in a **d** position and a Val to an Ile in an **a** position. According to Wagschal et al. (1999) the substitution of Ile to Leu, and Val to Ile in an **a** position would lead to a difference in the free energy of unfolding of these peptides. In their paper, the ΔG for unfolding of coiled-coil analogues with all twenty amino acids substituted into the core of a peptide were determined. The difference in the free energy of unfolding relative to the alanine analogue was then calculated for each analogue. Using the ΔΔG values for the Ile, Leu, and Val analogues of 3.88, 3.48, and 4.10 kcal/mol, respectively, the substitutions between the MmKif1A and AnBimC coiled-coils could thus be analyzed in a quantitative manner. Thus, an Ile to Leu substitution would decrease stability by 0.04kcal/mol and the substitution of Ile for Val would lead to a further destabilization by another 0.06kcal/mol.

Furthermore, the study conducted by Tripet et al. (2000) determined the ΔΔG free energy of unfolding for the substitution of all 20 natural amino acids relative to Ala in the **d** position. Subtracting the two ΔΔG values for the Leu and Phe analogues (3.8-1.2 kcal/mol) shows a difference of 2.6 kcal/mol in the stability between the MmKif1A and

AnBimC coiled-coils. Taking the determined differences in the ΔΔG of unfolding for the **a** and **d** substitutions between MmKif1A and AnBimC, there should be a 3.6 kcal/mol difference between their free energies of unfolding. This 3.6 kcal/mol would come through the substitutions of residues in the hydrophobic cores.

In the present study, the ΔGs of unfolding for the peptides were determined by denaturing the peptides with guanidine hydrochloride. ΔG^{H_2O} for each peptide was determined, in benign medium, by extrapolating from the ΔG_u values determined at various denaturant concentrations, in a similar manner to Wagschal et al. (1999) and Tripet et al. (2000) (Fig. VI-5B). The ΔG^{H_2O} of unfolding for MmKif1A was determined to be 11 kcal/mole while that of AnBimC was determined to be 8 kcal/mol. This is a difference of 3.0 kcal/mole, not far from the calculated value of 3.6 kcal/mole. This result suggests that differences in the hydrophobic core can explain differences in stability in this case, but helical propensity and electrostatics can make major contributions to stability (Lee et al., 2001).

Interestingly MmKif3B and AnBimC have the exact same hydrophobic core residues, except at the final **d** position. The difference in their $GdnHCl_{1/2}$ points is 1.7-0.6 = 1.1M, while the difference in their extrapolated $\Delta G^{H_2 0}$ values is 1.5 kcal/mole. The cross-sectional view of the coiled-coils formed by the neck regions of MmKif3B and AnBimC are shown in figure VI-6. Analysis of the **a** and **d** hydrophobic residues reveals the similarity between the hydrophobic core residues. The sequences are presented in a linear format below the cross-sectional view. The hydrophobic residues are

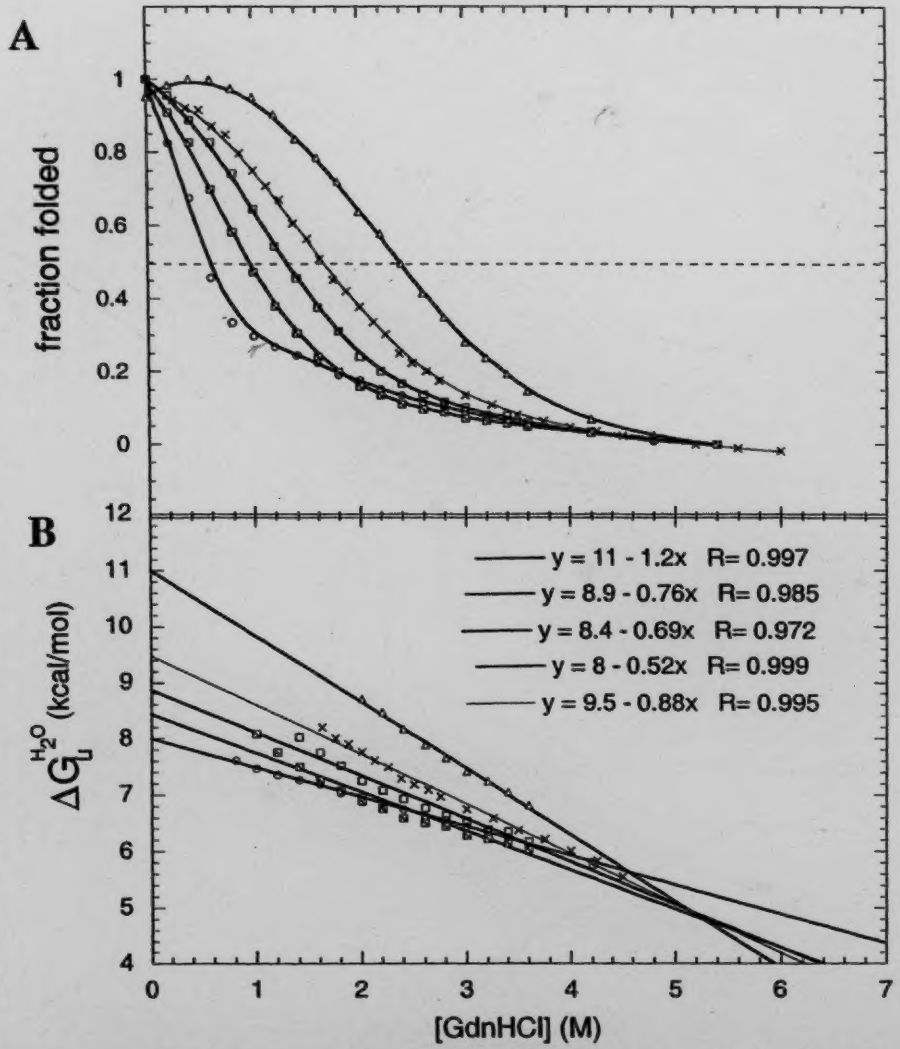

Figure VI-5. Denaturation profiles of the synthetic peptides. Panel A shows the denaturation profiles, with guanidine hydrochloride, of the coiled-coils formed by the neck regions in the examined proteins. Panel B shows the extrapolation of ΔG_u (the free energy of unfolding) values for each of the coiled-coil forming peptides. ΔG_u at each guanidine hydrochloride concentration was calculated using the equation $-RT\ln(K_D)$, where $K_D=(f_U/f_f)$. f_u is fraction unfolded and f_f is fraction folded for the peptide at each respective guanidine hydrochloride concentration. R, the ideal gas constant, was 0.0019872 kcal x K^{-1} x mol^{-1}, and T was 298K. MmKif1A (upward triangles), MmKif3B (crosses), XlEg5 (squares), CeUnc104 (hatched squares), and AnBimC (circles).

Table VI-2. Neck-region coiled-coil stability data

[a]Peptide	[b]$[\mathrm{GdnHCl}]_{1/2}$ (M)	[c]ΔG^{H_2O} kcal/mol	[d]$\Delta\Delta G$ kcal/mol
MmKif1A	2.4	11	3.0
MmKif3B	1.75	9.5	1.5
XlEg5	1.3	8.9	0.9
CeUnc104	1.0	8.4	0.4
AnBimC	0.6	8.0	0

[a] Reduced peptides AnBimC CeUnc104, XlEg5, MmKif1A, MmKif3A, MmKif3B. The amino acid sequence for each peptide is shown in Fig. VI-3.

[b] $\mathrm{GdnHCl}_{1/2}$ is the transition midpoint, the concentration of guanidine hydrochloride (M) required to give a 50% decrease in the molar ellipticity at 222 nm.

[c] ΔG^{H_2O} was determined by the extrapolation of ΔG_u values. ΔG_u at each guanidine hydrochloride concentration was calculated using the equation $-RT\ln(K_D)$, where ΔG_u is the free energy of unfolding for the peptides at various GdnHCl concentrations, ΔG^{H_2O}, is the free energy of unfolding in benign medium, $K_D=(f_U/f_f)$. f_u is fraction unfolded and f_f is fraction folded for the peptide at each respective guanidine hydrochloride concentration. R, the ideal gas constant, was 0.0019872 kcal x K^{-1} x mol^{-1}, and T was 298K.

[d] $\Delta\Delta G$ is the experimentally determined difference in the free energy of unfolding for the kinesin-like coiled-coil neck regions relative to the free energy of unfolding value obtained for AnBimC.

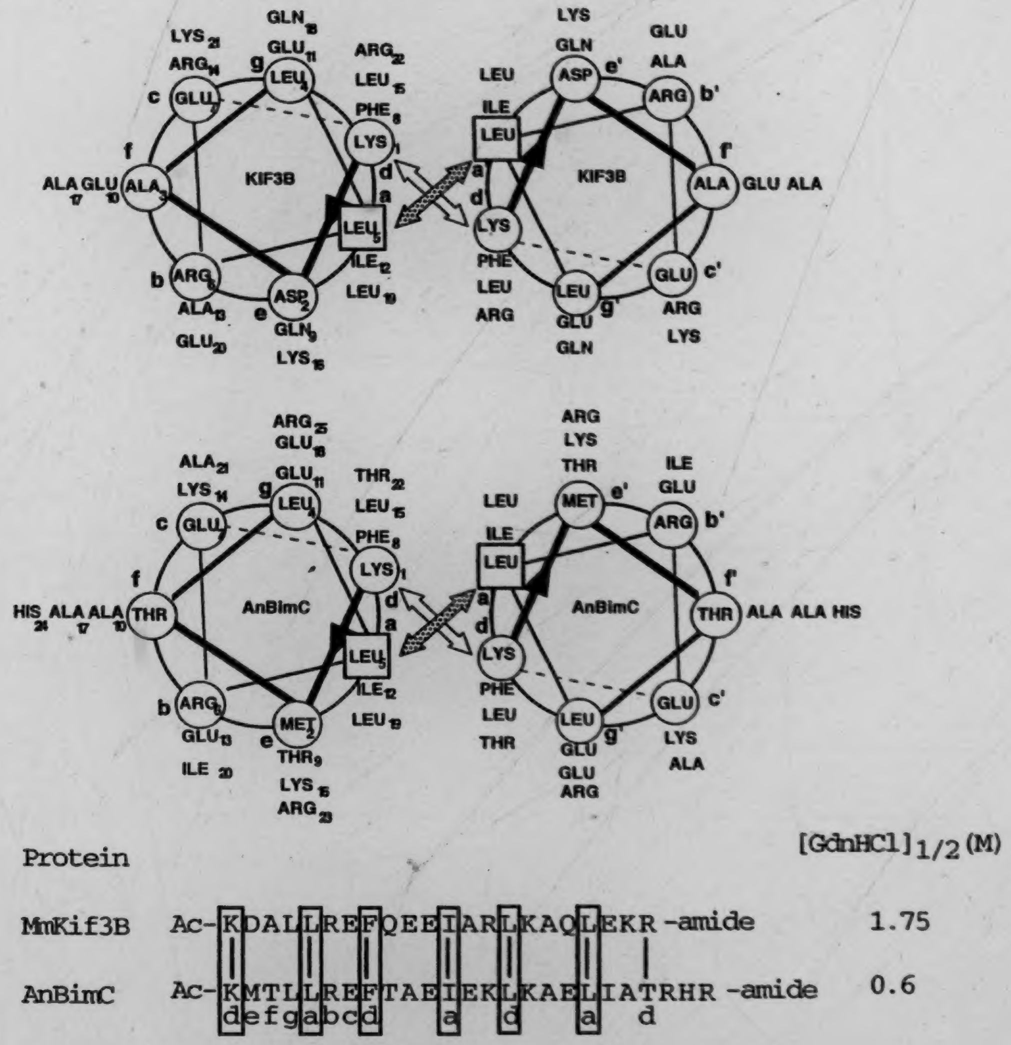
KIF3B
KIF3B
AnBimC
AnBimC
a
d
e
f
g
b
c
a'
d'
e'
f'
g'
b'
c'
LYS 1
ASP 2
ALA 3
LEU 4
LEU 5
ARG 6
GLU 7
PHE 8
ALA GLU ALA
GLU ALA
HIS ALA ALA
ALA ALA HIS
Protein
[GdnHCl]1/2 (M)
MmKif3B Ac-KDALLREFQEEIARLKAQLEKR-amide 1.75
AnBimC Ac-KMTLLREFTAEIEKLKAELIATRHR-amide 0.6
d e f g a b c d a d a d

Figure VI-6. A representative cross-sectional view of the α-helical coiled-coils formed by AnBimC, and Kif3B. The heptad defgabc, begins at a lysine (residue 1) for the two peptides. The two coiled-coils have the same hydrophobic **a** and **d** residues with the exception of the last **d** residue. Below the cross-sections is a linear representation of the sequences. The lines between the two sequences denote the **a** and **d** residues, and the boxes indicate similar hydrophobic residues.

shown in bold and a line is drawn between each core residue. Residues that are exactly identical are boxed. It is known that the ends of a coiled-coil "breathe", and it was elegantly depicted that mutations of Leu to Ala in the hydrophobic core positions are more destabilizing to coiled-coil structure than those made at the termini [Zhou et al., 1992a]. Therefore, the Arg to Thr substitution at the C-terminal **d** position is not likely to be as important for the difference in the stability between the coiled-coils. We hesitate to apply the results from Tripet et al. (2000) to describe the difference between an Arg to Thr substitution since the substitution data collected were for substitutions made directly in the center of the coiled-coil while the difference between MmKif3B and AnBimC is observed at the C-terminus. Interestingly, the coiled-coils of AnBimC and MmKif3B are only 3 heptads long. It was shown by Su et al. (1994) that 3 heptads are required to initiate the formation of a two-stranded coiled-coil for a model coiled-coil sequence. The peptides were shown to increase in stability with an increase in their lengths. Perhaps the 3 heptad coiled-coil is more sensitive to what would be considered a minor difference for a stable 4 or 5 heptad coiled-coil?

An analysis of the average helical propensity [Zhou et al., 1994c], throughout the sequences (Fig. VI-7) of MmKif3B and AnBimC, shows that the AnBimC sequence has a lower helical propensity overall. Remarkably, not only do both peptides have the same helical propensity patterns, the pattern seems to mimic the stability results determined for the individual heptads found for the 5 heptad neck coiled-coil of conventional kinesin [Tripet et al., 1997]. Helical propensity is a factor, which contributes to overall stability of the individual peptide backbones, and as was shown by Zhou et al. (1993b) and Kohn et al. (1997), that increasing the stability of helical structure of each peptide's backbone

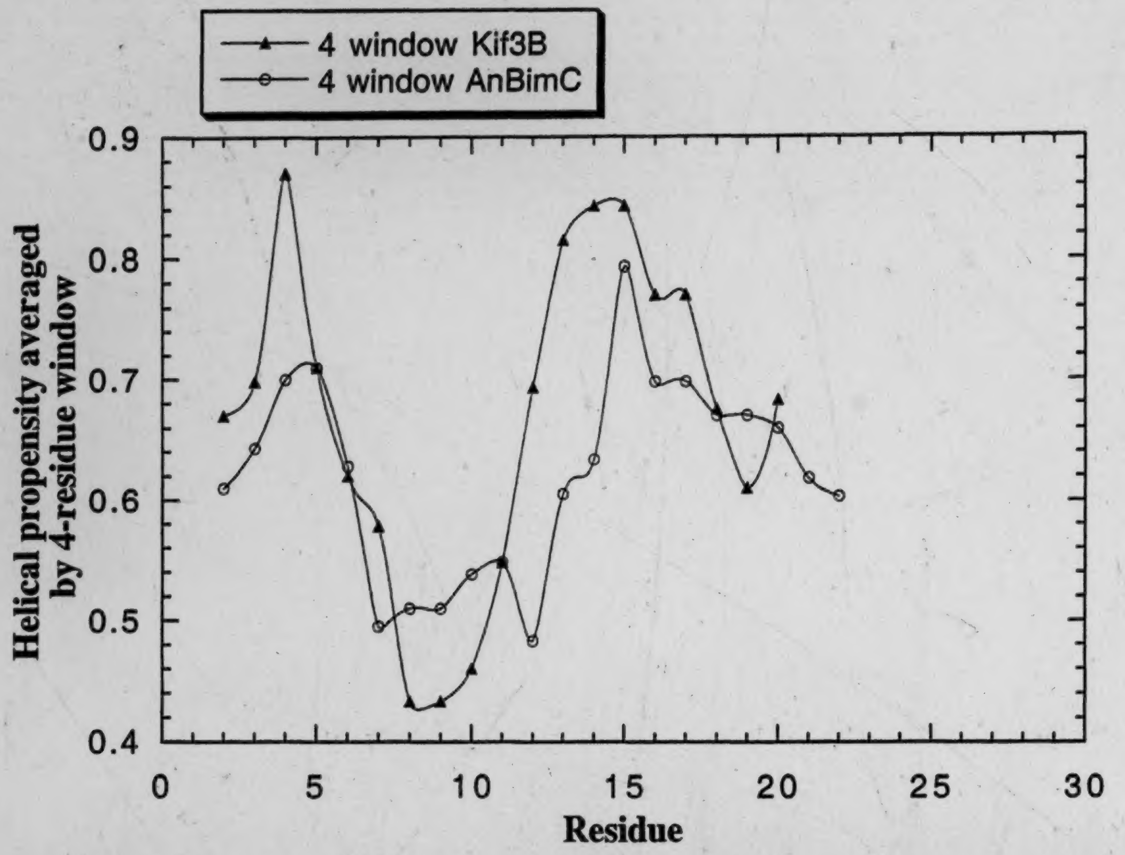

Figure VI-7. A 4-residue window helical propensity plot. The sequences of MmKif3B and AnBimC were summed using helical propensity values (Zhou et al., 1994c). Starting at the N-terminus, four residues were summed and averaged. This window of four residues was then incrementally moved to the C-terminus of the sequences, adding and averaging the helical propensity values of four residues at a time. MmKif3B (closed triangles) and AnBimC (open circles).

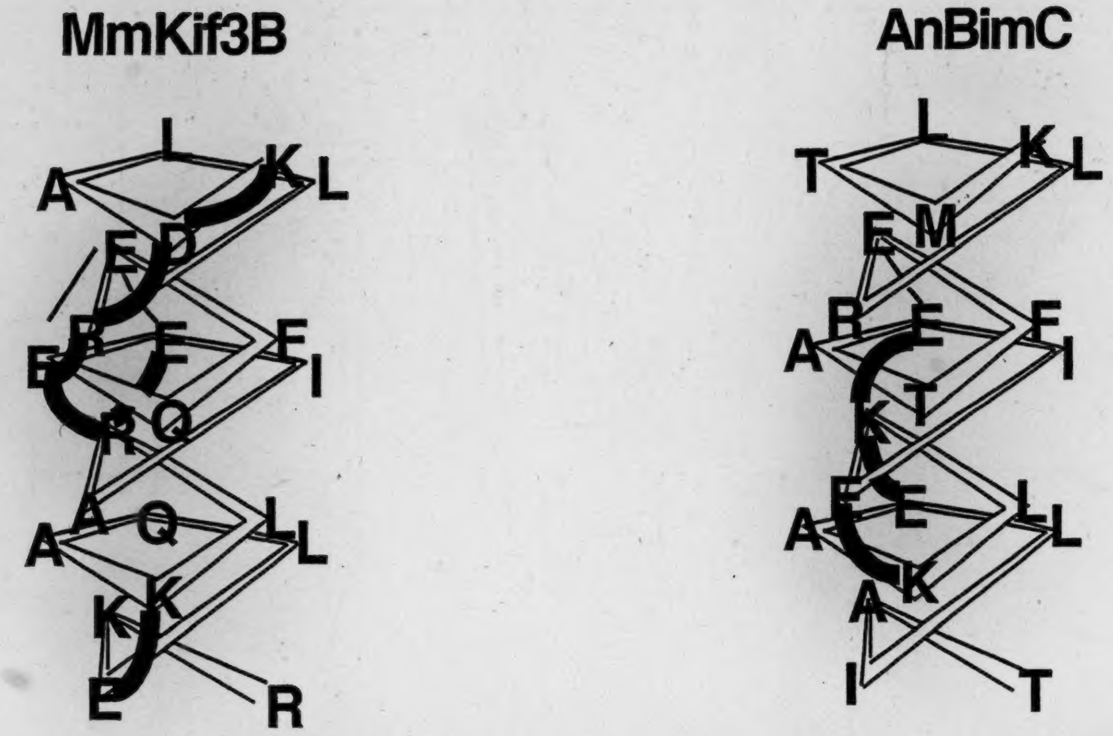
MmKif3B
L
A
K
L
E
D
R
E
F
F
I
E
R
Q
A
Q
L
A
L
K
K
E
R
AnBimC
L
T
K
L
E
M
R
E
F
A
I
T
K
E
E
L
A
L
A
K
I
T

Figure VI-8. A schematic representation of the intrachain ionic interactions for the residues in MmKif3B and AnBimC. The tops of the helices are the N-termini and the sequence winds its way down the helix. Electrostatic attractions are shown by dark, broad lines connecting the residues, while repulsions are shown by lighter, thin lines connecting the potentially interacting amino acid side-chains.

through intrachain electrostatic attractions led to the increased stability of the dimeric coiled-coil. Thus, factors that contribute to the stability of the helical backbone contribute to the stability of the dimer. In addition to simple electrostatic interactions, complex associations that lead to the formation of an ion network seem to have a greater stabilizing effect on protein structure. Ion networks have been found in thermophilic proteins [Vogt et al., 1997], and are thought to add resiliency to their folded structures [Aguilar et al., 1997]. The MmKif3B backbone has 6 potential intrahelical ionic attractions (Fig. VI-8) and 2 intrachain repulsions, while the backbone of AnBimC has 3 attractions and 1 repulsion. Though the net difference for intrachain attractions is +4 - +2 = +2, which is a small difference, the short length of these coiled-coils may exacerbate the difference. It is also apparent that MmKif3B's backbone electrostatic interactions create an extensive ion network. Furthermore, not only is the region of the backbone with the lowest helical propensity fortified by intrachain attractions, the N-terminal Lys also plays a role in this network, and this may serve to increase MmKif3B's stability relative to that of AnBimC, through decreasing N-terminal fraying of the backbone, leading to the concomitant increase in dimer stability.

Electrostatics:

The results generated from the systematic study of the complementary charged regions found in the Kif3A and Kif3B motor proteins lead to the interesting result showing how segments of sequence, abundant in positively charged amino acids, do not disrupt the stability of a coiled-coil when placed at the C-terminus of the coiled-coil. Modifying the side-chain of lysine to see how the aliphatic portion contributes in counteracting repulsions between the charged amino groups, would be an interesting next step.

Stalk region of Kif3A/Kif3B:

The next step in our research would also be to characterize the coiled-coil of the stalk region in Kif3A/Kif3B, C-terminal to the complementary charged hinge region. Once the regions capable of forming a coiled-coil are identified, we could determine which portions of the stalk coiled-coil, if any, can exclusively form heterodimer. Also, through studying the portions of the coiled-coil forming regions of the stalk separately, we might obtain some insight into which regions are more important for specifying heterodimer formation between the Kif3A and Kif3B motor proteins.

BIBLIOGRAPHY[4]

Adamson, J. G., Zhou, N. E., and Hodges, R. S. (1993) Structure, function and application of the coiled-coil protein folding motif. *Curr. Opin. Biotechnol.* **4,** 428-437.

Aguilar, C. F., Sanderson, I., Moracci, M., Ciaramella, M., Nucci, R., Rossi, M., and Pearl, L. H. (1997) Crystal structure of the b-Glycosidase from the hyperthermophlic Archeon *Sulfolobus solfataricus*: resilience as a key factor in thermostability. *J. Mol. Biol.* **271,** 789-802.

Allen, R., Metuzals, J., Ichiji, T., Brady, S., and Gilbert, S. P. (1982) Fast Axonal Transport in Squid Giant Axon. *Science* **218,** 1127-1128.

Allen, R. D., Weiss, D. G., Hayden, J. H., Brown, D. T., Fujiwake, H., and Simpson, M. (1985) Gliding movement of and bidirectional organelle transport along single native microtubules from squid axoplasm. Evidence for an active of microtubules in cytoplasmic transport. *J. Cell Biol.* **100,** 1736-1752.

Anderson, D. E., Becktel, W. J., and Dahlquist, F. W. (1990) pH-Induced denaturation of proteins: A single salt bridge contributes 3-5 kcal/mol to the free energy of folding of T4 lysozyme. *Biochemistry* **29,** 2403-2408.

Bagger, S. and Wagner, K. (1998) Molecular recognition of colbalt(III)-ligated peptides by serine proteases: The role of electrostatic effects. *J. Peptide Res.* **52,** 273-282.

Ball, H. L. M., P. (1996) Chemical synthesis and purification of proteins: A methodology. *Int. J. Peptide Protein Res.* **48,** 31-47.

Beech, P. L., Pagh-Roehl, K., Noda, Y., Hirokawa, N., Burnside, B., and Rosenbaum, J. L. (1996) Localization of kinesin superfamily proteins to the connecting cilium of fish photoreceptors. *J. Cell Sci.* **109,** 889-897.

Ben-Naim, A. (1991) The role of hydrogen bonds in protein folding and protein association. *J. Phys. Chem.* **95,** 1437-1444.

Betz, S. F., Bryson, J. W., and DeGrado, W. F. (1995) Native-like and structurally characterized designed alpha-helical bundles. *Curr. Opin. Struct. Biol.* **5,** 457-463.

Bloom, G., Wagner, M., Pfister, K., and Brady, S. (1988) Native Structure and Physical Properties of Bovine Kinesin and Identification of the ATP-binding Subunit Polypeptide. *Biochemistry* **27,** 3409-3416.

---

[4] Publications arising from this thesis are printed in bold type

Bodanszky, M. (1988) *Peptide Chemistry: A Practical Textbook.,. Springer_Verlag, New York.*

Brady, S. and Lasek, R. (1982) Fast Axonal Transport in Extruded Axoplasm from Squid Giant Axon. *Science* **218,** 1129-1131.

Brady, S. T. (1985) A novel brain ATPase with properties expected for the fast axonal transport motor. *Nature* **317,** 73-75.

Camacho, C. J., Weng, Z., Vajda, S., and DeLisi, C. (1999) Free energy landscapes of encounter complexes in protein-protein association. *Biophys. J.* **76,** 1166-1178.

Case, R. B., Pierce, D. W., Hom-Booher, N., Hart, C. L., and Vale, R. D. (1997) The directional preference of kinesin motors is specified by an element outside of the motor catalytic domain. *Cell* **90,** 959-66.

Chana, M. S., Tripet, B. P., Mant, C. T., and Hodges, R. S. (2002a) The Role of Unstructured Highly Charged Regions on the Stability and Specificity of Dimerization of Two-Stranded Alpha-Helical Coiled-coils: Analysis of the Neck-Hinge Region of the Kinesin-like Motor Protein MmKif3A. *J. Struct. Biol.* In press.

Chana, M. S., Tripet, B. P., Mant, C. M., and Hodges, R. S. (2002b) An Investigation into the effects of highly charged regions on the stability of the neck region coiled-coil of Kinesin-Like Motor Protein Kif3B. *Protein Sci.* Submitted.

Chana, M. S., Tripet, B. P., Mant, C. M., and Hodges, R. S. (2002c) Stability and specificity of heterodimer formation for the neck regions of the motor proteins Kif3A and Kif3B. *J. Biol. Chem.* Manuscript in preparation.

Chang, C. T., Wu, C. C., and Yang, J. T. (1978) Circular Dichroic Analysis of Protein Conformation Inclusion of the Beta Turns. *Anal. Biochem.* **91,** 13-31.

Chen, Y. H., Yang, J. T., and Chau, K. H. (1974) Determination of the Helix and Beta Form of Proteins in Aqueous Solution by Circular Dichroism. *Biochemistry* **13,** 3350-3359.

Cohen, C. and Parry, D. A. D. (1994) Alpha-helical coiled-coils: more facts and better predictions. *Science* **263,** 488-489.

Cohn, S., Ingold, A., and Scholey, J. (1987) Correlation between the ATPase and Microtubule translocating activities of Sea Urchin Egg Kinesin. *Nature* **328,** 160-163.

Cole, D. G., Chinn, S. W., Wedaman, K. P., Hall, K., Vuong, T., and Scholey, J. M. (1993) Novel heterotrimeric kinesin-related protein purified from sea urchin eggs. *Nature* **366,** 268-270.

Cole, D. G., Diener, D. R., Himelblau, A. L., Beech, P. L., Fuster, J. C., and Rosenbaum, J. L. (1998) Chlamydomonas Kinesin-II-dependent intraflagellar transport (IFT): IFT particles contain proteins required for Ciliary assembly in Caenorhabditis elegans sensory neurons. *J. Cell Biol.* **141,** 993-1008.

Creighton, T. E. (1990) Protein folding. *Biochem. J.* **270,** 1-16.

de Cuevas, M., Tao, T., and Goldstein, L. S. (1992) Evidence that the stalk of Drosophila kinesin heavy chain is an a-helical coiled-coil. *J. Cell Biol.* **116,** 957-965.

De Marco, V., Burkhard, P., Le Bot, N., Vernos, I., and Hoenger, A. (2001) Analysis of heterodimer formation by Xklp3A/B, a newly cloned kinesin-II from Xenopus laevis. *EMBO J.* **20,** 3370-3379.

DeGrado, W. F., Wasserman, Z. R., and Lear, J. D. (1989) Protein design, a minimalist approach. *Science* **243,** 622-628.

Dill, K. A. (1990) Dominant Forces in Protein Folding. *Biochemistry* **29,** 7133-7155.

Ellisman, M. H. and Porter, K. R. (1980) Microtrabecular structure of axoplasmic matrix: visualization of cross-linking structures and their distribution. *J. Cell Biol.* **87,** 464-79.

Feilds, G. B. (1997) Editor of *Solid Phase Peptide Synthesis: Methods in Enzymology vol. 289*.

Fisher, B. M., Shultz, L. W., and Raines, R. T. (1998) Coulombic effects of remote subsites on the active site of ribonuclease A. *Biochemistry* **37,** 17386-17401.

Fontenot, J. D., Ball, J. M., Miller, M. A., David, C. M., and Montelaro, R. C. (1991) A survey of potential problems and quality contol in peptide synthesis by the fluoroenylmethoxycarbonyl procedure. *J. Pep. Res.* **1,**19-25.

Gans, P. J., Lyu, P. C., Manning, M. C., Woody, R. W., and Kallenbach, N. R. (1991) The helix-coil transition in heterogeneous peptides with specific side-chain interactions: theory and comparison with CD spectral data. *Biopolymers* **31,** 1605-1614.

Gibbsons, I. R. and Rowe, A. J. (1965) Dynein: A protein with adenosine triphosphate activity from cilia. *Science* **149,** 424-426.

Goldstein, L. S. B. and Philp, A. V. (1999) The road less traveled: Emerging principles of kinesin motor utilization. *Annu. Rev. Cell Dev. Biol.* **15,** 141-83.

Goodson, H. V., Kang, S. J., and Endow, S. A. (1994) Molecular phylogeny of the kinesin family of microtubule motor proteins. *J. Cell Sci.* **107,** 1875-1884.

Grafstein, B. and Forman, D. S. (1980) Intracellular Transport in Neurons. *Physiological Reviews.* **60,** 1168-1210.

Hackney, D. D. (1988) Kinesin ATPase: rate-limiting ADP release. *Proc Natl Acad Sci* U S A. **85,** 6314-8.

Hackney, D. D. (1992) Kinesin and myosin ATPases: variations on a theme. *Philos Trans R Soc Lond B Biol Sci.* **336,** 13-7; discussion 17-8.

Hagihara, Y., Tan, Y., and Goto, Y. (1994) Comparison of the conformational stability of the molten globule and native states of horse cytochrome c. *J. Mol. Biol.* **237,** 336-348.

Hayes, D. B., Laue, T., and Philo, J. (1998) Sedimentation Interpretation Program, Version 1.01. Copyright (c) 1995-1998.

Hendsch, Z. S. and Tidor, B. (1994) Do salt bridges stablize proteins? A continuum electrostatic analysis. *Prot. Sci.* **3,** 211-226.

Hirokawa, N. and Yorifuji, H. (1986) Cytoskeletal Architecture of Reactivated Crayfish Axons, with special reference to crossbridges amoung microtubules and between microtubules and membrane organelles. *Cell Motil. Cytoskel.* **6,** 458-468.

Hirokawa, N., Pfister, K. K., Yorifuji, H., Wagner, M. C., Brady, S. T., and Bloom, G. S. (1989) Submolecular domains of bovine brain kinesin identified by electron microscopy and monoclonal antibody decoration. *Cell* **56,** 867-878.

Hiroto, Y., Nakata, T., Okada, Y., and Hirokawa, N. (1995) Kif3A/B: A Heterodimeric Kinesin Superfamily Protein That Works as a Microtubule Plus End-directed Motor for Membrane Organelle Transport. *J. Cell Biol.* **130,** 1387-1399.

Hodges, R. S., Sodek, J., Smillie, L. B., and Jurasek, L. (1972) Tropomyosin: amino acid sequence and coiled-coil structure. *Cold Spring Harbor Symp. Quant. Biol.* **37,** 299-310.

Hodges, R. S. (1992) Unzipping the secrets of coiled-coils. *Curr. Biol.* **2,** 122-124.

Hodges, R. S. (1996) De novo design of alpha-helical proteins: basic research to medical applications. *Biochem. Cell Biol.* **74,** 133-154.

Holzbaur, E. L. and Johnson, K. A. (1986) Rate of ATP synthesis by dynein. *Biochemistry.* **25,** 428-434.

Hunenberger, P. H., Helms, V., Narayanna, N., Taylor, S. S., and McCammon, J. A. (1999) Determinants of ligand binding to cAMP-dependent protein kinase . *Biochemistry* **38,** 2358-2366.

Ingold, A., Cohn, S., and Scholey, J. (1988) Inhibition of Kinesin-driven Microtubule Motility by Monoclonal Antibodies to Kinesin Heavy Chains. *J. Cell Biol.* **107,** 2657-2667.

Inoue, S. (1997) The role of microtuble assemby dynamics in mitotic force generation and functional organization of living cells. *J. Struc. Biol.* **118,** 87-93.

Kaiser, E. T. and Kezdy, F. J. (1983) Secondary structures of proteins and peptides in amphiphilic enviornments. *Proc. Natl. Acad. Sci. USA* **80,** 1137-1143.

Kamal, A. and Goldstein, L. S. B. (2000) Connecting vesicle transport to the cytoskeleton. *Curr. Opin. Cell Biol.* **12,** 503-508.

Kamtekar, S., Schiffer, J. M., Xiong, H., Babik, J. M., and Hecht, M. H. (1993) Protein design by binary patterning of polar and non-polar amino acids. *Science* **262,** 1680-1685.

Kim, A. J., and Endow, S. A. (2000) A kinesin family tree. *J. Cell Science.* **113,** 3681-2.

Kohn, W. D., Cyril, K. M., and Hodges, R. S. (1995a) Protein destabilization by electrostatic repulsions in the two-stranded alpha-helical coiled-coil/leucine zipper. *Protein Sci.* **4,** 237-250.

Kohn, W. D., Oscar, M. D., Kay, C. M., and Hodges, R. S. (1995b) The Effects of Interhelical Repulsions between Glutamic Acid Residues in Controlling the Dimerization and Stability of Two-stranded a-Helical Coiled-coils. *J. Biol. Chem.* **270,** 25495-25506.

Kohn, W. D., Kay, C. M., and Hodges, R. S. (1997a) Positional dependence of the effects of negatively charged Glu side chains on the stability of two-stranded alpha-helical coiled-coils. *J. Pept. Sci.* **3,** 209-223.

Kohn, W. D., Kay, C. M., and Hodges, R. S. (1997) Salt effects on protein stability: Two-stranded a-helical coiled-coils containing inter- or intrahelical ion pairs. *J. Mol. Biol.* **267,** 1039-1052.

Kohn, W. D. and Hodges, R. S. (1998) De novo design of alpha-helcal coiled-coils and bundles: models for development of protein design principles. *Trends Biotech.*

Kondo, S., Sato-Yoshitake, R., Noda, Y., Aizawa, H., Nakata, T., Matsuura, Y., and Hirokawa, N. (1994) Kif3A Is a New Microtubule-based Anterograde Motor in the Nerve-Axon. *J. Cell Biol.* **125,** 1095-1107.

Kozielske, F., Sack, S., Marx, A., Thormahlen, M., Schonbrunn, E., Biou, V., Thompson, A., Mandelkow, E. M., and Mandelkow, E. (1997) The crystal structure of dimeric kinesin and implications for microtubule-dependent motility. *Cell* **91,** 985-994.

Kull, J., Sablin, E., Lau, R., and Fletterick, R. (1996) Crystal structure of the kinesin motor domain reveals a structureal similarity to myosin. *Nature* **380,** 550-555.

Kuznetsov, S. A. and Gelfand, V. I. (1986) Bovine brain kinesin is a microtubule-activated ATPase. *Proc. Natl. Acad. Sci. USA* **83,** 8530-8534.

Kuznetsov, S. A., Vaisberg, E. A., Shanina, N. A., Magretova, N. N., Chernyak, V. Y., and Gelfand, V. I. (1988) The quaternary structure of bovine brain kinesin. *EMBO J.* **7,** 353-356.

Kuznetsov, S. A., Vaisverg, Y. A., Rothwell, S. W., Murphy, D. B., and Gelfand, V. I. (1989) Isolation of 45-kDa Fragment from the Kinesin Heavy Chain with Enhanced ATPase and Microtubule-binding Activities. *J. Biol. Chem.* **264,** 589-595.

Kwok, S. C., Tripet, B., Man, J. H., Chana, M. S., Lavigne, P., Mant, C. T., and Hodges, R. S. (1998) Structural cassette muagenesis in a de novo designed protien: proof of a novel concept for examining protein folding and stability. *Biopolymers* **47,** 101-123

Lasek, R. J. and Brady, S. T. (1985) Attachment of transported vesicles to microtubles in axoplasm is facilitated by AMP-PNP. *Nature* **316,** 645-647.

Lau, S. Y. M., Taneja, A. K. H., and Hodges, R. S. (1984a) Synthesis of a model protein of defined secondary and quaternary structure; effect of chain length on the stabilzation and formation of two-stranded a-helical coiled-coils. *J. Biol. Chem.* **259,** 13253-13261.

Lau, S. Y. M., Taneja, A. K., and Hodges, R. S. (1984b) Effects of solvents and hydrophobic supports on the secondary and quaternary structure of a model protein: reversed-phase and size-exclusion high performance liquid chromatography. *J. Chromatogr.* **317,** 129-140.

Lavigne, P., Kondejewski, L. H., Houston, M. E., Sonnichsen, F. D., Lix, B., Sykes, B. D., and Hodges, R. S. (1995) Preferential Heterodimeric Parallel Coiled-coil Formation by Synthetic Max and c-Myc Leucine Zippers: A Description of Putative Electrostatic Interactions Responsible for the Specificity of Heterodimerization. *J. Mol. Biol.* **254,** 505-520.

Lavigne, P., Sonnichsen, F. D., Kay, C. M., and Hodges, R. S. (1996) Interhelical salt bridges, coiled-coil stability, and specificity of dimerization. *Science* **271,** 1136-1138.

Lee, D. L., Lavigne, P., and Hodges, R.S. (2001) Are trigger sequences essential in the folding of two-stranded alpha-helical coiled-coils? *J Mol Biol.* **306,** 539-53.

Loladze, V. V., Ibarra-Molero, B., Sanchez-Ruiz, J. M., and Makhatadze, G. I. (1999) Engineering a Thermostable Protein via optimization of charge-charge interactions on the protein surface. *Biochemistry* **38,** 16419-16423.

Lounnas, V. and Wade, R. C. (1997) Exceptionally stable salt bridges in cytochrome P450cam have functional roles. *Biochemistry* **36,** 5402-5417.

Mant, C. T., Chao, H., and Hodges, R. S. (1997) Effect of mobile phase on the oligomerization state of a-helical coiled-coil peptides during high-performance size-exclusion chromatography. *J. Chromatograhpy A* **791,** 85-89.

Marszalek, J. R., Ruiz-Lozano, P., Roberts, E., Chien, K. R., and Goldstein, L. S. B. (1999) Situs inversus and embyonic ciliary morphogenesis defects in mouse mutants lacking the KIF3A subunit of kinesin-II. *Proc. Natl. Acad. Sci. USA* **96,** 5043-5048.

McDonald, H. B., Stewart, R. J., and Goldstein, L. S. (1990) The kinesin-like ncd protein of Drosophila is a minus end-directed microtubule motor. *Cell* **63,** 1159-65.

Merrifield, R. B. (1963) Solid-phase peptide synthesis I. The synthesis of a tetrapeptide. *J. Am. Chem. Soc.* **29,** 2149-2154.

Merrifield, B. (1997) Concept and early development of solid-phase peptide synthesis. *Methods Enzymol.* **289,** 3-13.

Miki, H., Setou, M., Kaneshiro, K., and Hirokawa, N. (2001) All kinesin superfamily protein, KIF, genes in mouse and human. *PNAS* **98,** 7004-7011.

Miller, R. and Lasek, R. (1985) Cross Bridges Mediate Anterograde and Reterograde Vesicle Transport along Microtubules in Squide Axoplasm. *J. Cell Biol.* **101,** 2181-2193.

Monera, O. D., Zhou, N. E., Kay, C. M., and Hodges, R. S. (1993) Comparsion of antiparallel and parallel two-stranded a-helical coiled-coils. Design, synthesis and characterization. *J. Biol. Chem.* **268,** 19218-19277.

Monera, O. D., Kay, C. M., and Hodges, R. S. (1994a) Protein denaturation with guanidine hydrochloride or urea provides a different estimate of stability depending on the contributions of electrostatic interactions. *Protein Sci.* **3,** 1984-1991.

Monera, O. D., Kay, C. M., and Hodges, R. S. (1994b) Electrostatic Interactions Control the Parallel and Antiparallel Orientation of a-Helical Chains in Two-Stranded a-Helical Coiled-coils. *Biochemistry* **33,** 3862-3871.

Morii, H., Takenawa, T., Arisaka, F., and T., S. (1997) Identification of kinesin neck region as a stable a-helical coiled-coil and its thermodynamic characterization. *Biochemistry* **36,** 1933-42.

Morris, R. L. and Scholey, J. M. (1997) Heterotrimeric Kinesin-II is required for the assembly of motile 9+2 ciliary axonemes on sea urchin embryos. *J. Cell Biol.* **138,** 1009-1022.

Muresan, V., Lyass, A., and Schnapp, B. J. (1999) The kinesin motor KIF3A is a component of the presynaptic ribbon in vertebrate photoreceptors. *J. Neurosci.* **19,** 1027-1037.

Nadassy, K., Wodak, S. J., and Janin, J. (1999) Structural features of protein-nucleic acid recognition sites. *Biochemistry* **38,** 1999-2017.

Novabiochem (2000) *Novabiochem Catalog and Peptide Synthesis Handbook '00/01. Novabiochem, San Diego, CA.*

O'Shea, E. K., Rutkowski, R., and Kim, P. S. (1989a) Evidence that the leucine zipper is a coiled-coil. *Science* **243,** 538-542.

O'Shea, E. K., Rutkowski, R., Stafford, W. F., and Kim, P. S. (1989b) Preferential heterodimer formation by isolated leucine zippers from Fos and Jun. *Science* **245,** 646-648.

O'Shea, E. K., Klemm, J. D., Kim, P. S., and Alber, T. (1991) X-ray structure of the GCN4 leucine zipper, a two-stranded, parallel coiled-coil. *Science* **254,** 539-544.

Ozeki, S., Kato, T., Holtzer, M. E., and Holtzer, A. (1991) The Kinetics of Chain Exchange in Two-Chain Coiled Coils: aa- and bb-Tropomyosin. *Biopolymers* **31,** 957-966

Pace, C. N., Shirley, B. A., Mcnutt, M., and Gajiwala, K. (1996) Forces contributing to the conformational stability of proteins. *Faseb J.* **10,** 75-83.

Pappenberger, G., Schurig, H., and Jaenicke, R. (1997) Disrupton of an ionic network leads to accelerated thermal denaturation of D-glyceraldehyde-3-phosphate dehydrogenase from the hyperthermophilic bacterium Thermotoga maritima. *J. Mol. Biol.* **274,** 676-683.

Penningroth, S., Rose, P., and Peterson, D. (1987) Evidence that the 116kDa component of kinesin binds and hydrolyzes ATP. *FEBS J.* **222,** 204-210.

Pfister, K. K., Wafner, M. C., Stenoien, D. L., Brady, S. T., and Bloom, G. S. (1989) Monoclonal Antibodies to Kinesin Heavy and Light Chains Stain Vesicle-like Structures, but not Microtubules, in Cultured Cells. *J. Cell. Biol.* **108,** 1453-1463.

Pontius, B. W. and Berg, P. (1990) Renaturation of complementary DNA strands mediated by purified mammalian heterogeneous nuclear ribonucleoprotein A1 protein: Implications for a mechanism for rapid molecular assembly. *Proc. Natl. Acad. Sci. USA.* **87,** 8403-8407.

Pontius, B. W. (1993) Close encounters: why unstructured polymeric domains can increase rates of specific macromolecular association. *TIBS.* **18,** 181-186.

Privalov, P. L. and Gill, S. J. (1988) Stability of protein structure and hydrophobic interaction. *Advan. Protein Chem.* **39,** 191-234.

Rabanal, F., DeGrado, W. F., and Dutton, P. L. (1996) Use of 2,2'-dithiobis(5-nitropyridine) for the heterodimerization of cysteine containing peptides. Introduction of the 5-nitro-2-pyridinesulfenyl group. *Tetrahedron Letters* **37,** 1347-1350.

Radic, Z., Kirchhoff, P. D., Quinn, D. M., McCammon, J. A., and Taylor, P. (1997) Electrostatic influence on the kinetics of ligand binding to acetylcholinesterase. *J. Biol. Chem.* **272,** 23265-23277.

Rashid, D. J., Wedaman, K. P., and Scholey, J. M. (1995) Heterodimerization of the two motor subunits of the heterotrimeric kinesin, KRP85/95. *J. Mol. Biol.* **252,** 157-62.

Rice, S., Lin, A. W., Safer, D., Hart, C. L., Naber, N., Carragher, B. O., Cain, S. M., Pechatnikova, E., Wilson-Kubalek, E. M., Whittaker, M., Pate, E., Cooke, R., Taylor, E. W., Milligan, R. A., and Vale, R. D. (1999) A structural change in the kinesin motor protein that drives motility. *Nature* **402,** 778-84.

Romberg, L. and Vale, R. D. (1993) Chemomechanical cycle of kinesin differes from that of myosin. *Nature* **361,** 168-170.

Romberg, L., Pierce, D. W., and Vale, R. D. (1998) Role of the Kinesin Neck Region in Processive Microtubule-based Motility. *J. Cell Biol.* **140,** 1407-1416.

Sack, S., Muller, J., Marx, A., Thormahlen, M., Mandelkow, M., Brady, S., and Mandelkow, E. (1997) Xray Structure of Motor and Neck Domains from Rat Brain Kinesin. *Biochemistry* **36,** 16155-16165.

Sadhu, A. and Taylor, E.W. (1992) A kinetic study of the kinesin ATPase. *J. Biol. Chem.* **267,** 11352-11359.

Schmitt, F. O., (1968) Fibrous proteins-neuronal organelles. *Proc. Natl. Acad. Sci.* USA **60,** 1092-1101

Schnapp, B., Vale, R., Sheetz, M., and Reese, T. (1985) Single Microtubules from Squide Axoplasm Support Bidirectional Movement of Organelles. *Cell* **40,** 455-462.

Schreiber, G. a. F., A.R. (1996) Rapid, electrostatically assisted association of proteins. *Nat. Struct. Biol.* **3,** 427-431.

Serada, T. J., Mant, C. T., Quinn, A. M., and Hodges, R. S. (1993) Effect of the a-amino group on peptide retention behaviour in reversed-phase chromatography. Determination of the pKa values of the a-amino group of 19 different N-terminal amino acide residues. *J. Chromatogr.* **646,** 17-30.

Smith, R. S. (1980) The short term accumulation of axonally transported oranelles in the region of localized lesions of single myelinated axons. *J. Neurocytology* **9,** 39-65.

Soriano, G. M., Ponamarev, M. V., Piskorowski, R. A., and Cramer, W. A. (1998) Identification of the basic residues of cytochrome f responsible for electrostatic docking interactions with plastocyanin in vitro: Relevance to the electron transger reaction in vivo. *Biochemistry* **37,** 15120-15128.

Stewart, J. Y., J. (1984) *Solid Phase Peptide Synthesis,. Pierce Chemical Co., Rockford, Illinois.*

Su, J. Y., Hodges, R. S., and Kay, C. M. (1994) Effect of Chain Length on the Formation and Stability of Synthetic a-Helical Coiled-Coils. *Biochemistry* **33,** 15501-15510.

Summers, K., and Gibbons, I.R. (1971) Adenosine-triphosphate induced sliding of tubules in trypsin-treated flagella of sea urchin sperm. *Proc. Natl. Acad. Sci. USA* **68,** 3092-3096.

Takeda, S., Yonekawa, Y., Tanaka, Y., Okada, Y., Nonaka, S., and Hirokawa, N. (1999) Left-Right Asymmetry and Kinesin superfamily protein KIF3A: New insights in determination of laterality and mesoderm induction by kif3A-/- Mice analysis. *J. Cell Biol.* **145,** 825-836.

Taylor, E. W. (1992) *Heart and Cardiovascular System* (eds Fozzard, H. A. Raven: New York) 1281-1293.

Thorn, K. S., Ubersax, J. A., and Vale, R. D. (2000) Engineering the Processive Run Length of the Kinesin Motor. *J. Cell Biol.* **151,** 1093-1100.

Tripet, B., Vale, R. D., and Hodges, R. S. (1997) Demonstration of Coiled-coil Interactions within the Kinesin Neck Region Using Synthetic Peptides. *J. Biol. Chem.* **272,** 8946-8956.

Tripet, B., Wagschal, K., Lavigne, P., Mant, C. T., and Hodges, R. S. (2000) Effects of side-chain characteristics on stability and oligomerization state of a de novo designed model coiled-coil: 20 amino acid substitutions in position "d". *J. Mol. Biol.* **300,** 377-402.

Tsukita, S. and Ishikawa, H. (1980) The movement of membranous organelles in axons. *J. Cell Biol.* **84,** 513-530.

Tytell, M., Black, M., Garner, J., and Lasek, R. (1981) Axonal Transport: Each Major Rate Component Reflects the Movement of Distinct Macromolecular Complexes. *Science* **214,** 179-181.

Vale, R., Schnapp, B., Reese, T., and Sheetz, M. (1985a) Movement of Organelles Along Filaments dissociated from the Axoplasm of the Squid Giant Axon. *Cell* **40,** 449-454.

Vale, R., Schnapp, B., Reese, T. S., and Sheetz, M. (1985b) Organelle, Bead, and Microtubules Translocations Promoted by Soluble Factors from the Squid Giant Axon. *Cell* **40,** 559-569.

Vale, R. D., Reese, T., and Sheetz, M. (1985c) Identification of a Novel Force-Generating Protein, Kinesin, Involved in Microtubule-Based Motility. *Cell* **42,** 39-50.

Vale, R. D. (1996) Switches, Latches, and Amplifiers: Common Themes of G Proteins and Molecular Motors. *J. Cell Biol.* **135,** 291-302.

Vale, R. D. a. F., R.J. (1997) The Design Plan of Kinesin Motors. *Ann. Rev. Cell Developmental Biol.* **13,** 745-777.

Vaughan, C. K., Buckle, A. M., and Fersht, A. R. (1999) Structural response to mutation at a protein-protein interface. *J. Mol. Biol.* **286,** 1487-1506.

Vijayakumar, M., Wong, K., Schreiber, G., Fersht, A. R., Szabo, A., and Zhou, H. (1998) Electrostatic enhancement of diffusion-controlled protein-protein association: Comparison of theory and experiment on barnase and barstar. *J. Mol. Biol.* **278,** 1015-1024.

Vogt, G., Woell, S., and Argos, P. (1997) Protein thermal stability, hydrogen bonds and ion pairs. *J. Mol. Biol.* **269,** 631-643.

Wade, R. C., Gabdoulline, R. R., Ludemann, S. K., and Lounnas, V. (1998) Electrostatic steering and ionic tethering in enzyme-ligand binding: Insights from simulations. *Proc. Natl. Acad. Sci. USA* **95,** 5942-5949.

Wagschal, K., Tripet, B., Lavigne, P., Mant, C. T., and Hodges, R. S. (1999) The role of position a in determing the stability and oligomerization state of alpha-helical coiled-coils: 20 amino acid stability coefficients in the hydrophobic core of proteins. *Protein Sci.* **8,** 2312-2329.

Waldburger, C. D., Schildbach, J. F., and Sauer, R. T. (1995) Are buried salt bridges important for protein stability and conformational specificity? *J.Struc. Biol.* **2,** 122-128.

Wedaman, K. P., Meyer, D. W., Rashid, D. J., Cole, D. G., and Scholey, J. M. (1996) Sequence and Submolecular Localization of the 115-kD Accessory Subunit of the Heterotrimeric Kinesin-II (KRP85/95) Complex. *J. Cell Biol.* **132,** 371-380.

Weiss, D. G. and Gross, G. W. (1982) The microstream hypothesis of axoplasmic transport : characteristics, predictions and compatibility with data. In Axoplasmic Transport. *D.G. Weiss, ed. (Berlin:Springer-Verlag).* 330-341.

William, S. M., Porter, M. E., Cohn, S. A., Scholey, J. M., Raff, E. C., and McIntosh, J. R. (1988) Drosophila kinesin: characterization of microtubule motility and ATPase. *Proc. Natl. Acad. Sci. USA* **85,** 1109-1113.

Xiong, H., Buckwalter, B. L., Shieh, H. M., and Hecht, M. H. (1995) Periodicity of polar and nonpolar amino acids is the major determinant of secondary structure in self assembling oligomeric peptides. *Proc. Natl. Acad. Sci. USA* **92,** 6349-6353.

Yamazaki, H., Nakata, T., Okada, Y., and Hirokawa, N. (1995) Kif3A/B: A heterodimeric kinesin superfamily protein that works as a mictrotubule plus-end directed motor for membrane organelle transport. *J. Cell Biol.* **130,** 1387-1399.

Yamazaki, H., Nakata, T., Okada, Y., and Hirokawa, N. (1996) Cloning and characterizatio of KAP3: A novel kinesin superfamily-associated protein of Kif3A/3B. *Proc. Natl. Acad. Sci. USA.* **93,** 8443-8448.

Yang, J. T., Laymon, R. A., and Goldstein, L. S. (1989) A three-domain structure of kinesin heavy chain revealed by DNA sequence and microtubule binding analyses. *Cell* **56,** 879-89.

Zhou, N. E., Kay, C. M., and Hodges, R. S. (1992a) Synthetic model proteins: the relative contribution of leucince residues at the nonequivalent positions of the 3-4 hydrophobic repeat to the stability of the two-stranded a-helical coiled-coil. *Biochemistry* **31,** 5739-5746.

Zhou, N. E., Kay, C. M., and Hodges, R. S. (1992b) Synthetic model proteins. Postional effects of interchain hydrophobic interactions on stability of two stranded a-helical coiled-coils. *J. Biol. Chem.* **267,** 2664-2670.

Zhou, N. E., Zhu, B.-Y., Kay, C. M., and Hodges, R. S. (1992c) The two stranded a-helical coiled-coil is an ideal model for studying protein stability and subunit interactions. *Biopolymers* **32,** 419-426.

Zhou, N. E., Kay, C. M., and Hodges, R. S. (1993) Disulfide bond contribuition to protein stability: Positional effects of substitution in the hydrophobic core of the two-stranded a-helical coiled-coil. *Biochemistry* **32,** 3178-3187.

Zhou, N. E., Zhu, B. Y., Cyril, K. M., and Hodges, R. S. (1993b) Importance of intra-chain ionic interactions in stabilzing alpha-helices in proteins. *Biology and Chemistry: Proceedings of the 1992 Chinese Peptide Symposium* 217-220.

Zhou, N. E., Kay, C. M., and Hodges, R. S. (1994a) The Role of Interhelical Ionic Interactions in Controlling Protein Folding and Stability. *J. Mol. Bio.* **237,** 500-512.

Zhou, N. E., Cyril, K. M., and Hodges, R. S. (1994b) The net energetic contribution of interhelical electrostatic attractions to coiled-coil stability. *Protein Eng.* **7,** 1365-1372.

Zhou, N. E., Monera, O. D., Cyril, K. M., and Hodges, R. S. (1994c) Alpha-Helical Propensities of Amino Acids in the Hydrophobic Face of an Amphipathic Alpha-Helix. *Protein and Peptide Letters* **1,** 114-119.